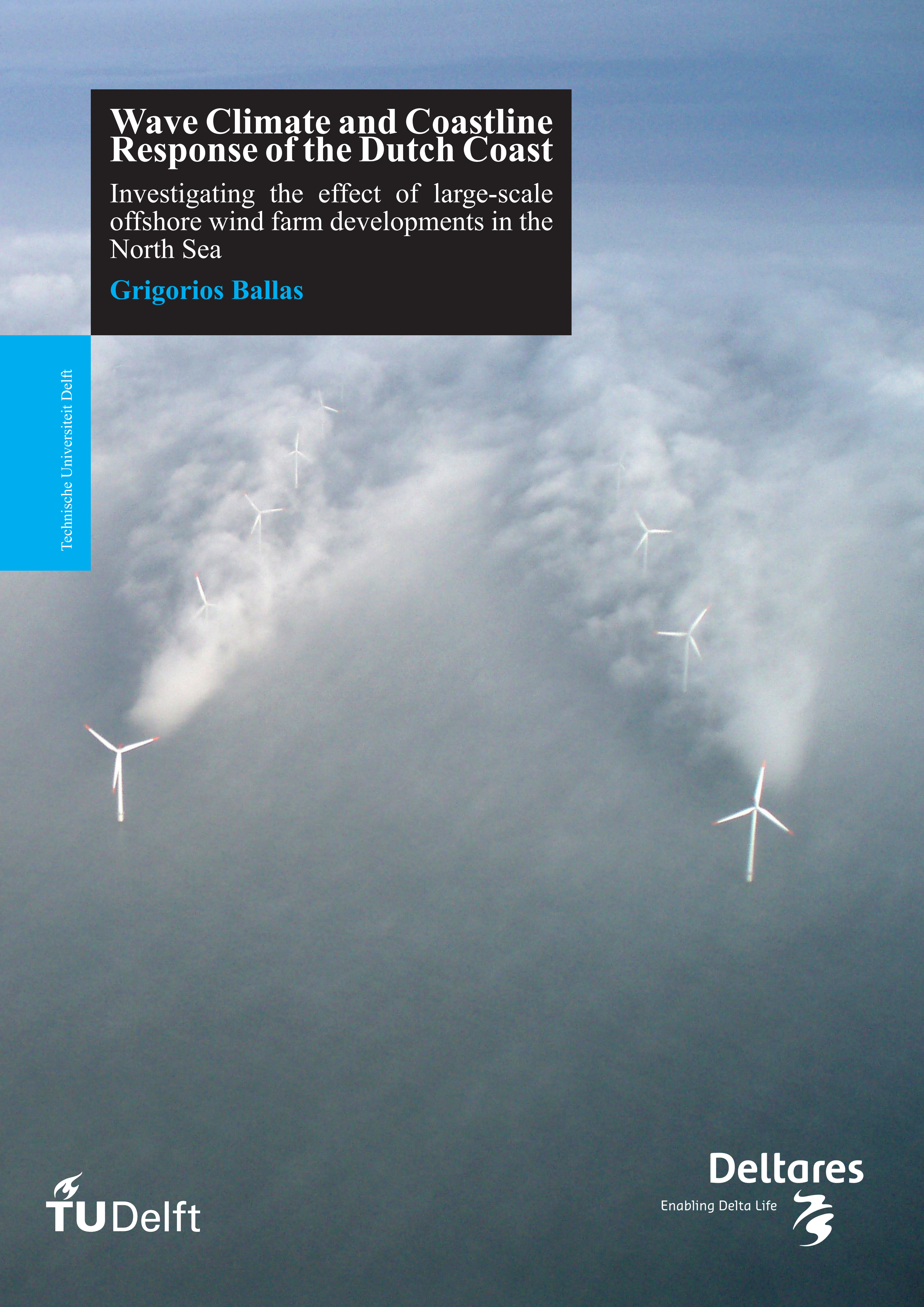

Wave Climate and Coastline Response of the Dutch Coast

Investigating the effect of large-scale offshore wind farm developments in the North Sea

Grigorios Ballas

Technische Universiteit Delft

TU Delft

Deltares
Enabling Delta Life

Wave Climate and Coastline Response of the Dutch Coast

Investigating the effect of large-scale offshore wind farm developments in the North Sea

by

Grigorios Ballas

in partial fulfillment of the requirements for the degree of

Master of Science
in Civil Engineering

at Delft University of Technology,
to be defended publicly on Thursday November 15th, 2018 at 2:00 PM.

Thesis committee:	Prof. dr. ir. S.G.J. (Stefan) Aarninkhof	TU Delft
	Ir. R. (Roderik) Hoekstra	Deltares, TU Delft
	Ir. E. (Emiel) Moerman	Deltares
	Prof. dr. ir. M. (Marcel) Zijlema	TU Delft

An electronic version of this thesis is available at
http://repository.tudelft.nl/.

Correspondence with the author may be directed to
gri.ballas@gmail.com.

TU Delft

Deltares
Enabling Delta Life

Cover photo: Wakes at Horns Rev I OWF in Denmark. The condensed water vapor makes it possible to observe the turbulence behind the wind turbines. Image retrieved from Hasager, Rasmussen, Peña, Jensen, and Réthoré (2013).

Contents

Abstract

To counteract the effect of climate change, a global agreement was put into force in 2016, aiming to limit the increase in average global warming and reduce greenhouse gas emissions. In that respect, European countries are investing in cleaner sources of energy and predominantly offshore wind, which has seen a rapid growth over the last years. The North Sea is a region suitable for developing offshore wind energy, given its strong wind climate and the relatively shallow waters. Many large-scale offshore wind farm (OWF) developments are currently ongoing in that region, while many more are planned and consented for the coming decades.

The concept of large-scale OWF developments has spurred many discussions addressing its potential effect on the greater North Sea region. However, the long-term effect on the surrounding coastal areas has never been studied in detail. Especially for a low-lying country as the Netherlands, assessing the impact of large-scale OWFs is of great importance. This study aims at exploring the effect of future large-scale OWFs in the North Sea, focusing on the wave climate and the coastline response of the Dutch coast.

Based on the roadmap for developing offshore wind energy until 2050, existing and future designated OWF areas are accounted in the North Sea region. The effect of OWFs on wind is introduced in a schematized way, with a constant decrease in wind speed of 20% inside the OWF areas, based on literature knowledge. Supplementary, based on the vision of creating an artificial energy island for storing and redistributing the wind farm generated electricity, a 5 km^2 island is introduced, approximately 30 km away from the Dutch coast. The effect on the nearshore wave climate is studied using the numerical model SWAN, while the resulting effect on the alongshore morphology is assessed using coastline model Unibest-CL+.

The impact of future OWFs on the nearshore wave climate is found to be dependent on the size, shape, orientation and distance from the coast of the individual wind farms. Results show a mean decrease in significant wave height in the order of 1 – 2%. In addition, slight changes in wave direction are observed. The effect on wave climate reduces the alongshore sediment transport at the Dutch coast, by an order of 10% with respect to present values. This results in net-induced erosion, which requires nourishment. The study shows that the areas north of Zandvoort and Petten need the greatest nourishment volumes, in the range of 1.5 – 2.5 m^3/m/year. This is an additional 1% on the current annual nourishment volumes supplied along the Dutch coast.

The underlying study has proved to be effective in quantifying the chain of effects of OWFs and identifying potential hot-spots along the Dutch coast. The knowledge acquired from these effects can be used to optimize future OWF planning in relation to coastline maintenance policies.

Keywords: large-scale offshore wind farms, North Sea, Dutch coast, energy island, coastal engineering, long-term morphodynamics, wave modeling, coastline modeling, coastal management, SWAN, Unibest-CL+.

Acknowledgements

This thesis concludes my studies for obtaining the Master of Science in Hydraulic Engineering at Delft University of Technology. Looking back on this two-year journey, I feel extremely grateful to have had the opportunity to experience life in the Netherlands and expose myself to a highly motivating and demanding academic environment.

Reaching the end of this work, I would like to express my gratitude to all the people that helped me in this research and supported me during the last months.

First, I would like to give special thanks to the members of my graduation committee, for investing their time in me and for their overall contribution to my progress.

I would like to acknowledge Professor Stefan Aarninkhof, for his immediate interest and enthusiasm on the research topic and his willingness to chair the committee. His experience and insightful questions helped me improve my research.

I am also extremely grateful to my research supervisors at Deltares with whom I was working on a daily basis. I would like to thank Roderik Hoekstra for giving me the opportunity to work at the company and showing me how to interact in a professional environment. His critical thinking and day-to-day supervision were critical for steering this work in the right direction. I would like to equally thank Emiel Moerman who was always there to help me on every sort of difficulty with wave modeling, and also for improving my programming skills. His ideas and recommendations were extremely important to finalize this thesis.

At TU Delft, I would like to thank Marcel Zijlema who expressed his interest in being part of this work and for sharing his valuable ideas and experience in SWAN.

However, this research could not have been possible without the contribution of more people within Deltares. I would like to express my appreciation to Bas Huisman for providing the Unibest model and for giving me all the tips and tools regarding coastline modeling. Even though he was not part of the committee, he always showed interest in my progress and was always willing to share his knowledge and ideas. I would also like to thank Sofia Caires who gave her insight at the first stages of this research, helping me update the research approach and providing sources for the literature review. Also, I would like to thank Caroline Gautier who always had the time to help me with SWAN related issues.

Of course, I could not forget to thank all my fellow students who made my stay at Deltares enjoyable. The interesting talks during the coffee and lunch breaks helped me relief myself from doubts and worries, giving me strength and motivation to continue the hard work.

Additionally, I would like to specially mention Sienna White for devoting her time in proofreading this report.

I am also extremely grateful to my girlfriend Maro, for her care and patience as well as her eagerness to hear about my research on a daily basis, even though she was also working on her own Master Thesis at the same time.

Last but far from least, I would like to thank my father, my mother and my brother, who always support me and motivate me to pursue my dreams.

Grigorios Ballas
Delft, October 2018

List of Figures

List of Tables

List of Symbols

Symbol	Units	Description
C_{fric}	m^{2}s^{-3}	Friction coefficient
H_{m0}	m	Significant wave height
Q_s	m^3/year	Net alongshore sediment transport
T_p	s	Peak wave period
U_{10}	m/s	Hourly mean wind speed 10 m above water surface
X	°E $\vee$ m	Longitude $\vee$ Alongshore distance from Hoek van Holland
Y	°N $\vee$ m	Latitude $\vee$ Coastline change with respect to 2018
ΔS	m^3/year	Change in net sediment transport due to OWFs/energy island
ΔY	m	Change in coastline position due to OWFs/energy island
ζ	-	Dimensionless Monin-Obukhov length
σ_θ	degrees (°)	(One-sided) wave spectral directional width
ϕ	°N[a]	Mean wave direction
ϕ_{coast}	degrees (°)	Wave approach angle with respect to shore normal

[a] Degrees in nautical convention, expressed as the direction where the waves come from, measured clockwise from geographic North. Not to be confused with latitude.

List of Abbreviations

Abbreviation	Description
ASAR	Advanced Synthetic Aperture Radar
C3S	Copernicus Climate Change Service
DCSM	Dutch Continental Shelf Model
EC	European Commission
ECMWF	European Center for Medium-Range Weather Forecasts
Envisat	Environmental satellite
ERS	European Remote-Sensing satellite
EU	European Union
EWEA[1]	European Wind Energy Association
EZ	Egmond aan Zee
FF	Far Field
GHG	Greenhouse Gas
HCWD	Holland Coast Wadden Sea Model
HKN	Hollandse Kust Noord
HKNW	Hollandse Kust Noordwest
HKW	Hollandse Kust West
HKZ	Hollandse Kust Zuid
HKZW	Hollandse Kust Zuidwest
IABR	International Architecture Biennale Rotterdam
IEA	International Energy Agency

Continued

Abbreviation	Description
LES	Large Eddy Simulation
LIDAR	Light Detection and Ranging
LUD	Luchterduinen Wind Farm
MKL	Momentary coastline position (kustlijnpositie)
MSL	Mean Sea Level
NAP	Normaal Amsterdams Peil
NF	Near Field
OFWEC	Offshore Wind Energy Capacity
ONWEC	Onshore Wind Energy Capacity
OWEZ	Offshore Wind Farm Egmond aan Zee
OWF	Offshore Wind Farm
PAWP	Princess Amalia Wind Park
RES	Renewable Energy Sources
SAR	Synthetic Aperture Radar
SWAN	Simulating Waves Nearshore
TI	Turbulence Intensity
UN	United Nations
VD	Velocity Deficit
WA	Wake Area
WEC	Wind Energy Capacity
WFA	Wind Farm Area
WL	Wake Length

[1] EWEA has rebranded to WindEurope. The old name is used for citing relevant literature references.

1

Introduction

In order to counteract the effect of climate change, a global agreement was adopted aiming to limit the increase in average global temperature and reduce greenhouse gas emissions. As part of this, European countries are investing in renewable energy sources and predominantly wind energy, which has seen a rapid growth over the last years. Given the strong wind climate and the relatively shallow waters, the North Sea is a region where many large-scale offshore wind farm (OWF) developments are already ongoing while many more are planned for the coming decades. The effect of large-scale OWF developments on the surrounding coastal areas though has never been studied in detail. Especially for a low-lying country as the Netherlands, assessing the impact of large-scale OWFs is of great importance. This study aims at exploring the cumulative effect of large-scale OWF developments on the nearshore wave climate and the coastline response of the Dutch coast.

1.1. Background

At the Paris Conference of the Parties (COP21) in December 2015 (UN, 2015a) the first-ever global climate agreement was adopted. A plan to combat climate change was set out by 195 countries aiming to limit the increase in average global temperature to well below 2°C while making efforts to hold the increase to 1.5°C above pre-industrial levels (EC, 2015; UN, 2015b). The Paris agreement was formally ratified and put into force on 4 November 2016 (UN, 2016). From that moment the European Union (EU) is facing the challenge to implement the Agreement. Realizing a low-carbon economy is considered the best applicable option and should be therefore highly prioritized (Müller, Haesen, Ramaekers, & Verkaik, 2017). Prior to the Paris Conference the European Commission (EC) presented a roadmap (EC, 2011) suggesting the most cost-effective way of reaching the overall energy target: a reduction in domestic Greenhouse Gas (GHG) emissions by 40% in 2030, 60% in 2040 and 80 – 95 % in 2050 compared to 1990 levels (Figure 1.1). Following the plan of the EU to decarbonize its power generation, European countries are investing in renewable energy sources (RES) and predominantly wind energy, which has seen a rapid growth over the last years. As a matter of fact, in 2016 wind energy overtook coal as the 2nd largest form of power generation capacity in EU (WindEurope, 2018a).

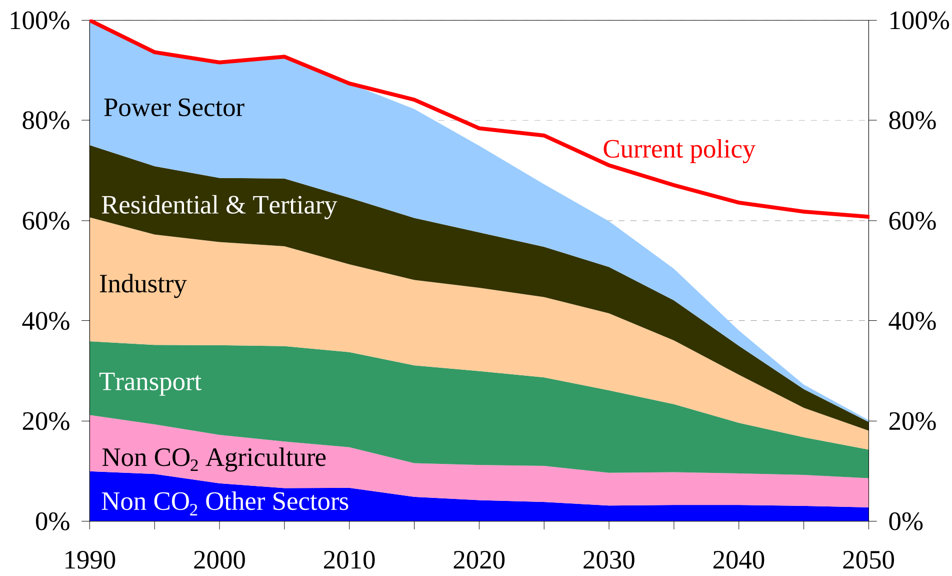

Figure 1.1: EU domestic GHG emissions compared to 1990 levels (EC, 2011).

The total wind energy capacity (WEC) in EU (consisting of onshore and offshore wind energy installations) is expected to rise in the coming decades. Projections are presented in Figure 1.2.

According to the European Commission (EC) WEC is expected to reach 207 GW in 2020, 255 GW in 2030 and 368 GW by 2050 (EC, 2016). The International Energy Agency (IEA) presents the ”new policies” scenario according to which the WEC will reach 190 GW in 2020 and 217 GW

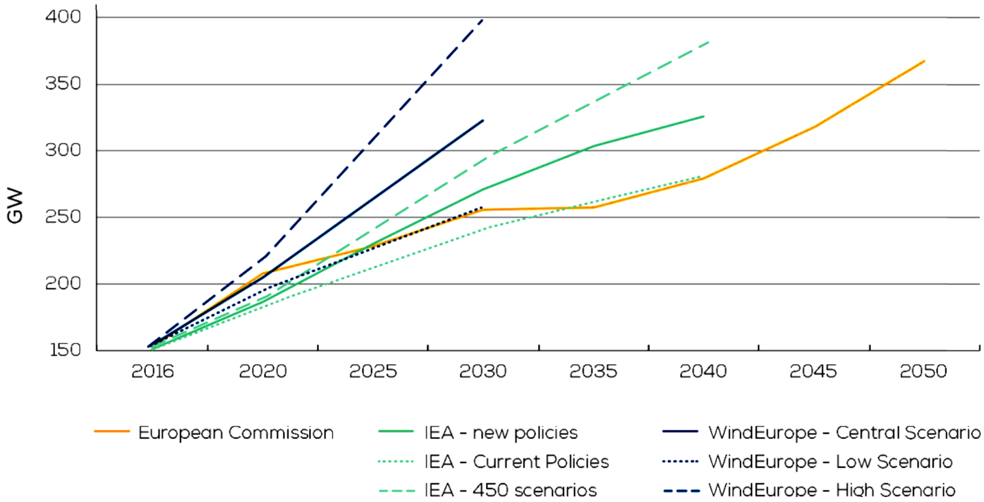

Figure 1.2: Projections of installed WEC in EU extending to 2050 (WindEurope, 2017b).

in 2030. WindEurope[1] estimates greater numbers suggesting a central scenario of 210 GW in 2020 and 323 GW in 2030.

Such an increase in WEC should be realized in a large spatial scale. Since land is mainly reserved for other uses the future intention is to develop offshore wind farms (OWFs). The potential to increase the offshore wind energy capacity (OFWEC) is greater for countries surrounding the North Sea, due to the strong winds blowing in the region in combination with the relatively shallow water depths. The installed WEC in the North Sea at the end of 2017 is shown in Table 1.1.

Table 1.1: Installed ONWEC and OFWEC (GW) in North Sea countries at the end of 2017.

Country	**Year**	
	2017	
	ONWEC[1]	**OFWEC**[2]
Belgium	1.966	0.877
Denmark	4.21	1.266
Germany	50.777	5.355
Netherlands	3.223	1.118
United Kingdom	12.037	6.835
Norway	1.16	0.002
Total	73.37	15.45
	88.83	

[1] WindEurope (2018a, 2018b).
[2] WindEurope (2018b).

At the end of 2017 the total installed WEC in the North Sea countries was 88.83 GW with ONWEC being 73.37 GW and OFWEC amounting to 15.45 GW.

[1]Formerly European Wind Energy Association (EWEA).

The installed wind capacity is expected to be much greater in the future. Table 1.2 gives more details. In a central scenario, WindEurope predicts WEC to reach 107.3 GW in 2020 and 159.7 GW in 2030. As for OFWEC, this is expected to increase to 24.57 GW in 2020 and 57.3 GW in 2030.

Table 1.2: Projections of installed ONWEC and OFWEC (GW) in North Sea countries in years 2020 and 2030.

Country	**Year**			
	2020[1]		**2030**[2]	
	ONWEC	**OFWEC**	**ONWEC**	**OFWEC**
Belgium	2.574	2.112	3.4/4.4/4.4	1.6/4/4
Denmark	4.456	2.171	3.65/5/6.5	3.4/4.3/6.13
Germany	58.811	7.608	60/70/71	14/15/20
Netherlands	4.91	2.418	8/8/15	4.5/11.5/18.5
United Kingdom	11.986	10.256	13/15/20	18/22.5/30
Norway[3]	–		–	
Total	82.74	24.57	88.05/102.4/116.9	41.5/57.3/78.63
	107.3		129.55/159.7/195.53	

[1] Presenting a central scenario (GWEC, 2017; WindEurope, 2017a, 2017c).
[2] Presenting a low/central/high scenario (WindEurope, 2017b).
[3] Projections account for EU countries. Norway is not part of the EU but it is presented here since it is a North Sea country.

The increase in OFWEC means more OWFs in the North Sea. In fact many OWFs are currently being developed and many more are planned and consented for the coming decades as shown in Figure 1.3.

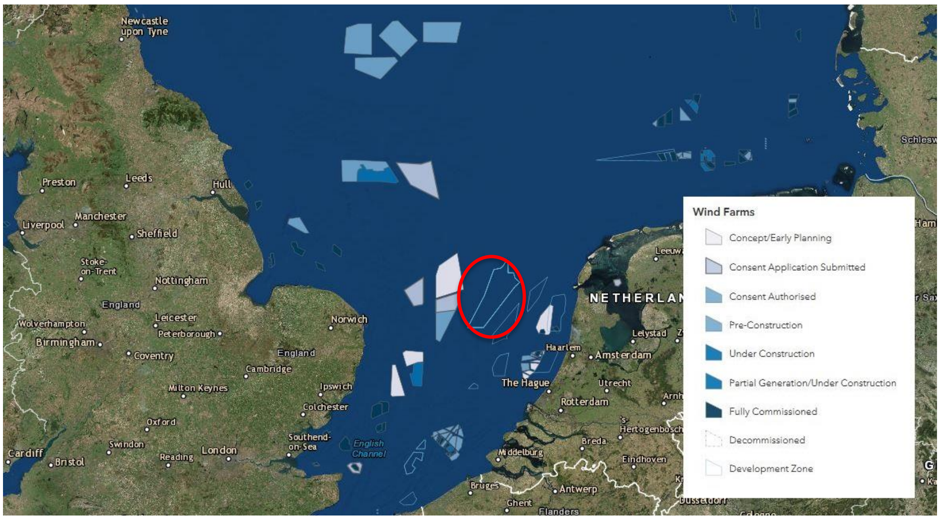

Figure 1.3: Current and planned OWF developments in the North Sea. The red circle shows IJmuiden Ver, which is expected to cover an area of around 1,000 km^2 (4C Offshore, 2018).

Future OWFs in the North Sea will be located further from the shore. Using current concepts to interconnect these OWFs (such as radial/individual grid connections via AC cables) will result in an increasing cost level since the offshore distances are longer and the waters are deeper. In addition, the generated electricity from OWFs must be easily transmitted between the North Sea countries while any surplus should be stored for later use. To achieve this in a cost-efficient way a possible approach is to establish an international network, where the OWFs are interconnected using one or multiple energy hubs. To that end many concepts have been proposed, one of which is an artificial energy island, depicted in Figure 1.4.

Figure 1.4: Artistic impression of an energy island in the North Sea surrounded by wind turbines (TenneT, Energinet, Gasunie, & Port of Rotterdam, 2018).

The island could be surrounded by OWFs and interconnect all North Sea countries (Netherlands, United Kingdom, Belgium, Norway, Germany and Denmark). It could also serve other needs, such as creating opportunities for work and housing. Furthermore, the island could integrate many more functions in the North Sea, such as mining of oil and gas, fisheries, shipping, military practice grounds, habitat for ecology, cabling etc. An island area of 6 km^2 has been suggested in the media. It is important to note however that an energy island is one of the potential solutions for storing and redistributing the offshore generated wind energy. The Dutch government is supporting further technical solutions to upscale the OFWEC in the North Sea, and has not reached a final decision yet.

The idea of large-scale OWF developments in the North sea has been visualized by Sijmons (2014) who presented a model showing the energy transition by 2020, 2030 and 2040/2050 (Figure 1.5). A similar model has been presented at the 2016 International Architecture Biennale Rotterdam (IABR) meeting (Figure 1.6). Both models demonstrate the increase in OWFs and a tendency to realize such infrastructure further from the coast, at deeper water.

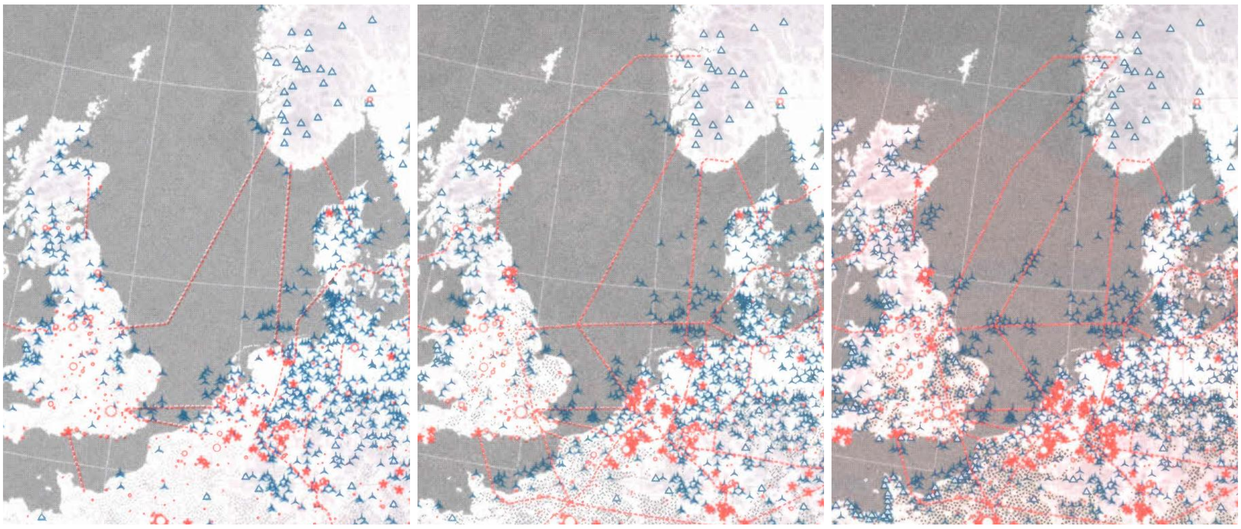

(a) 2020 (b) 2030 (c) 2040/2050

Figure 1.5: Growth model showing the energy transition in Europe. OWFs are indicated with blue color. Three future development stages are presented: (a) 2020, (b) 2030 and (c) 2040/2050 (Sijmons, 2014).

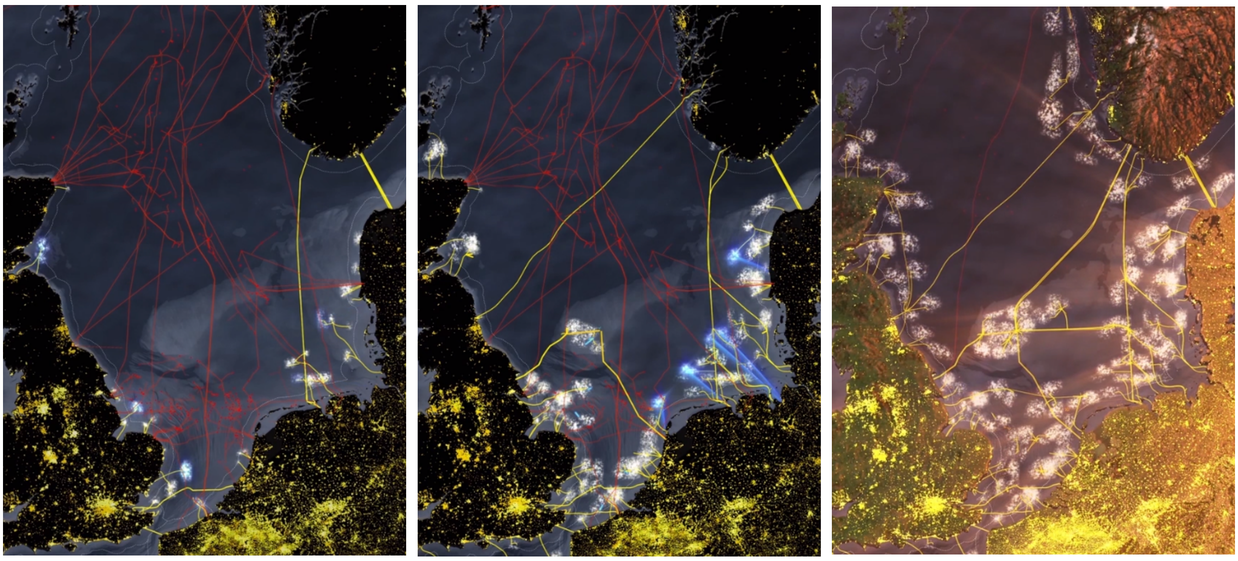

(a) 2020 (b) 2030 (c) 2050

Figure 1.6: Growth model presented in the IABR 2016 meeting indicating the progressive increase of OWFs in the North Sea. Three future development stages are shown: (a) 2020, (b) 2030 when an energy island construction at Dogger Bank could begin and (c) 2050.

1.2. Motivation

The concept of large-scale OWF developments has spurred many discussions addressing its potential long-run effect on the greater North Sea region (Jongbloed, van der Wal, & Lindeboom, 2014). These developments have never existed on a such a big scale, thus their effect on ecological aspects, coastal processes, waves, water levels and wind forcing is poorly understood (Clark, Schroeder, & Baschek, 2014). Furthermore, little attention has been given to an additional effect which is of great importance for the Netherlands. OWFs affect the wind climate which is responsible for wave generation and propagation. If the effect on waves is significant close to the coast, OWFs could alter the alongshore sediment transport and hence the coastal morphology[2]. Moreover, the additional effect of an energy island can further affect the wave climate, since the island would directly block wave propagation. The potential effect of large-scale OWF developments on various physical processes is presented schematically in Figure 1.7.

One could argue that a single OWF cannot cause a significant change in wave height; looking at the entire North Sea, waves have enough fetch length to grow and OWFs affect wind in a very small proportion of that length. Consider though a future scenario in which the North Sea is occupied by numerous OWFs as visualized in Figure 1.5 and Figure 1.6. In such a case the wind will be affected in a significant part of the fetch length something that should be taken into account when trying to predict the nearshore wave climate and the alongshore sediment budget in coastal regions.

Especially in the Netherlands, preserving the coastline position is of vital importance resulting in frequent updates of the coastal maintenance policy. Since 1991, the Dutch government adopted a decision to maintain the coastline to its 1990 position (Roeland & Piet, 1995). This was redefined in 2001 to account for sea level rise (Van Koningsveld & Mulder, 2004). The increasing interest in protecting the Dutch coast is a key point for motivating further investigation on the potential effect of large-scale OWF developments.

Looking at the future, not only the number of OWFs will increase. The need to grow the OFWEC in rates greater than ever (Table 1.2) will also result in bigger OWF areas. In addition, it is obvious that future technological advancements will also allow for bigger wind turbines operating within OWFs. Such expectations could lead to an intensified effect on wave climate and coastal morphology. The above suggest that the effect of large-scale OWFs is worth investigating.

1.3. Scientific and societal significance

It is a great challenge to investigate the effect of large-scale OWF developments in the North Sea, which is a highly dynamic environment accommodating many human activities and a rich natural habitat (Jongbloed et al., 2014). OWF development is a new industry which has not reached maximum capacities in offshore areas, and therefore has not triggered the need to consider potential effects. This is however going to change in the future as previously explained.

From an academic standpoint up till now, the main research focused on increasing the performance of wind turbines. Little research has investigated large-scale secondary effects on various physical processes in the North Sea. This knowledge limitation is expected to open up a new and multidisciplinary field which will receive a great deal of attention in the coming years. Studying the effect of large-scale OWF developments is also relevant for the industry since more knowledge

[2] Alongshore sediment transport is predominantly driven by waves propagating to the coast.

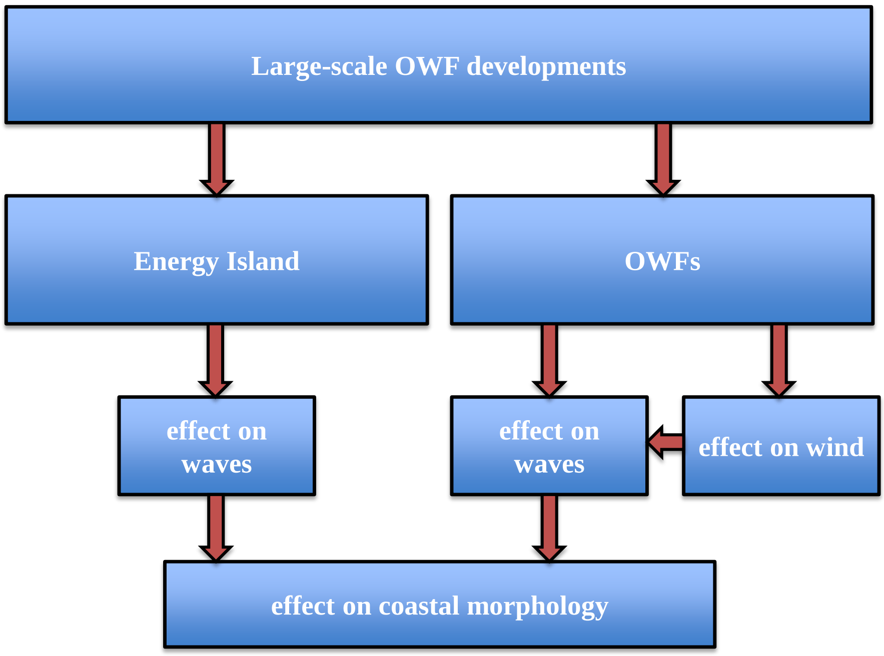

Figure 1.7: Effect of large-scale OWF developments on various physical processes.

must be acquired to tackle potential negative effects (or even benefit from positive outcomes) of such infrastructure. For example, predicting the effect of OWFs on wave climate is necessary to further optimize the tidal windows and to plan vessel movements close to ports (Gautier & Caires, 2015). Furthermore, especially for the Netherlands, it is crucial to predict the effect on coastal morphology since this is linked to safety against floods. Therefore, understanding the effect of large-scale OWF developments on the nearshore wave climate and the coastline response of the Dutch coast will give a better insight on future design of OWFs for the benefit of the shoreline evolution of the Netherlands.

1.4. Knowledge gap and research focus

To our knowledge, a study regarding the combined effect of many OWFs on wave climate and the potential for coastline change has never been conducted. There are only limited studies that take into account a single OWF and only one study that investigates the effect of an OWF on the shoreline development. More information is given in Chapter 2.

OWFs are relatively new developments, therefore their large-scale effect on the wind climate has not been studied extensively either. For example there is still no well established knowledge on how the 10-m wind speed (U_{10}[3]) is affected in the vicinity of an OWF and the dependencies of this effect. Various studies have addressed this issue with numerical models (Ainslie, 1988; Cui, Li, Liu, & Gao, 2015; González-Longatt, Wall, & Terzija, 2012; Segtnan & Christakos, 2015). However, models require thorough validation using wind speed measurements over large spatial scales.

[3]Hourly mean wind speed 10 m above water surface, which is forcing wave generation in the open sea.

This has just recently become possible using remote sensing techniques, especially SAR measurements. More information on wind speed measurements using SAR is given in Appendix A.

This study acknowledges the knowledge gap on the effect of OWFs on wind. The aim of this thesis however is not to increase the understanding of this phenomenon, because the focus is on coastal engineering applications. The effect of OWFs on wind climate is introduced in a schematized way assuming a wind speed decrease inside the OWF areas, taken as the mean value of measurements reported in literature. This is expected to decrease the uncertainty of this parameter as much as possible.

The main goal of this work is to understand the contribution of large-scale OWF developments in changing the wave climate in the nearshore and the resulting effect on the Dutch coast. The focus is to identify the proportion of wave height change caused by OWFs in relation to a baseline situation, where no OWFs are present. Continuously, the interest is directed to the Dutch coast where the affected wave climate is expected to alter the alongshore sediment transport and therefore the evolution of the shoreline. In addition, an island is included in the simulations to investigate its effect in combination with OWF developments.

1.5. Research questions and objectives

The research objective of this thesis is to understand how large-scale OWF developments in the North Sea affect the nearshore wave climate of the Netherlands as well as the evolution of the Dutch coast. The research objective is fulfilled by answering the following questions:

1. **What is the effect on the nearshore wave climate along the Dutch coast resulting from various OWF development stages in the North Sea?**
    (a) How can we explain these phenomena?
2. **What is the effect on the sediment transport along the Dutch coast resulting from various OWF development stages in the North Sea?**
    (a) How is this change related to the effect on wave climate?
3. **Can we plan the development of large-scale OWFs in the North Sea, for the benefit of the Dutch coast?**
    (a) How close to the Dutch coast is the effect from existing and future OWFs significant for affecting the alongshore morphology?
    (b) Can we identify locations (hot-spots) of significant erosion and thus nourishment need?
    (c) What knowledge have we acquired on future design of OWFs?

As seen from the above questions, first the effect of OWFs on wave climate is identified (Question 1). This is realized by presenting the change in significant wave height and wave direction due to OWFs in relation to a baseline scenario (no OWFs). The mechanism that causes these changes (subquestion 1a) is explained in Chapter 6 and more details are given in Appendix D.

The change in wave height and direction should be significant enough to force changes in alongshore sediment transport and thus affect the coastal morphology (Question 2). The dependence between wave climate and coastal morphology (subquestion 2a) is investigated along the -9 m NAP[4] depth contour, which is assumed to be the nearshore margin.

Results from previous questions are used to determine a plan for OWF developments for the benefit of the Dutch coast (Question 3). The regions near the Dutch coast where the effect on wave climate is most significant (subquestion 3a) are defined by looking back at results from Question 1. Locations along the Dutch coast that need the greatest nourishment volumes (subquestion 3b) are identified by looking at results from Question 2. The above findings are used to acquire knowledge for developing OWFs for the benefit of the Dutch coast (subquestion 3c).

1.6. Research approach and strategy

Research material

To study the effect of OWFs in the North Sea first the current and future designated OWF areas are retrieved from existing databases (4C Offshore, 2018; EMODnet, 2018). In addition, to account for the temporal character of OWF developments a timeframe is considered. Since the development of RES seeks to contribute to the 2050 climate goals it is reasonable to consider a timeframe extending till 2050. A clear distinction is made between OWFs already present in the North Sea (development stage 2018 with OFWEC equal to 15.45 GW), and OWFs to be created in the future (development stages 2023 and 2030 with OFWEC of approximately 25 GW and 57 GW respectively, see Table 1.2). In addition, hypothetical[5] OWFs are considered in the final stage of the timeframe (development stage 2050). It is acknowledged that predictions regarding OWF presence in the North Sea become less certain the further in the future. However, the main idea is that the North Sea will be more congested with OWFs, and this is what is demonstrated here. Supplementary, an energy island is considered in year 2030 at various locations in the North Sea.

Research approach

The wave climate is predicted using SWAN, a third-generation wave model capable of computing wave characteristics over a defined domain (Holthuijsen, Booij, & Ris, 1993). The metocean data to force SWAN computations is retrieved from the ERA5 reanalysis dataset (ECMWF, 2018). To express the long-term wind climate in the North Sea a representative year is selected. The representative wind climate is used to force SWAN simulations. The effect of OWFs on wind is schematized by decreasing the wind speed inside the OWF areas by 20% based on current knowledge (see Chapter 2). SWAN simulations consist of a baseline case (no OWFs), cases accounting

[4] Normaal Amsterdams Peil: a vertical datum; 0 m NAP is approximately equal to the mean sea level (MSL).
[5] Existing databases do not provide information further in the future therefore an assumption is made for 2050.

for OWFs at the defined development stages (2018, 2023, 2030 and 2050) and cases including OWFs together with energy island options.

The effect on the Dutch coast is investigated with Unibest-CL+, a coastline model that simulates longshore processes and related morphodynamics of the coastline (WL|Delft Hydraulics, 1992). The model is forced with the annual wave climate resulting from SWAN simulations and computes the net sediment transport and coastline change from 2018 till 2050 accounting for a baseline case, an OWF presence case and a combined OWF-island case.

Looking at the wave modeling results an offshore region is determined further from which the effect of existing and planned OWFs on the nearshore wave climate is insignificant. Significant effect is considered a change in wave height greater than 1% or a change in wave direction greater than 0.5°. The effect on wave climate has an immediate effect on the alongshore sediment transport. The gradient of the change in net sediment transport along the Dutch coast indicates the additional accretion/erosion rate induced by OWFs which can be translated to nourishment need. The nourishment need for counteracting the effect of OWFs is compared with historical nourishment volumes to determine whether it is significant to include these in the Dutch coastal maintenance policy.

Analysis and presentation of results

Wave modeling results are illustrated by depicting the geographical distribution of significant wave height and direction. Results are available for a 1-year hindcast and are averaged to end up to the annual mean quantities. Furthermore, the effect of OWF developments on wave climate is expressed as the annual mean change in wave height and direction due to OWFs. The wave height change is presented as a percentage relative to the baseline value (case with no OWFs). The change in wave direction is shown in absolute terms, measured in degrees. As explained above, the -9 m NAP contour is considered to be the nearshore margin. Therefore, every plot is accompanied by an extra figure showing the alongshore distribution of the corresponding quantities at the -9 m NAP contour. Additionally, figures includes the upper (3^{rd}) and lower (1^{st}) quartiles of the 1-year simulation to illustrate the range of computed values. Wave modeling results are presented in Section 5.2.

Regarding coastline modeling the net sediment transport along the Dutch coast as well as the coastline change with respect to 2018 are presented as a function of time. More specifically, results are shown for years 2023, 2030 and 2050 (corresponding to development stages 2018, 2023 and 2030). The effect of OWFs is expressed as the difference between the quantities in the OWF case and and baseline case (no OWFs). To identify regions of nourishment need, the gradient of the change in net sediment transport due to OWFs is computed. Coastline modeling results are presented in Section 5.2.

1.7. Thesis outline

The thesis report is structured as follows. The necessary theory that supports the study is presented in Chapter 2 using literature references where necessary. Chapter 3 gives more insight on the chosen approach and research strategy. Wave and coastline modeling is explained in Chapter 4. The obtained results are presented in Chapter 5 and an extensive discussion of the findings is provided in Chapter 6. Conclusions from this and further recommendations are presented in Chapter 7. In addition, Appendix A provides basic information on SAR wind speed measurements near OWFs. Appendix B shows wind speed statistics of the entire ERA5 dataset retrieved for this study. Appendix C displays supplementary results of the effect of OWF developments on wave climate. Appendix D elaborates more on the mechanism behind the effect of OWFs on wave climate. Finally, Appendix E contains information on the model set-up and the post-processing of data.

2

Literature review

This chapter contains the literature review of the underlying study. It is split up into three parts. The first one discusses the effect of OWFs on wind. This is mainly elaborated by looking at remote sensing measurements. Continuously, the focus is directed on the effect of OWFs on waves. It is found that little research has been conducted on this field, especially taking into account large-scale OWF developments (such as the future OWFs in the North Sea). Finally, one study dealing with the effect of OWFs on coastal morphology is presented. This is the only one found in literature.

2.1. Relevant research fields

This study is related to two basic research fields. The first one focuses on the effect of one or multiple OWFs on wind climate and more specifically on the 10-m wind speed, denoted by U_{10}. The second one examines the effect of one or multiple OWFs on wave climate. In addition, since waves are generated by wind and coastal morphology is affected by the nearshore wave climate, this study necessitates knowledge on the (indirect) effect of one or multiple OWFs on coastline evolution. The link between the aforementioned research fields was already presented in Figure 1.7.

2.2. Effect of single OWF on wind

An OWF consists of multiple wind turbines. Wind turbines affect atmospheric wind as it passes through. When wind interacts with a wind turbine, part of its kinetic energy is used to turn the turbine rotor, generating electricity. This results in loss of kinetic energy, mainly at hub height (around 100 m above sea surface), creating turbulence and a wake behind each turbine (Ainslie, 1988).

Vertical effect

For a single turbine, wind speed decreases close to the hub height; near the surface though, it can sometimes increase due to turbulence generated by the turbine, as presented in Figure 2.1.

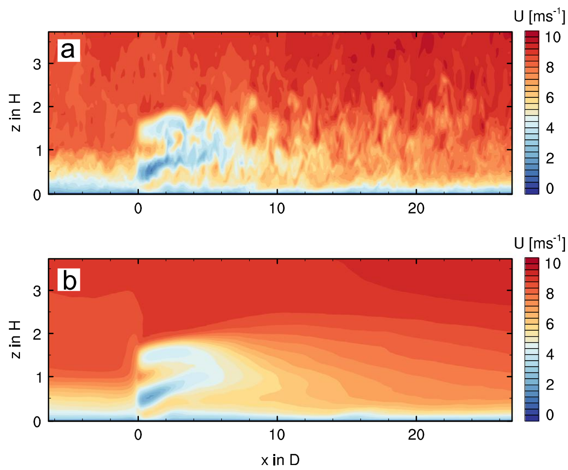

(a)

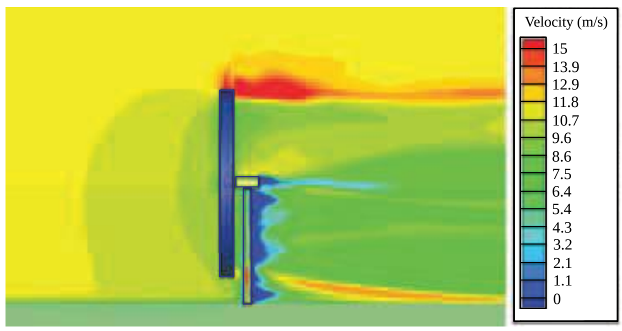

(b)

Figure 2.1: Examples of wind speed increase downwind of a wind turbine. (a) Upper panel: instantaneous wind speed. Lower panel: averaged wind speed. H = 67 m (hub height), D = 93 m (rotor diameter). Results from Dörenkämper, Witha, Steinfeld, Heinemann, and Kühn (2015). (b) Results from Cui et al. (2015).

In absence of a wind turbine the undisturbed wind speed increases nearly logarithmically with distance from sea surface. Its variation from a logarithmic profile depends mostly on atmospheric stability, the temperature gradient between air and water. Atmospheric stability is distinguished into three categories: *stable*, *unstable*, and *neutral*. In a stable atmosphere air temperature is greater than sea temperature. Wind speed increases with altitude with almost a linear trend (constant gradient) while mixing and sea surface stress decrease. In an unstable atmosphere the air temperature is lower than sea temperature. Wind speed increases with altitude with a decreasing gradient and mixing and sea surface stress increase. A neutral atmosphere is a situation in between, in which air and sea temperature are equal. Undisturbed wind speed profiles at various atmospheric states are shown in Figure 2.2.

As discussed above, wind speed might increase close to sea surface when interacting with a wind turbine. This mostly happens in a stable atmosphere as illustrated in Figure 2.3.

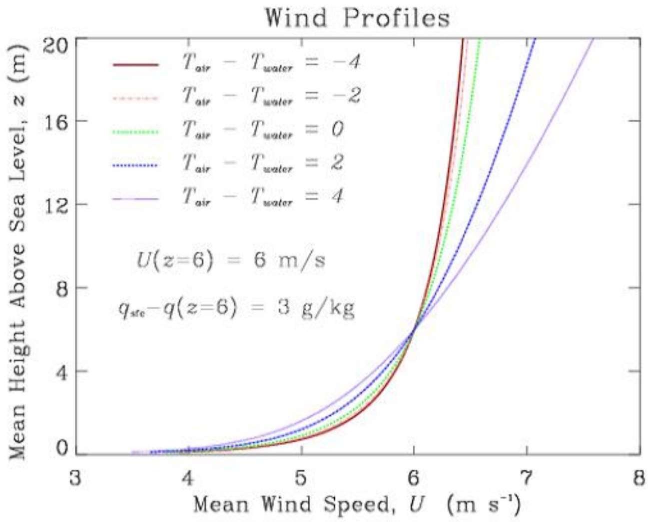

Figure 2.2: Vertical profile of undisturbed wind as a function of atmospheric stability. The green line corresponds to a neutral atmosphere, the red and orange lines to an unstable atmosphere and the blue and magenta lines to a stable atmosphere.

(a) neutral atmosphere

(b) stable atmosphere

Figure 2.3: Schematic representation of the effect of a wind turbine on the vertical structure of wind speed, depending on various atmospheric states. Figure (a) depicts a neutral atmosphere, where wind speed decreases all the way from hub height to sea surface. Figure (b) depicts a stable atmosphere, where wind speed decreases at hub height and increases close to sea surface.

Apart from extracting kinetic energy from wind, a wind turbine can have an additional effect, known as *blockage effect*. Wind turbines act as solid obstacles on wind, making the air flow divert around them. This results in wind speed increase just outside the rotor swept area[1], due to conservation of momentum. This phenomenon has been described in a number of experimental and numerical studies (Sarlak, Nishino, Martínez-Tossas, Meneveau, & Sørensen, 2016; Zaghi, Muscari, & Di Mascio, 2016). Therefore, the blockage effect can lead to an increase of the 10-m wind speed.

Spatial effect

The effect of an OWF on wind is a more complex phenomenon. In such a case the combined effect of multiple wind turbines must be taken into account. Wakes merge with each other and the flow pattern becomes even more unclear. Rajewski et al. (2013) and Dörenkämper et al. (2015) linked the turbulence intensity (TI) and the dimensionless Monin-Obukhov length (ζ)[2] within an OWF to the atmospheric stability. A stable atmosphere results in less wind turbulence (less mixing, low TI and positive ζ). An unstable atmosphere is characterized by increased turbulence (more mixing, high TI and negative ζ). A neutral atmosphere is an intermediate state.

To study the spatial effect of OWFs on wind numerical models are being used, called *wake models*. The use of numerical models is still preferred over field measurements, since it is difficult and expensive to perform measurements covering large spatial scales. The simplest and most common wake model is the ”stand-alone” Jensen model (Jensen, 1983). Furthermore, parametric wake models have been created by schematizing OWFs in exising atmospheric models. Parametric models can take into account characteristics of wind turbines within an OWF (Frandsen et al., 2006; Paskyabi, 2015; Segtnan & Christakos, 2015) and extend to multiple wakes (Christensen, Kristensen, & Deigaard, 2014; González-Longatt et al., 2012). Many parametric models exclude atmospheric stability effects; however wind speed reduction tends to be larger in stable than in unstable conditions, and wakes are longer (Platis et al., 2018). These effects however can be better accounted for using Large Eddy Simulation (LES) models. Figure 2.4 shows the results for the 10-m wind speed using a LES model covering the Borselle OWF. An increase in wind speed between the OWFs is visible, resulting from the effects discussed above. Within the OWF areas wind speed decrease is observed. Even with LES though, it is difficult to perform long-term computations for areas covering more than 2 to 3 OWFs because simulations become computationally expensive.

From the above it becomes apparent that the effect of a single OWF on wind is rather a complex phenomenon. The current study does not account for all the parameters that affect the wind speed. The effect of OWFs on wind is expressed with a simplified schematization. Before moving to that part, some useful definitions are given in the following section.

[1]The rotor swept area is defined as the circular plane created by the rotating turbine blades.
[2]These quantities are not further explained because this study focuses on coastal engineering applications.

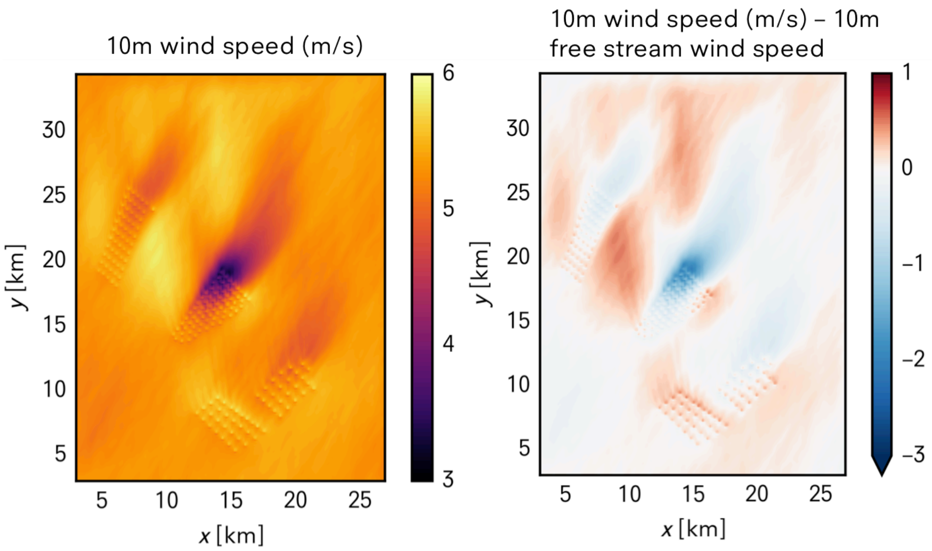

Figure 2.4: Daily average 10-m wind speed at Borselle OWF computed with a LES model. Left panel: disturbed wind speed. Right panel: difference between disturbed and undisturbed (free-stream) wind speed.

2.3. Definitions

Wind farm area and wake area

The current work does not focus on (relatively) small scale dependencies between wind turbines within an OWF but instead deals with larger scale effects. Therefore, the OWF is observed as a whole. To study the effect of OWFs on wind two regions are distinguished: the area within the OWF, called Wind Farm Area (WFA), and the area downwind from the last wind turbine array, called Wake Area (WA). It is important to note that the term "Wake Area" for an OWF does not refer to the wake resulting from a simple turbine, but it is instead the cumulative effect observed downwind from the OWF. The length of the WA is simply called Wake Length (WL). Usually the largest change in the 10-m wind speed is observed at the downwind edge of the WFA. The wind speed recovers to its initial undisturbed value within the WA.

Wake length

The Wake Length is defined as the distance downwind from the last turbine array where the 10-m wind speed is significantly close to the upstream-undisturbed value. An example of the change in 10-m wind speed as a function of the downwind distance from an OWF is presented in Figure 2.5.

In the field, the Wake Length is determined by analyzing large-scale remote sensing measurements of 10-m wind speed, which should be accurate enough to capture the effect of OWFs on wind. More information on such measurements is provided in Appendix A.

It has been found that the WL mainly depends on atmospheric stability which is linked to TI and ζ as previously explained. The dependence of WL on TI and ζ has been observed in many studies (Christiansen & Hasager, 2005; Hasager et al., 2017, 2013; Li & Lehner, 2013; Platis et al.,

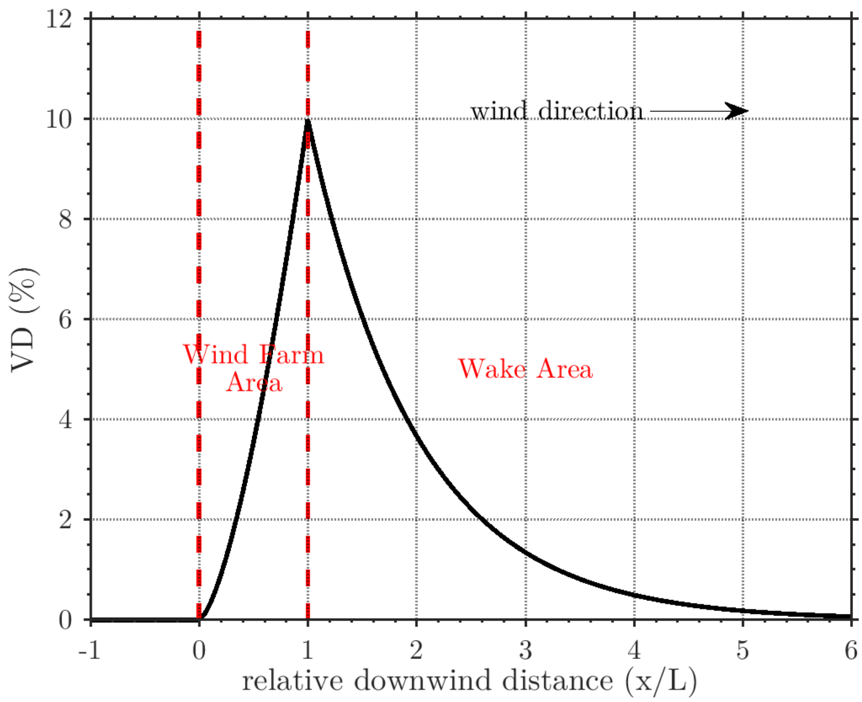

Figure 2.5: Velocity deficit as a function of distance from the upwind edge of an OWF, based on SAR measurements by Christensen et al. (2013). L is the OWF dimension parallel to wind direction. The dashed red lines indicate the Wind Farm Area (WFA). The maximum velocity deficit occurs at the downwind edge of the WFA.

2018). Results show that in a stable atmosphere WLs are maximum whereas the opposite happens in an unstable atmosphere. Nevertheless, another factor that should be taken into account is the orientation of the turbine arrays within an OWF with respect to wind direction. It has been observed that when turbine arrays are parallel to wind direction, less turbulence is generated, allowing for greater WLs (Li & Lehner, 2013).

An extensive amount of references regarding the effect of OWFs on wind (and waves) is given by Clark et al. (2014). In their report they identify two regions, the “Near-Field” (NF) that refers to changes within the OWF and up to 2 km downwind and the “Far-Field” (FF) which considers the situation at least 2 km downwind of an OWF. For consistency, the same definitions will be used in the following. It is important to note that according to the authors few studies investigate the FF effect of OWFs.

Velocity deficit

To study the change in 10-m wind speed in the presence of an OWF, most studies determine the wind speed or Velocity Deficit (VD), which is expressed by the following formula:

$$\mathrm{VD} = \frac{U_{\text{freestream}} - U_{\text{wake}}}{U_{\text{freestream}}} \times 100\% \tag{2.1}$$

where $U_{\text{freestream}}$ is the undisturbed 10-m wind speed upwind of the OWF and U_{wake} the 10-m wind speed inside or downwind of the OWFs. The above equation implies that positive values of VD correspond to a decrease in 10-m wind speed.

The 10-m wind speed is usually determined by meteorological observations at fixed points in space, given as a time-series with 10-minute ensemble averaging. However, an approach like this is difficult to follow when measurements covering great spatial scales are required. A recent solution for obtaining large-scale 10-m wind speed measurements is remote sensing. A drawback of such a technique though is that wind speed is measured at specific time instances (the moments at which the satellite/aircraft passes above the area of interest) meaning that no timeseries can be obtained. In addition, the measured wind speed is averaged spatially, to remove noise. More information can be found in Appendix A.

Velocity deficit measurements

The first to use high resolution SAR images for identifying the wake characteristics of an OWF were Christiansen and Hasager (2005). They analyzed 10-m wind speed maps derived from the ERS-2 SAR and Envisat ASAR satellites at Horns Rev 1 OWF in Denmark. Horns Rev 1 consists of 80 turbines (in 10 rows of 8) and covers and area of 3.9 km $\times$ 5 km (19.5 km^2). It is located 14 – 20 km offshore. The authors investigated two scenarios of wind direction. In the first scenario wind was blowing onshore, where near-neutral stability was observed. The WL was 20 km and within this area significant VD fluctuations were observed. In the second scenario wind was offshore directed in an unstable atmosphere resulting in a WL of 5 km with less VD fluctuations In both cases a maximum VD of 8% was reported.

Li and Lehner (2013) studied the effect of Germany's Alpha Ventus OWF on wind speed using X-band SAR images from the TerraSAR-X imaging radar. This radar provides better spatial quality compared to the ERS-2 SAR and Envisat ASAR satellites used in the study of Christiansen and Hasager (2005). Alpha Ventus consists of 12 turbines (in 3 rows of 4) and covers an area of 2.4 km $\times$ 1.6 km (4 km^2). It is located 56 km offshore. The researchers identified two scenarios by explicitly referring to atmospheric stability. The first scenario considered a stable atmosphere with a maximum VD of 23.2% observed 5 km away from the downwind edge of the OWF and a WL of 18 km. Turbine wakes merged quickly to form a uniform wind farm wake. In the second case, related to a neutral atmosphere, turbine wakes merged slower, resulting in a slightly shorter wind farm wake equal to 14 km and a maximum VD of 24.4%.

Finally, Platis et al. (2018) performed in-situ measurements with an airborne multi-hole flow probe together with an assessment of SAR images and models to identify the existence and characteristics of OWF wakes on the German Bight. They confirmed that WLs ranging from 10 km to 70 km exist for stable atmospheric conditions, with a maximum VD of 40%, whereas for neutral atmospheres these are moderate (10 – 25 km) and significantly smaller for unstable conditions (0 – 10 km).

2.4. Effect of multiple OWFs on wind

While research is thorough on the formation and dynamics of individual turbine wakes and OWF wakes, the collective effect of multiple OWFs is less understood (Christiansen & Hasager, 2005; Hasager et al., 2015). Relevant effects consider the interaction of far wakes with the higher atmosphere, formation of internal boundary layers and interaction between far wakes and sea. Evidence of wakes that extend for tens of kilometers has been found in satellite images, see Figure 2.6.

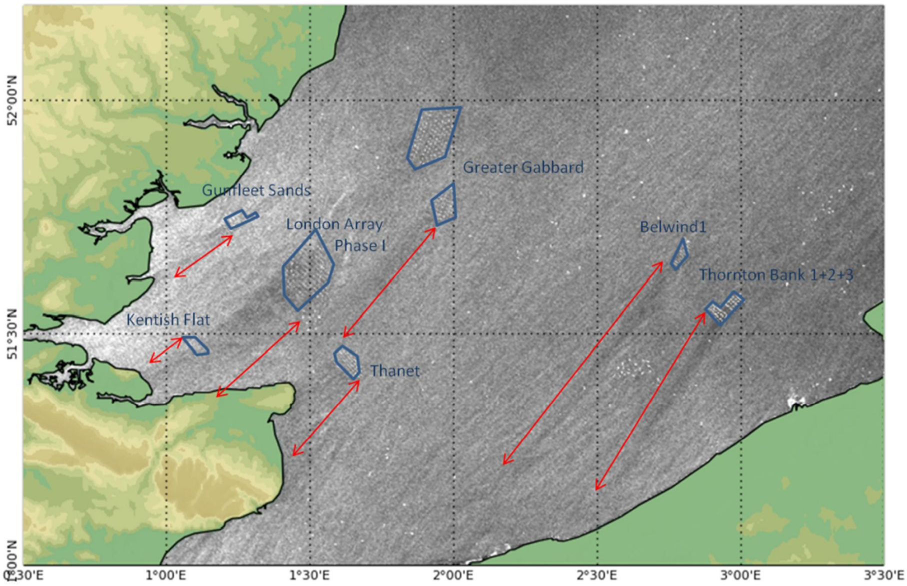

Figure 2.6: SAR image showing large-scale wakes at the southern North Sea. OWF areas are enclosed in blue polygons. Wakes (red arrows) are extending for tens of kilometers. Prevailing wind blows from northeast. Image from Hasager et al. (2015).

Numerical models have also found such phenomena, like the simulations of Platis et al. (2018) and LES results already presented in Figure 2.4. However, the currently available knowledge on these large-scale effects still originates from few and relatively small OWFs compared to future scenarios (see Figure 1.5 and Figure 1.6). A schematic description of the effect of one or multiple OWFs on wind is given in Figure 2.7.

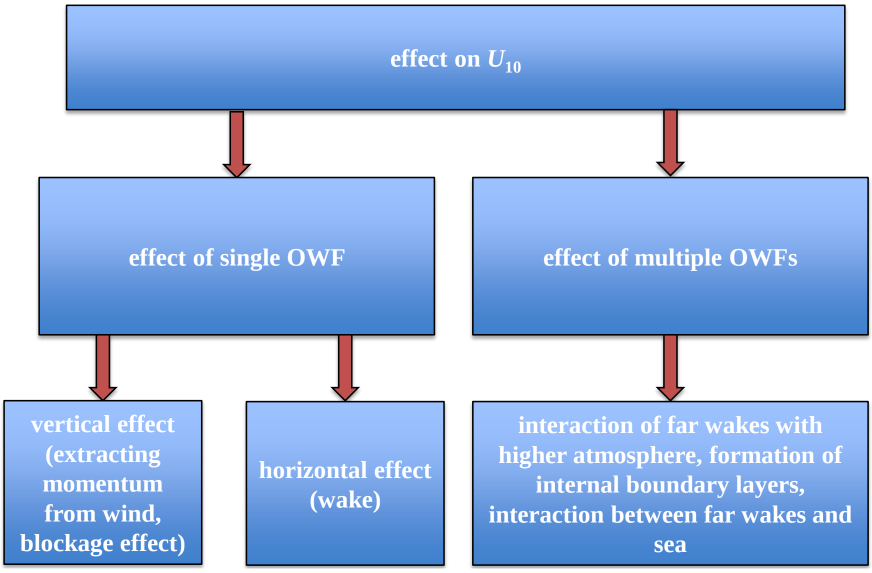

Figure 2.7: Overview of the effect of one or multiple OWFs on wind.

2.5. Effect on wave climate

An OWF can affect waves in two ways. The first one is blocking of wave energy by turbine monopiles, which serve as obstacles causing wave diffraction/refraction. The second one is an indirect effect; the modification of wind speed by OWFs, which affects wave generation and thus propagation to the shore. A third effect has also been reported by Christensen et al. (2013), which is the dissipation due to drag resistance. This results from the drag force exerted on waves as they hit the turbine monopiles. During this interaction eddies are generated and part of the incoming wave energy is transformed into turbulent kinetic energy. However, the authors proved that this effect is insignificant compared to the first two. An overview of the effect of OWFs on waves is given in Figure 2.8.

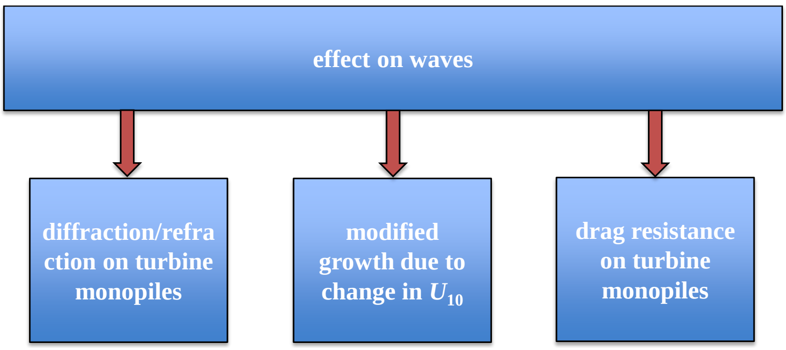

Figure 2.8: Overview of the effect of OWFs on waves.

Effect on significant wave height

Beiboer and Cooper (2002) investigated the effect of OWFs on wave height. They considered the presence of an OWF on two locations. In the first one, referred to as ”reasonable worst case scenario", the OWF was located around 1.5 km away from the coast, with an arrangement of 30 turbines in 3 rows of 10 and a turbine spacing of 300 m (resulting in an area of 1.6 km^2). This location accounted for the NF effect. In the second location, referred to as "typical scenario", the OWF was situated approximately 7 km away from the coast and consisted of 30 turbines in 3 rows of 10, with a separation of 700 m between rows and 400 m within each row (resulting in an area of 5 km^2). This location investigated the FF effect. The researchers used the wave-flow model MIKE21 and introduced the OWF on top of a sandbank on the original sea bed. They also used a 15 m nested grid to model the wind turbine monopiles. To account for the hydraulic resistance offered by the turbine support structures, they increased the bed roughness within the OWFs, and also altered the wave conditions locally by including source/sink terms. In their study they did not account for the effect of OWF on wind. For the "reasonably worst case scenario", they found a relative wave height change of 0.5% and 1.5%, corresponding to baseline values of 2.5 m and 1 m respectively (NF effect). For the "typical case scenario" the relative change was 0.1% and 0.3% for baseline values of 2.5 m and 1 m (FF effect). The authors concluded that the FF effect of an OWF is insignificant while very small influences are observed in the NF.

Alari and Raudsepp (2012) used the numerical model SWAN to investigate the effect of two OWFs on wave height. The OWFs were located in the Baltic Sea, at northwest of Estonia. The first one (wind farm 1) was situated WSW from the Kopu Peninsula and consisted of 55 turbines in parallel rows with a minimum spacing of 1000 m (resulting in an area of 37 km^2). The OWF was located 5 – 15 km away from the coast. The second one (wind farm 2) was located 13 – 20 km away from Hiiumaa island and consisted of 35 turbines (resulting in an area of 18 km^2). The researchers did not account for wind speed change but only diffraction/refraction of waves on turbine monopiles. Their model consisted of multiple nested grids, with the finer one having a size of 25 m. This was five times greater than the turbine diameter. Therefore, to account for the turbine monopiles they assumed a turbine diameter of 25 m and divided the computed wave height by 5, using the assumption of linear scaling. They found a change in wave height of 0.25% to 2% in the nearshore (FF effect). They reasoned that taking the effect of the OWF on wind into account would not further affect the wave height in the nearshore because the effect would be diminished by wave transformation processes.

Rodriguez Gandara and Harris (2012) studied the effect of a hypothetical OWF on waves by including both wind speed reduction, using the results of a wind wake model, as well as dissipation induced by turbines. The OWF in their study consisted of 432 turbines (in 24 rows of 18) and covered a region of 39 km × 17 km (resulting in an area of 663 km^2). It was situated 12 km away from the coast. The wake model predicted a maximum velocity deficit of 10% at a distance 5 km away from the downwind OWF boundary. The dissipation coefficient was derived using a wave agitation model on a subsection of the OWF. The simulation of the whole OWF with the latter model was computationally impossible. The results indicated that wave blockage is more severe than wind wake effects. The relative change in wave height considering the combined effect was 8.5% in the NF and approximately 6.7% in the FF.

In contrast with the previous study Christensen et al. (2013) found that wake effects are more dominant in changing the wave height. The authors used MIKE21 to study the effect of Denmark's Horns Rev 1 OWF on waves. They implemented a simple VD formulation based on measurements by Christiansen and Hasager (2005) which led to a maximum 10-m wind speed decrease of 10%. The OWF was considered a continuum, meaning the reduced wind speed was evenly distributed within the WFA. The study showed that for moderate wind speed (equal to 10 m/s) the wave height in the NF is reduced by 1/3 due to reflection/diffraction and by 2/3 due to wind speed change. The total reduction amounted to 5%. In the FF the reduced wind speed contributed almost entirely to the wave height change and the reduction was around 1%. It is further stressed by the authors that the results can be dependent on the OWF size.

2.6. Effect on coastal morphology

There is hardly any study that investigates the effect of OWFs on coastal morphology. To our knowledge only Christensen et al. (2014) have addressed this subject. They applied the results of their previous study (Christensen et al., 2013) to a so-called one-line coastline model to investigate the impact of an OWF on the shoreline development for a 100-year period. They considered a typical OWF size of 5 km $\times$ 5 km (25 km^2) and investigated the effect on the coast for three different OWF locations, situated 5 km, 10 km and 20 km away from the coast (Figure 2.9). They observed sediment accumulation on the lee side of the OWF leading to the formation of a salient, in a manner similar to a shore-parallel breakwater. The effect was more prominent for the OWF closer to the coast where a maximum shoreline advance of 50 m (30 m for the OWF 10 km offshore; 10 m for the OWF 20 km offshore) and a maximum retreat of 10 m (8 m for the OWF 10 km offshore; 4 m for the OWF 20 km offshore) were observed within the 100-year period.

2.7. Discussion

From the work that has already been carried out, it is obvious that the effect of OWFs on wind and waves has not been studied in great detail. Regarding the effect on wind, current models are taking into account the effect of a single OWF by including only few of its parameters. In addition, these models require thorough validation with high resolution, large-scale spatial measurements of 10-m wind speed. This has only become possible in recent years with advanced remote sensing techniques, such as SAR measurements.

All studies agree on the fact that atmospheric stability influences the Wake Length. It is also mentioned that the orientation of the turbine arrays with respect to wind can further modify the Wake Length without however explaining the underlying mechanism. As for Velocity Deficit, it does not seem to be dependent on one specific factor. It seems reasonable to say that there are many parameters that could play a role in wind speed change, such as the number of wind

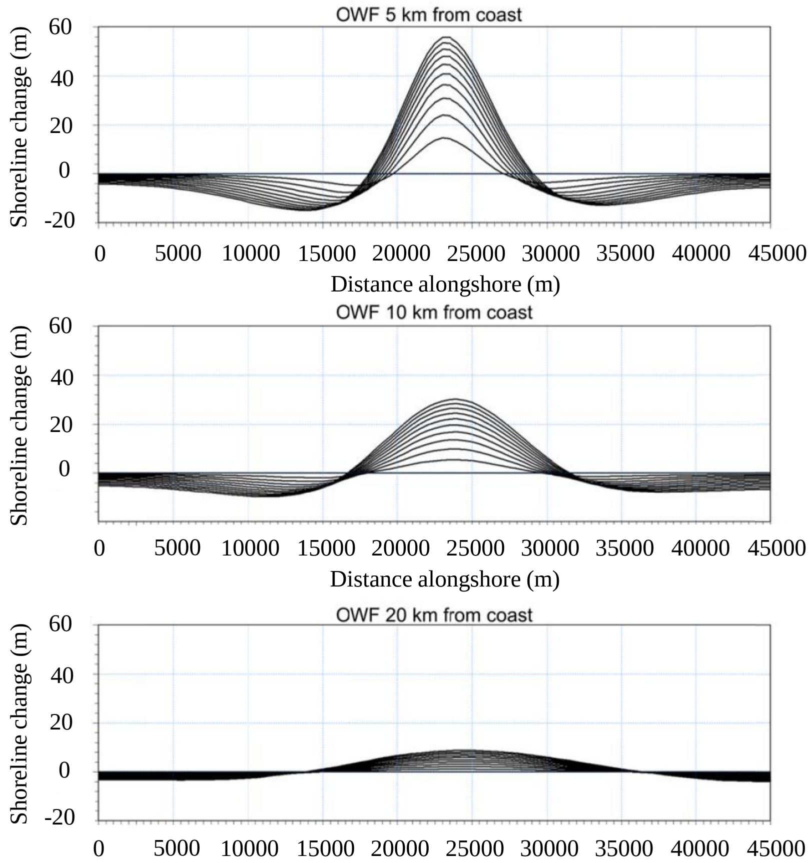

Figure 2.9: Coastline change resulting from a single OWF for a period of 100 years (Christensen et al., 2014).

turbines in operation, the wind turbine characteristics (height, blade size etc.), the OWF area as well as the wind speed magnitude itself. However, no study has been found that takes into account such factors when large-scale effects are investigated. It is also important to note that none of the above studies found an increase in 10-m wind speed close to sea surface. This is in contrast with LES results shown in Figure 2.4. A possible explanation could be that the above studies did not account for the temporal variation of wind speed, because this is computed from a single satellite image (a snapshot in time). Furthermore, in the analysis of satellite images the 10-m wind speed is averaged spatially, to remove noise (see Appendix A for more information). Therefore, a possible increase in wind speed could be either non-existent or averaged out. In contrast, results from LES are obtained by just averaging wind speed in time. Since no spatial averaging occurs, locations of predominantly wind speed increase still show an increase when averaged in time. Even in the LES of Figure 2.4 though, an increase in wind speed is never observed within the WFA of WA, but in between OWFs. Therefore, it is possible that an increase in 10-m wind speed hardly happens inside or downwind of an OWF. This of course needs further investigation.

It is also noted that contradicting views exist regarding the factor contributing most to wave height change in the presence of an OWF. Rodriguez Gandara and Harris (2012) conclude that it is the dissipation due to turbine monopiles whereas Christensen et al. (2013) argue that the modified wind field is more dominant. Rodriguez Gandara and Harris (2012) considered a much bigger OWF compared to Christensen et al. (2013). Such a size is comparable to IJmuiden Ver OWF (see Figure 1.3). Therefore, it could be the OWF size that determines the most dominant factor. Nevertheless, this should be supported by more studies in the future. The scope of this thesis is not to explore such an investigation but to use the current knowledge available. In any case though it is obvious that a large-scale OWF as the one modeled by Rodriguez Gandara and Harris (2012) has a much greater effect on wave height.

The following tables summarize the information on the effect of OWFs on wind, waves and coastal morphology, as discussed in this chapter.

Table 2.1: Effect of OWFs on wind for various atmospheric states. VD = maximum Velocity Deficit, WL = Wake Length.

Study	**OWF area (km^2)**	**Atmospheric state**		
		stable	**neutral**	**unstable**
Christiansen and Hasager (2005)	19.5	–	VD = 8% WL = 20 km	VD = 8% WL = 5 km
Li and Lehner (2013)	4	VD = 23.2% WL = 18 km	VD = 24.4% WL = 14 km	–
Platis et al. (2018)	–	VD = 40% WL = 10 – 70 km	WL = 10 – 25 km	WL = 0 – 10 km

Table 2.2: Effect of OWFs on waves. The table indicates the relative wave height change together with the baseline value, as well as the processes that were included in each study.

Study	OWF area (km^2)	Distance from coast (km)	Near-field	Far-field	Processes
Beiboer and Cooper (2002)	1.6 (NF) ; 5 (FF)	1.5 (NF) ; 7 (FF)	0.5% (2.5 m) ; 1.5% (1 m)	0.1% (2.5 m) ; 0.3% (1 m)	drag resistance, diffraction/re-fraction
Alari and Raudsepp (2012)	37 ; 18	5 – 15 ; 13 – 20	–	0.25 ; 2%	diffraction,refraction
Rodriguez Gandara and Harris (2012)	663	12	8.5% (1.24 m)	6.7% (1.05 m)	drag resistance, diffraction/re-fraction, wind speed change
Christensen et al. (2013)	19.5	14 – 20	5%	1%	diffraction,refraction, wind speed change

Table 2.3: Effect of OWFs on coastline morphology. The table indicates the maximum coastline accretion (A) and erosion (E) within a 100-year period.

Study	Distance from coast		
	5 km	10 km	20 km
Christensen et al. (2014)	A = 50 m, E = 10 m	A = 30 m, E = 8 m	A = 10 m, E = 4 m

3

Approach

The following chapter presents the approach followed in this work. First a study area is determined covering the whole North Sea. Out of many years of wind speed data, a representative one is chosen to describe the long-term wind climate in the North Sea and to force wave computations. Information on the area and location of existing and future OWFs is retrieved from an available database. Within the OWF areas a constant wind speed decrease of 20% is assumed, based on literature review. The original spatial resolution of the wind input grid is too coarse to properly resolve the OWF areas, therefore its mesh size is reduced by a factor of 6. To account for the increase in number of OWFs with time, a timeframe is determined, leading to four development stages (2018, 2023, 2030, 2050 and 2050A as an alternative). In addition, an island option is considered, based on the vision for creating an artificial energy island in the North Sea. Each development stage and each island option accounts for a 1-year simulation in SWAN, using the wind input from the representative year. The output at the -9 m NAP contour is forced into Unibest-CL+ to compute the coastal morphology for a 32-year period, starting in 2018 and ending in 2050.

3.1. Study area

To study the effect of large-scale OWF developments three domains of interest are considered. To better capture the occurring processes in the nearshore the domain resolution increases in the direction to the Netherlands. The domains of interest are depicted in Figure 3.1. The largest domain includes the whole North Sea and part of the North Atlantic Ocean and extends to the edges of the continental shelf. This is the computational domain of the SWAN Dutch Continental Shelf Model (SWAN-DCSM). Within SWAN-DCSM a medium-scale domain is defined where OWF developments will take place in between 2018 – 2050. This is the wind input grid that takes into account a 20% wind speed decrease within the OWF areas. To study the effect of OWFs on the Dutch wave climate and coastal response a smaller domain is defined close to the Netherlands. This is the computational domain of SWAN Holland Coast Wadden Sea model (SWAN-HCWD)[1]. In SWAN-HCWD the -9 m NAP contour (depicted with red color) defines the nearshore margin.

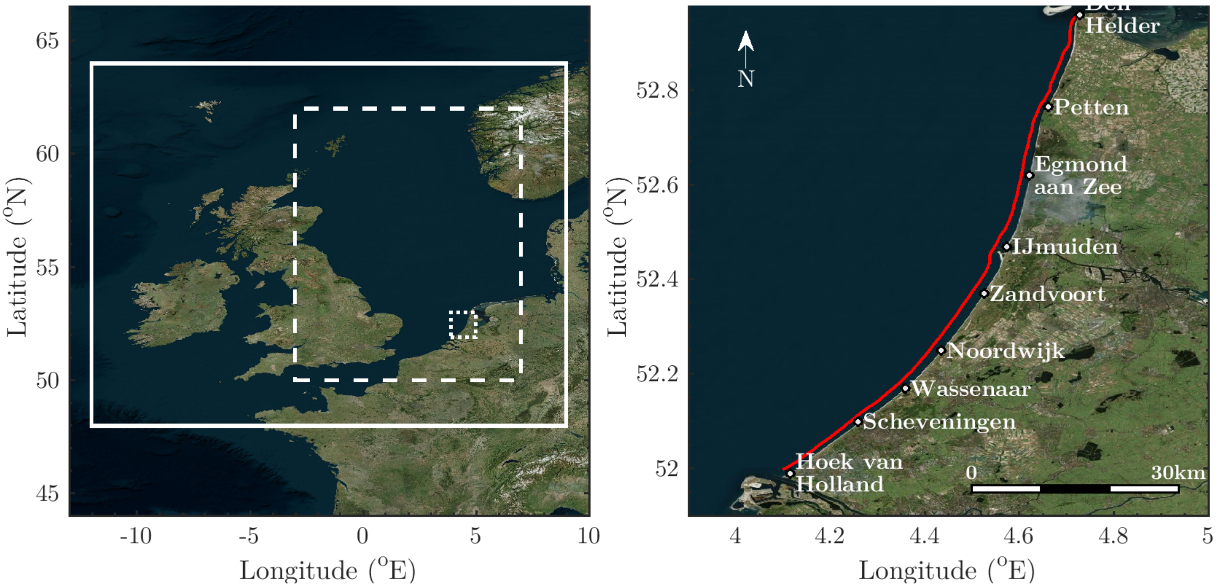

Figure 3.1: Left panel: Domain of interest for wave modeling (solid line), OWF developments (dashed line) and effect of OWFs on the nearshore wave climate and coastline response of the Dutch coast (dotted line). Right panel: zoomed view of the smaller domain of interest (SWAN-HCWD). The -9 m NAP contour is depicted with red color.

3.2. Representative year for wave modeling

Wave modeling requires an accurate representation of forcing conditions. These can be wind over the computational domain and (if needed) waves at the boundaries. In this study wave boundary conditions are provided at the edges of SWAN-DCSM while time and spatially varying 10-m wind is forced over the entire computational domain. The metocean data is obtained from the ERA5 climate reanalysis dataset (ECMWF, 2018). ERA5 is being developed by the Copernicus Climate

[1] More information on SWAN-DCSM and SWAN-HCWD is given in Chapter 4.

Change Service (C3S) and data processing is carried out by the European Center for Medium-Range Weather Forecasts (ECMWF). The entire ERA5 dataset covers the period from 2000 to present and provides information on atmospheric, land-surface and sea-state parameters with a temporal resolution of 1 hour and a spatial resolution of approximately 31 km ($\approx 0.3°$).

For the scope of this study an 8-year hindcast of 10-m wind speed (U_{10}), significant wave height (H_{m0}), peak wave period (T_p) and (one-sided) wave spectral directional width (σ_θ) is retrieved, covering period 2010 – 2017. The aim is to obtain a dataset large enough to properly describe the long term wind and wave climate in the North Sea. However, only one year is used for modeling due to time limitation and restrictions regarding the size of output data. The most representative year for describing period 2010 – 2017 is 2016 which is chosen for wave modeling. The selection is made on basis of U_{10}, the parameter that mostly affects wave generation in the open sea.

To determine the representative year three characteristic locations are defined: a *nearshore location* close to the Dutch coast, an *offshore location* in the middle of the North Sea and a *storm location* at the northern edge of the North Sea. These locations are considered satisfactory for describing the wind climate at the entire North Sea, since they contain information all the way from wave generation (*storm location*) to propagation (*offshore location*) and transformation in the nearshore (*nearshore location*). The 10-m wind speed statistics at these locations are depicted with wind roses for every individual year as well as for the full 2010 – 2017 period (see Section B.1). Figure 3.2 shows wind roses of the full period and the representative year for wave modeling. The resemblance is very satisfactory.

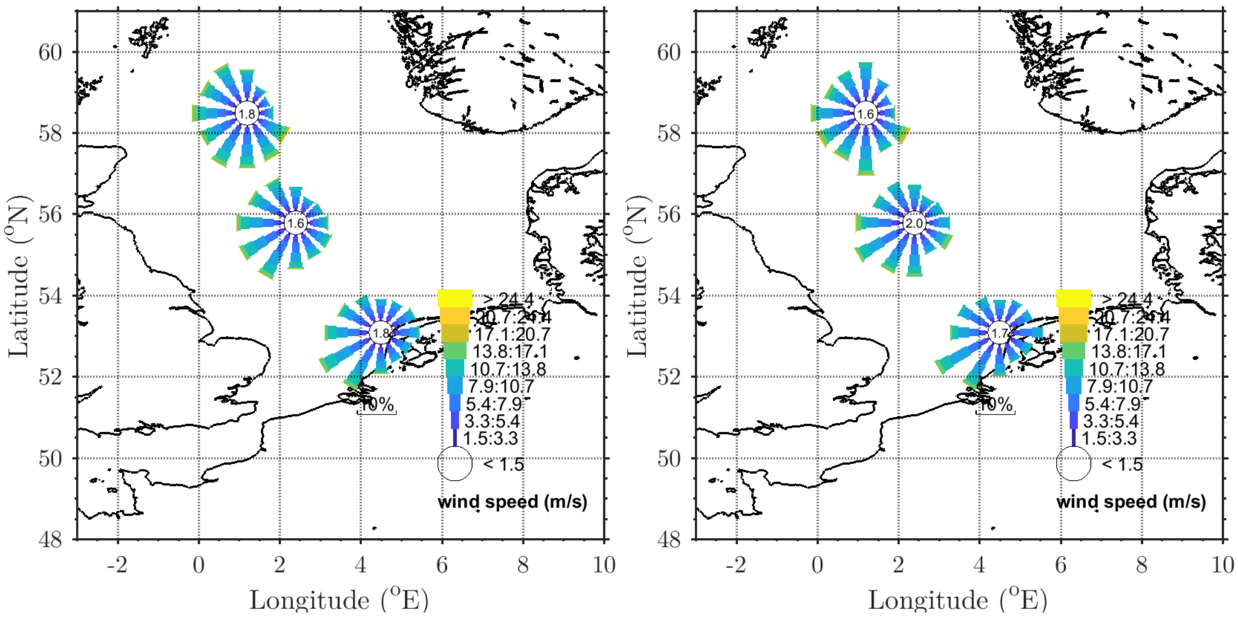

Figure 3.2: Wind roses of period 2010 – 2017 (left) and representative year 2016 (right) based on 10-m wind speed from the ERA5 dataset.

3.3. OWF development stages

The increase of OWFs with time is introduced with *development stages*. These are defined as significant years of OWF construction in the North Sea. This study considers *development stages* 2018, 2023, 2030 and 2050. The OWFs of each development stage are shown in Figure 3.3.

The choice of development stages is based on years most taken into account in OFWEC projections and national energy plans. As discussed in Section 1.1, it is common for studies to make projections for 2020 and 2030 (see Table 1.2). Here 2023 is considered over 2020 to comply with the Dutch Energy plan for OWF development (Noordzeeloket, 2018). The majority of planned OWFs will be realized by 2030. This would enable the construction of an energy island close to IJmuiden Ver (a pilot project towards realizing a bigger energy island in the North Sea). Year 2050 could not have been left out since it is the deadline for fulfilling the Paris climate agreement. It should be stressed that OWF developments in 2050 are not based on any specific source as no database contains projections so far in the future. The assumed OWFs is just a speculation, based on visions presented in Figure 1.5 and Figure 1.6. For that reason two scenarios of OWF developments in year 2050 are considered by changing the location of OWFs while retaining their total area.

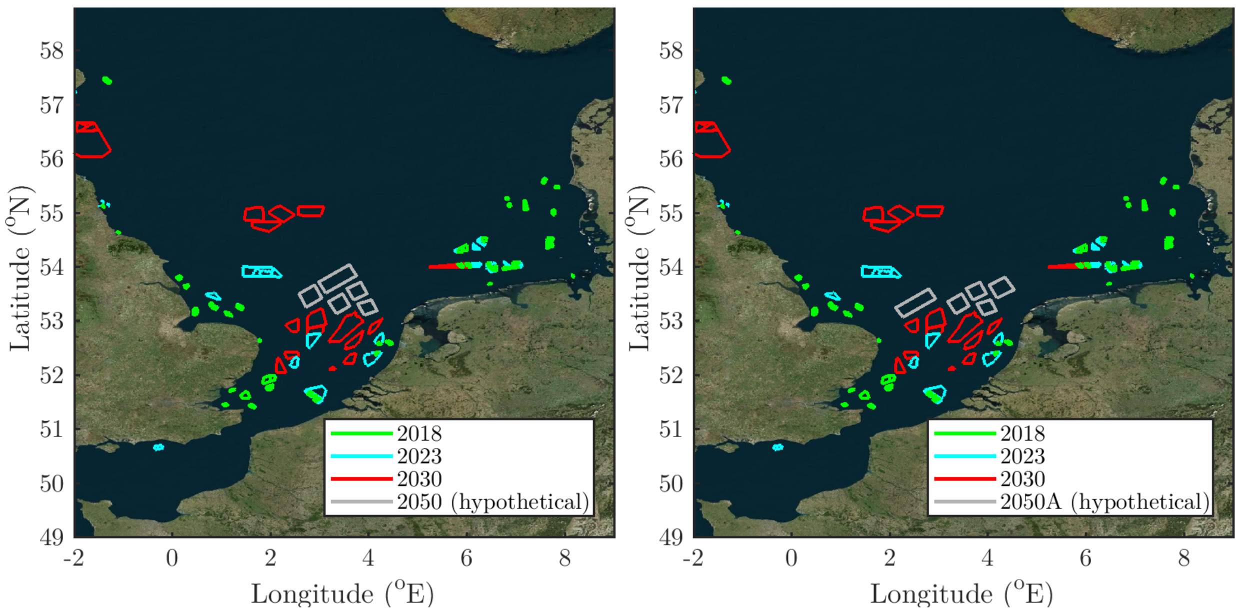

Figure 3.3: OWF areas in the North Sea categorized in development stages.

As seen in Figure 3.3, there is a clear relation between development stages and OWF size and distance from the Dutch coast. Therefore, it is possible to categorize OWFs into zones based on size and distance. This is done by looking at the details of existing and future Dutch OWF developments, shown in Table 3.1. Note that the OWF size is directly computed as the polygon area provided by the database, while the distance is measured from the center of gravity of the polygon to the nearest point at the Dutch coast. In addition, OWFs further away from the Dutch coast (bounded by Hoek van Holland and Den Helder) such as Borssele have been excluded from the table.

Table 3.1: Details of existing and future Dutch OWF developments.

OWF name[1]	Area (km^2)	Location with respect to Dutch coast	Offshore distance (km)
		2018	
PAWP	17	IJmuiden	25
LUD	16	Noordwijk	23
OWEZ	27	Egmond aan Zee	13
		2023	
HKZ	370	The Hague region	25
HKN	175	IJmuiden region	25
		2030	
IJmuiden Ver	1170	IJmuiden region	80
HKW	350	Zandvoort	60
HKNW	190	Petten	40
HKZW	230	Scheveningen	45

[1] PAWP = Princess Amalia Wind Park, LUD = Luchterduinen, OWEZ = OWF Egmond aan Zee, HK = Hollandse Kust: Z = Zuid, N = Noord, NW = Noordwest, ZW = Zuidwest.

Using the information from Table 3.1, an average OWF size as well as a range of distance from the Dutch coast is assigned to each development stage. This is shown in Table 3.2. OWFs in 2018 are located around 13 – 25 km offshore with an average size of 20 m^2, while OWFs developed in 2023, 2030, and 2050 are situated approximately 25 km, 40 – 80 km, and 80 – 100 km away from the Dutch coast with an average size of 270 m^2, 485 m^2 and 740 m^2, respectively. For the hypothetical development stage 2050/2050A the above values are directly computed based on the assumed areas.

Table 3.2: OWF development stages and assigned size and distance from the Dutch coast.

Year	Average OWF size (km^2)	Offshore distance (km)
2018	20	13 – 25
2023	270	25
2030	485	40 – 80
2050, 2050A	740	80 – 100

To introduce the OWFs in the ERA5 10-m wind grid information regarding their area and location is needed. This is obtained from the European Marine Observation and Data Network (EMODnet, 2018). The geographical distribution of the OWFs in the database was already presented in Figure 1.3. It should be noted however that EMODnet does not show the end date of each OWF construction but it rather indicates the development progress. This is reasonable since the time horizon of OWF developments extends far into the future which makes planning quite uncertain. Defining scenarios simplifies this uncertainty. Every intermediate OWF construction is assumed to be realized at the end of each *development stage*. In this way all the OWFs are taken into account just not at the specific moment of their construction. Such level of detail in OWF increase with time is considered satisfactory for the scope of this thesis.

3.4. Velocity deficit schematization

As discussed in Section 2.2 OWFs affect wind by changing the 10-m wind speed therefore causing a Velocity Deficit. Analyses of SAR images indicated maximum VDs of 8% – 40% (Table 2.1). These maxima are located close to the downwind edge of the Wind Farm Area while VD progressively approaches zero while reaching the verge of the Wake Area (see Figure 2.5). In this thesis, a simpler schematization is used for expressing VD. The WA is omitted and a constant VD is assumed within the WFA. Based on the range of observed VDs, a mean value of 20% is considered. Figure 3.4 compares the schematized VD with the one measured in Christiansen and Hasager (2005).

One can say that the proposed ”no-Wake Area” schematization underestimates the effect of OWFs on wind. As seen in Section 2.2 the Wake Length can extend for tens of kilometers, meaning it could reach close to the coast and thus significantly affect the nearshore wave climate. However, no information is known on the persistence of a wake in time and therefore an assumption of an infinitely fixed wake downwind of an OWF could result in overestimating the effect on wave climate. In addition, it should be reminded that the range of observed VDs in literature refers to maximum values. This study uses an average of these values. Therefore it is assumed that the absence of wakes is well counteracted by assuming a more intense effect within the WFA, taken as an average of maximum observed VDs.

3.5. Wind grid refinement

For OWF areas to be properly resolved within the wind grid, their dimensions must be bigger than the resolution of the grid itself. As discussed above, the spatial resolution of ERA5 is 31 km ($\approx 0.3°$), much greater than most OWF dimensions. This requires the grid to be refined. After testing many grid sizes, the optimal[2] resolution is 5 km ($\approx 0.05°$). Figure 3.5 shows the OWF areas resolved in the original and the refined ERA5 grid respectively. An overview of the tested grid sizes is presented in Appendix B.

3.6. Energy island

As explained in Section 1.1 there is a vision of creating an artificial energy island for storing and redistributing offshore wind energy. The construction of such an island is expected to take place at an offshore location in the North Sea while its size is suggested to be around 6 km^2. A candidate

[2] It is obvious that the smaller the grid size, the better the OWF area resolution. At the same time though, the computational time for generating the ”modified” wind grid increases. The optimal grid size requires the less computational time possible while resolving the OWF areas satisfactorily.

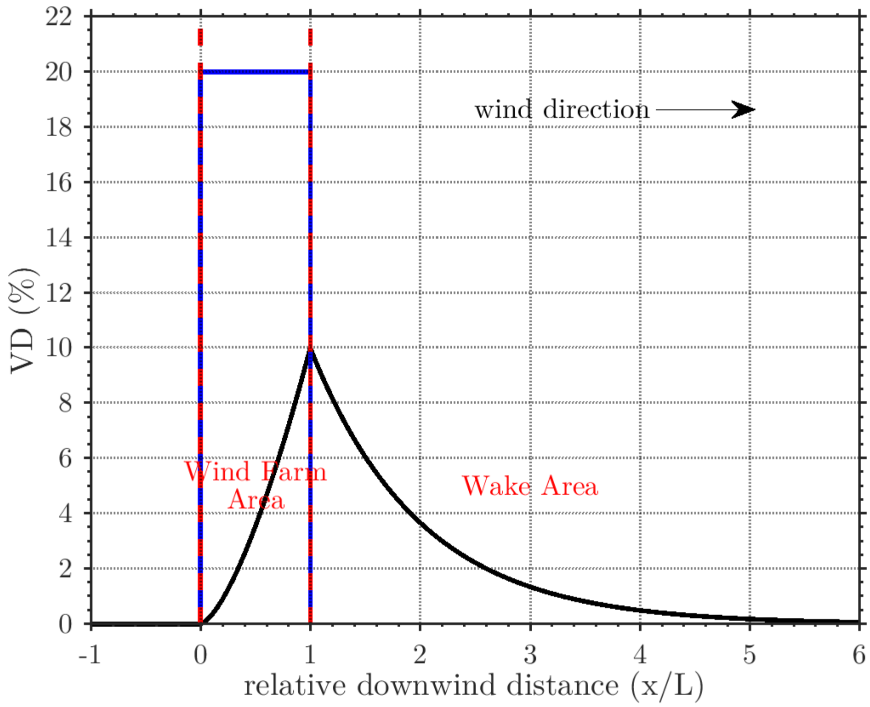

Figure 3.4: Schematized Velocity Deficit (blue line) versus measured Velocity Deficit (black line, after Christiansen and Hasager (2005)) along an OWF. The dashed red lines indicate the Wind Farm Area.

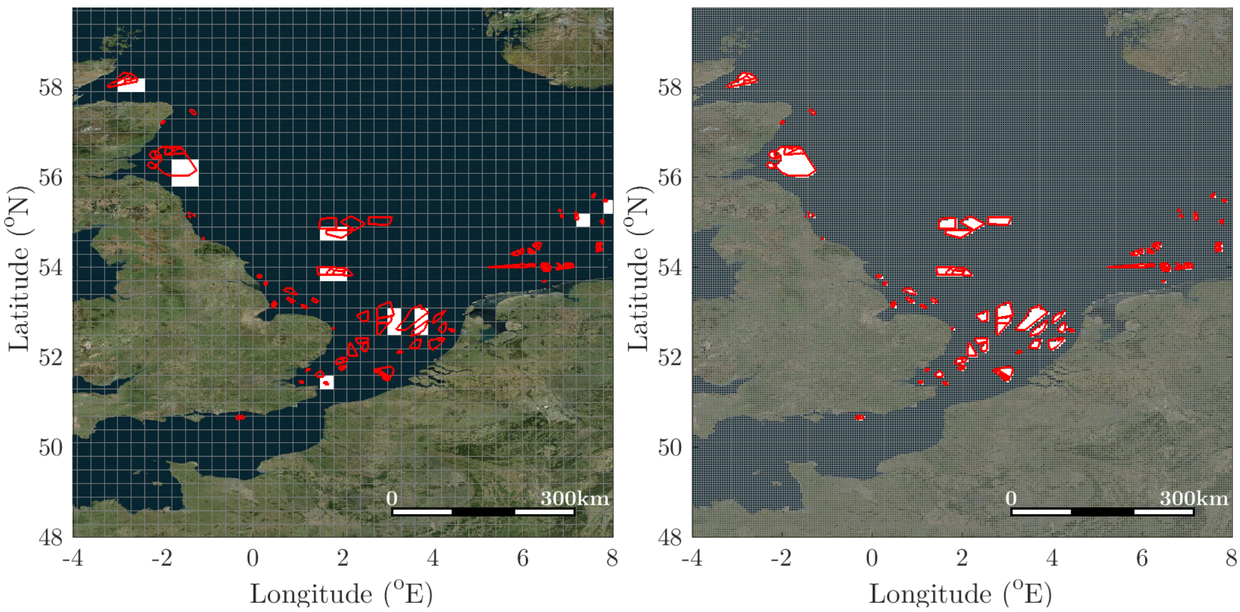

(a) ΔX = 31 km ($\approx 0.3°$)

(b) ΔX = 5 km ($\approx 0.05°$)

Figure 3.5: OWF areas resolved in (a) original and (b) refined ERA5 wind grid. The OWFs are shown with red polygons. The resolved areas are depicted with white color and the grid lines are illustrated with gray color.

site is Dogger bank which is extremely shallow, while strong winds blow in the nearby area. To explore the potential for constructing such an island a pilot project has been put into discussion considering an energy island at IJmuiden Ver OWF. Regarding its size this is expected to be smaller compared to its successor.

Since an energy island is expected to influence the nearshore wave climate of the Netherlands, it is included in simulations together with future OWFs. More specifically an island of 5 km^2 is assumed southwest of Hollandse Kust Noord Holland (*Island 4*). The resolution of the computational domain did not allow for modeling an island of such a small size further offshore (close to IJmuiden Ver or near Dogger Bank).

At the first stages of this study though, three island scenarios had been considered: one southwest of Hollandse Kust Noord Holland (*Island 1*), one northeast of IJmuiden Ver (*Island 2*) and one northwest of IJmuinen Ver (*Island 3*). However, these islands have a size of 20 km^2 which is considered unrealistic in the context of OWF developments. Therefore, the effect of these islands on the nearshore wave climate of the Netherlands is separately investigated in Appendix C since it could be of interest in other applications. The locations of the island scenarios are depicted in Figure 3.6. It should be noted that the selected island sizes are the smallest possible given the resolution of the chosen computational domains. This will become more clear in Chapter 4 where the modeling procedure is discussed.

Following the same reasoning with OWF development stages, the distance of each island scenario from the coast is determined, using IJmuiden as a reference location. *Island 3* is located 95 km away from the Dutch coast, *Island 2* lies 70 km offshore, while *Island 1* and *Island 4* are located 33 km away from the Dutch coast. Table 3.3 gives further details.

Table 3.3: Specifications of energy island scenarios.

Island ID	**Area (km^2)**	**Location**	**Depth (m)**	**Distance from IJmuiden (km)**
1	20	4.12 °N, 52.58 °E	22	33
2	20	3.67 °N, 52.78 °E	30	70
3	20	3.38 °N, 52.92 °E	30	95
4	5	4.12 °N, 52.58 °E	22	33

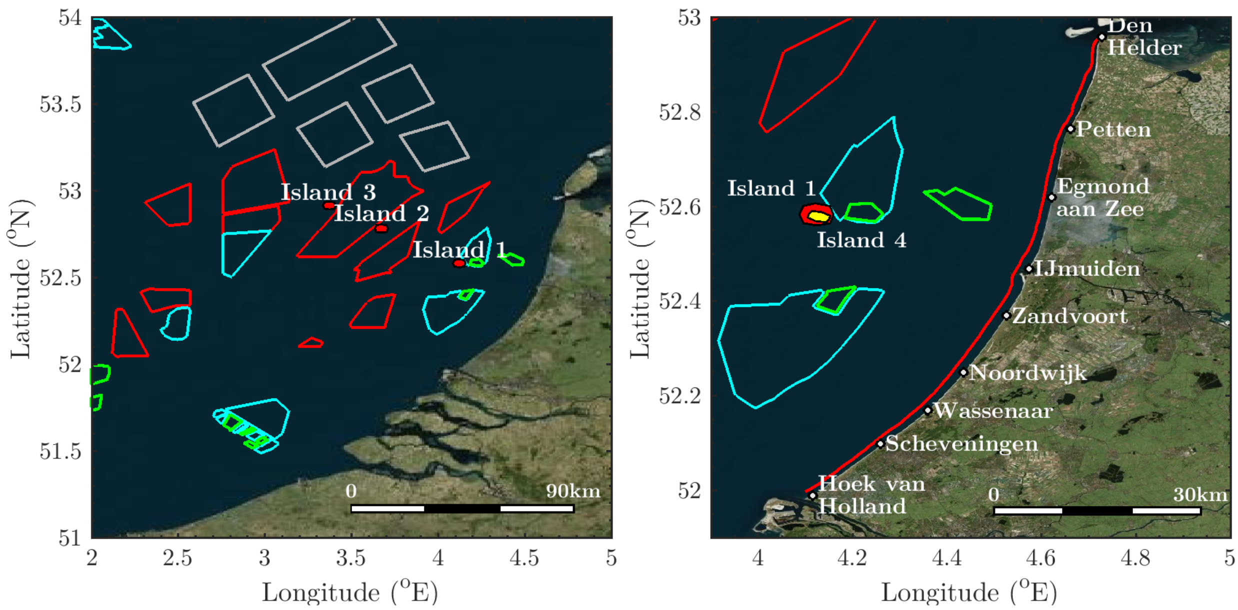

Figure 3.6: Energy island scenarios in the southern North Sea. Left image: islands with an area of 20 km^2 (indicated with red color). Right image: island of 20 km^2 (red) vs island of 5 km^2 island (yellow) both located 33 km away from the Dutch coast.

3.7. Modeling approach

This section gives an overview of the modeling approach. This is illustrated in Figure 3.7. The modeling consists of wave and coastline simulations. Detailed information on the set-up of each model is presented in Chapter 4.

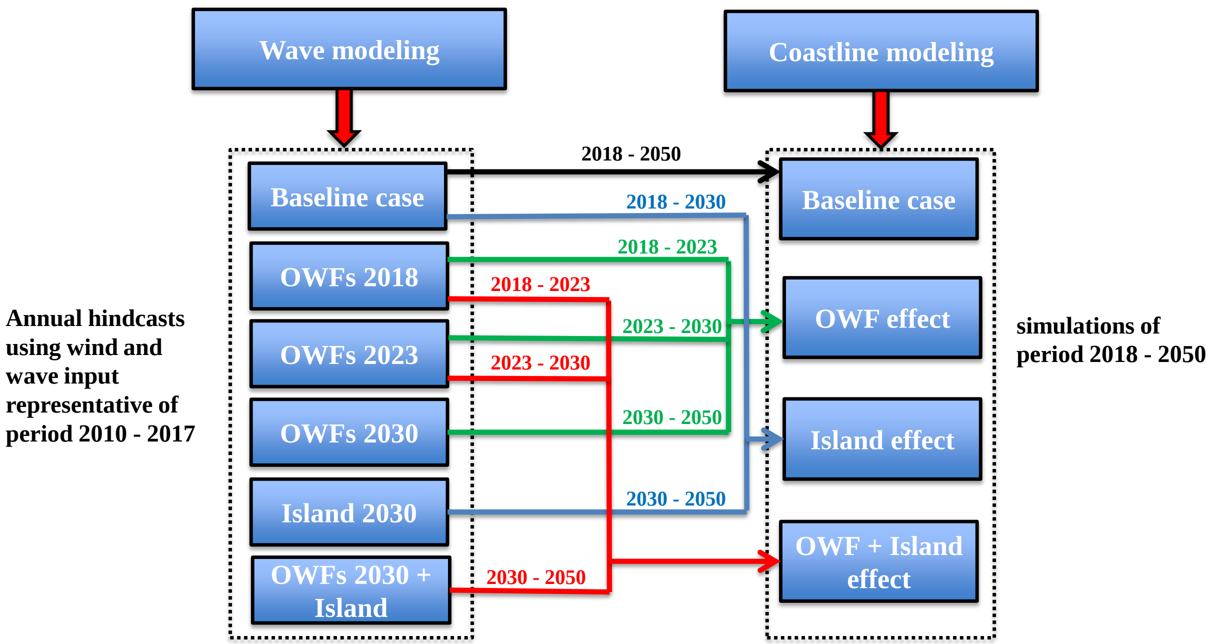

Figure 3.7: Overview of modeling approach.

Wave modeling is carried out by performing hindcasts using the same representative year. The hindcasts account separately for the baseline case (no OWFs) as well as development stages 2018, 2023, 2030, 2050/2050A and an island with and without OWFs in 2030 and 2050. Figure 3.7 does not indicate the hindcasts of development stages 2050 and 2050A for simplicity.

Coastline modeling is carried out for period 2018 – 2050. The resulting output of wave modeling, consisting of 1-year of data, is used as boundary condition in coastline modeling forcing the model at each time step (1 year) of the simulation.

Four coastline simulations are carried out. In the first one, accounting for the baseline case, the coastline model receives boundary conditions from the wave output of the baseline case (black line in Figure 3.7). The second simulation accounts for OWFs in period 2018 – 2050. Sub-period 2018 – 2023 gets boundary conditions from the wave output of 2018 and the same reasoning applies for the other sub-periods (2023 – 2030 is forced with the 2023 wave output, and period 2030 – 2050 with the 2030 wave output, see green lines in Figure 3.7). The third simulation considers the island alone. Period 2018 – 2030 is forced with the wave output of the baseline case (the island is assumed to be realized in 2030) while period 2030 – 2050 is forced with the wave output accounting for the island presence (blue lines in Figure 3.7). The last simulation considers OWFs together with an island. The boundary conditions for period 2018 – 2030 originate from the wave output accounting for OWFs (boundary conditions provided with the reasoning as explained above) while period 2030 – 2050 receives boundary conditions from the wave output accounting for the combined effect of OWFs and an island (red lines in Figure 3.7).

4

Wave and coastline modeling

This chapter discusses the modeling procedure. Wave computations are carried out using the numerical model SWAN. Two domains are considered, each one having its own bathymetry. The coarser one spreads across the entire North Sea and is used to compute boundary conditions for a finer domain that covers the region near the Dutch coast. Currents and water level fluctuations are excluded from computations for simplicity. Coastline modeling is performed with numerical model Unibest-CL+. The output from wave modeling at the -9 m NAP contour is provided as boundary condition in the coastline model, schematized into 40 wave height classes and 36 directional sectors. The initial coastline position of the Dutch coast as well as the cross-shore bathymetry are derived from the JARKUS database.

4.1. SWAN wave modeling

Wave modeling is carried out with SWAN, a numerical model developed at Delft University of Technology that is used worldwide to estimate wave parameters in coastal applications (Holthuijsen et al., 1993; Ris, Holthuijsen, & Booij, 1994; SWAN team, 2018b). The SWAN version used is 41.20A, parallelized with OpenMP and run at a Linux 64-bit platform. The wave model consists of a coarse grid for computing boundary conditions and a finer one for predicting the wave climate in the nearshore. Both grids are set-up in spherical coordinates. The coarse grid originates from the SWAN-Dutch Continental Shelf Model (DCSM). This is part of the SWAN-North Sea model that runs operationally within FEWS-North Sea (Gautier & Caires, 2015). In this study the latest release of SWAN-DCSM is used, which is version j15-v1. The finer grid is similar to SWAN-Kustrook, a Deltares model operated for Rijkswaterstaat. However, in this study the finer grid does not extend as far to the offshore as SWAN-Kustrook. The model runs internally at Deltares and henceforth will be called SWAN-HCWD (Holland Coast Wadden Sea Model).

Computational grids

The SWAN-DCSM and SWAN-HCWD grids are presented in Figure 4.1. The computational grid of SWAN-DCSM is rectangular with a resolution of 1/20° × 1/30° (≈ 3.6 km × 3.6 km)[1].

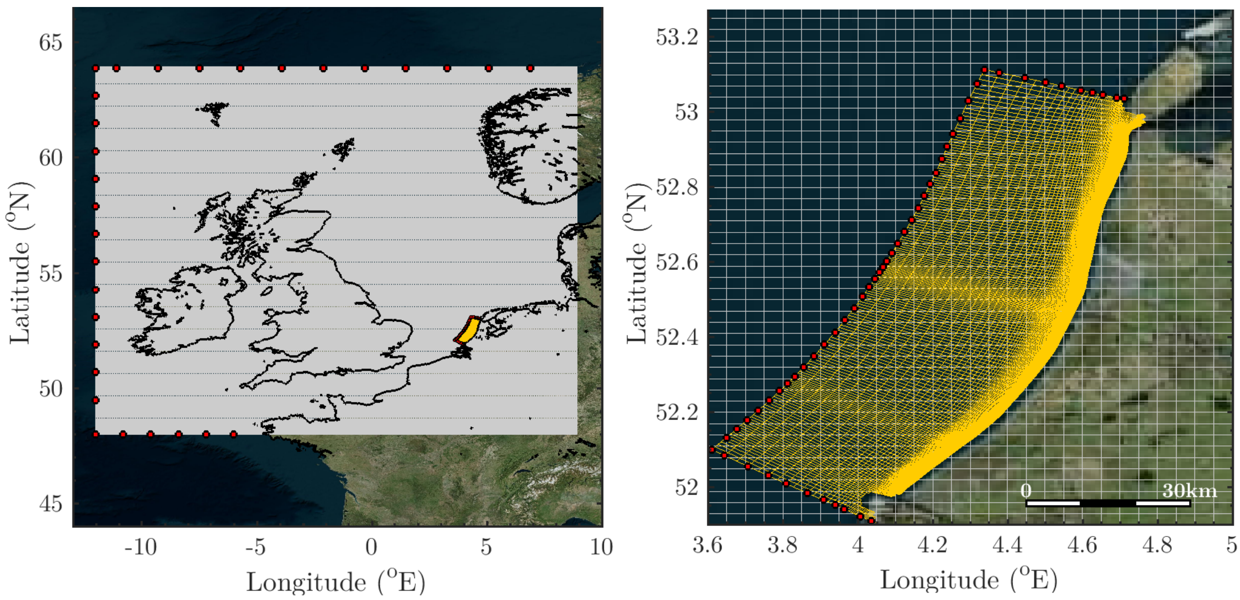

Figure 4.1: SWAN-DCSM and SWAN-HCWD computational grids (in gray and yellow color respectively). Left image: far-field view. Right image: zoomed view of SWAN-HCWD. Boundary/nesting points in both grids are depicted with red dots.

SWAN-DCSM is used to provide boundary conditions for the nested grid SWAN-HCWD. The latter is used in shallower areas near the Dutch coast where higher resolution is required to

[1] Note that the coordinate system is spherical. This means that the mesh size in the longitudinal coordinate is not constant when expressed in meters. Here the maximum mesh size is presented.

properly represent the spatial bathymetric variation. The SWAN-HCWD grid is curvilinear with a resolution varying from 40 m in the nearshore to 3 km in the offshore.

To save computational time, part of the original SWAN-HCWD grid is removed. This is the region west of Maasvlakte and north of the Mardiep inlet, in the Wadden Sea. The removed regions are not expected to influence the nearshore wave climate of the Dutch coast. It is known that the Dutch coast is predominantly affected by the nearshore wave climate in the coastal stretch between the Marsdiep tidal inlet in the North and the long jetty near Hoek van Holland in the South.

The directional domain of both grids is the full circle and is divided into 45 bins of 8° each. The frequency range is 0.03 Hz – 0.6 Hz (1.7 – 33.3 s). This is divided by SWAN into 31 bins with a resolution proportional to the frequency itself (defined as $\Delta f = 0.1f$). Detailed characteristics of the two grids are presented in Table 4.3, located in Section 4.3.

Bathymetry

The SWAN-DCSM grid uses the same bathymetry as in the operational SWAN-North Sea model (Gautier & Caires, 2015). To save computational time the bathymetry at some areas expected to be irrelevant for waves is removed. These areas are the Irish Sea and some Norwegian fjords. The bathymetry of SWAN-HCWD is based on bathymetry datasets of the Dutch coast for 2004 (supplemented with 2003 data). Even though this source is somewhat outdated this is not expected to affect the final result since the aim is not to perform a forecast in the future but to assess the potential impact of OWFs on the Dutch coast. The bathymetries of SWAN-DCSM and SWAN-HCWD are depicted in Figure 4.2.

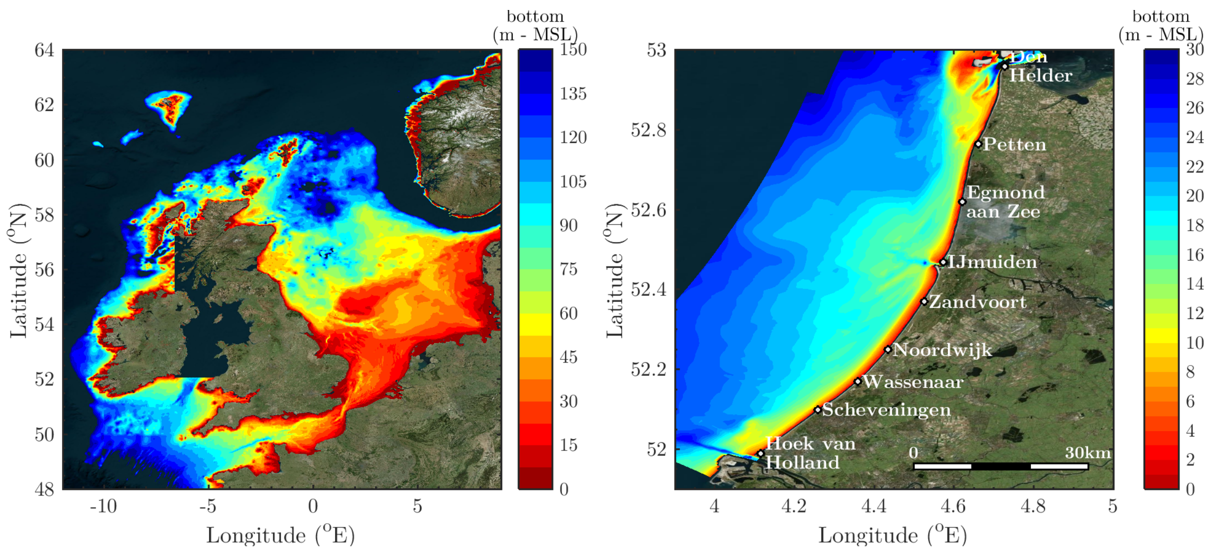

Figure 4.2: SWAN-DCSM and SWAN-HCWD bathymetries.

SWAN-DCSM does not resolve the wave height satisfactory close to the coast. There are two reasons for this. The first one is the low spatial resolution of the computational grid (0.03° ≈ 3.3 km) and the second one is that there is too much offset between the SWAN-DCSM bathymetry and the real bathymetry close to the Dutch coast. These reasons led to nest the finer resolution SWAN-HCWD into SWAN-DCSM.

Wave boundary conditions

The wave boundary conditions of SWAN-DCSM originate from ERA5, the new ECMWF climate reanalysis dataset (ECMWF, 2018). The wave grid of ERA5 is regular with a resolution of 0.3 $\times$ 0.3°. Since the ERA5 domain covers the SWAN-DCSM grid it could be possible to omit part of SWAN-DCSM and define wave boundary conditions closer to the coast, to save computational time. However, this is not considered a reasonable option since the wave model of ERA5 takes into account less shallow water physics compared to SWAN. Therefore, the entire SWAN-DCSM domain is selected since this is expected to provide better physical resolution and accuracy. An even bigger computational domain is not expected to increase the quality of results in the nearshore.

SWAN-DCSM receives wave boundary conditions (wave height, peak period and directional spreading) at 32 locations along its northern, western and southern boundaries and converts these into 2D spectra. In the same manner the nested SWAN-HCWD grid receives 2D wave spectra at 55 locations along its wet boundaries, computed by SWAN-DCSM. The boundary locations of each model are indicated with red dots in Figure 4.1. For both models the boundaries are given at every computational time step which is equal to 1 hour.

Water levels, currents and wind

No water level fluctuations are assumed at the boundaries of SWAN-DCSM and SWAN-HCWD. The same applies to currents. Omitting currents and water levels is reasonable for SWAN-DCSM since it is meant for deep water computations. On the other hand, this is a limitation for SWAN-HCWD, which is designed for coastal areas and therefore should properly describe the tidal influence and the wave-current interactions. However, omitting water levels and currents is a simplification which is expected to not influence the results significantly. This is because it is the pure wave action itself that predominantly affects the coastal.

Wind input for both SWAN-DCSM and SWAN-HCWD comes from the ERA5 dataset and is supplied on a regular grid with a resolution of $0.05\times0.05°$. This is the refined wind grid which, as explained in Section 3.5, is necessary to properly resolve the OWF areas and therefore the wind speed decrease inside them. The wind fields are provided at every computational time step, which is equal to 1 hour.

Physics

The following physical settings are applied in both SWAN-DCSM and SWAN-HCWD:

GEN3 KOMEN

WCAP KOMEN delta=1

FRIC JONSWAP cfjon=0.038

BREA CONST alpha=1.0 gamma=0.73.

These settings are default in the current SWAN version 41.20A. With the GEN3 option SWAN is run in third-generation mode for wind input, quadruplet interactions and whitecapping. The KOMEN option assumes an exponential wave energy growth due to wind according to Komen et al. (1984). The whitecapping is formulated according to Komen et al. (1984) with a value for δ equal to 1, similar to the current operational SWAN-North Sea model. For wave breaking, the default Battjes and Jansen (1978) settings are applied with a constant breaker index of 0.73 and a proportionality coefficient for the rate of energy dissipation equal to 1. The bottom friction uses the standard JONSWAP formulation, with a coefficient of 0.038 m^2s^{-3}. Within the operational SWAN North Sea model SWAN-DCSM uses a friction coefficient of 0.028 m^2s^{-3}. However, as later explained, the simulations here are performed using a quasi-stationary approach (every time step solved in stationary mode) which results in slightly bigger wave heights. Therefore the use of a higher friction coefficient is expected to counteract this effect leading to satisfactory results. Quadruplets (deep water non-linear wave interactions) are activated by default on both grids. In the computations of SWAN-DCSM, triads (shallow water non-linear wave interactions) are deactivated. In SWAN-HCWD they are activated using the following (default) settings:

TRIAD itriad=1 trfac=0.8 cutfr=2.5

These options enable the LTA approximation method for the triad computation with a 0.8 proportionality coefficient and a maximum frequency 2.5 times bigger than the mean value. For more information on the chosen settings and the relevant literature, reference is made to the SWAN Scientific and Technical Documentation (SWAN team, 2018a).

Obstacles

The energy island is considered in the model as an obstacle with the following settings:

OBST TRANS 0 REFL 0.3 RSPEC LINE X_1 Y_1 ... X_n Y_n

Using the above options the island is considered having a zero transmission coefficient and a reflection coefficient equal to 30%. Assigning a zero transmission coefficient ensures that no energy passes through the island. For the reflection coefficient the value is typical for breakwaters.

It is important to note that the modeling of the island neglects the necessary landfill to decrease the adjacent water depth. This means that the depth is not shallow enough to enable dissipation due to bottom friction and depth-induced wave breaking. Therefore, the incoming wave height will be bigger compared to the case of a landfill thus leading to a higher reflected wave.

Numerics

The numerical solver of the model is set up as follows:

PROP BSBT

STOPC 0.01 0.01 0.005 99 STAT 50 0.01 0.1

which means that the first order upwind BSBT (Backward in Space, Backward in Time) scheme is used. The stopping criterion is formulated for stationary computations according to Zijlema and van der Westhuysen (2005). This requires that the absolute change in H_{m0} from one iteration to the next is less than 1 cm or the relative change less than 1% and the normalized curvature of the iteration curve of H_{m0} less than 0.5%. This is formulated as follows:

$$|\Delta H^s_{m0}(i,j)| < 0.01 \text{ or } \frac{|\Delta H^s_{m0}(i,j)|}{H^{s-1}_{m0}(i,j)} < 0.01 \tag{4.1}$$

and

$$\frac{|H^s_{m0}(i,j) - (H^{s-1}_{m0}(i,j) + H^{s-2}_{m0}(i,j) + H^{s-3}_{m0}(i,j)|}{2H^s_{m0}(i,j)} < 0.005 \tag{4.2}$$

The above criterion should be fulfilled in more than 99% of all wet grid points and the maximum number of iterations to do so is set equal to 50. This value turned out to be quite big since in general the model used no more than 10 iterations during the first 5 to 10 time steps and no more than 5 iterations thereafter. In addition, the frequency dependent under-relaxation constant α and the action density limiter γ are set equal to their default values, namely 0.01 and 0.1 respectively.

Timing

The time step of the quasi-stationary computations is set to one hour. The initial goal was to perform non-stationary runs. However these resulted in inconsistent results for the relative wave height change. A comparison between non-stationary and quasi-stationary computations in SWAN-DCSM is presented in Figure 4.3. It can be seen that results from non-stationary computations show changes in wave height away from the areas of OWF influence. For example on January 1st 08:00:00 UTC a wave height decrease of 5% is observed at the Strait of Dover as well as the eastern coast of UK and the Wadden Sea. In addition, at the same time step as well as on June 1st 20:00:00 UTC a decrease of around 1.5% is observed at the central part of the North Sea, north of Dogger Bank, even though no OWFs are present there. Such inconsistent results do not make it possible to derive the relative effect of OWFs in a clear way. Quasi-stationary runs on the other hand do not show these inconsistencies. The effect on wave height is only present in the area adjacent to the OWFs. Therefore quasi-stationary runs are chosen instead of non-stationary runs.

A possible explanation for the inconsistent change in wave height away from OWFs could be a numerical error that propagates through the domain with time. This is however not further investigated. Nevertheless, to make sure that the output of the previous time step does not influence the input of the next one, the wave field prior to each computation is initialized using the following command:

COMPUTE STAT yyyymmdd.hh

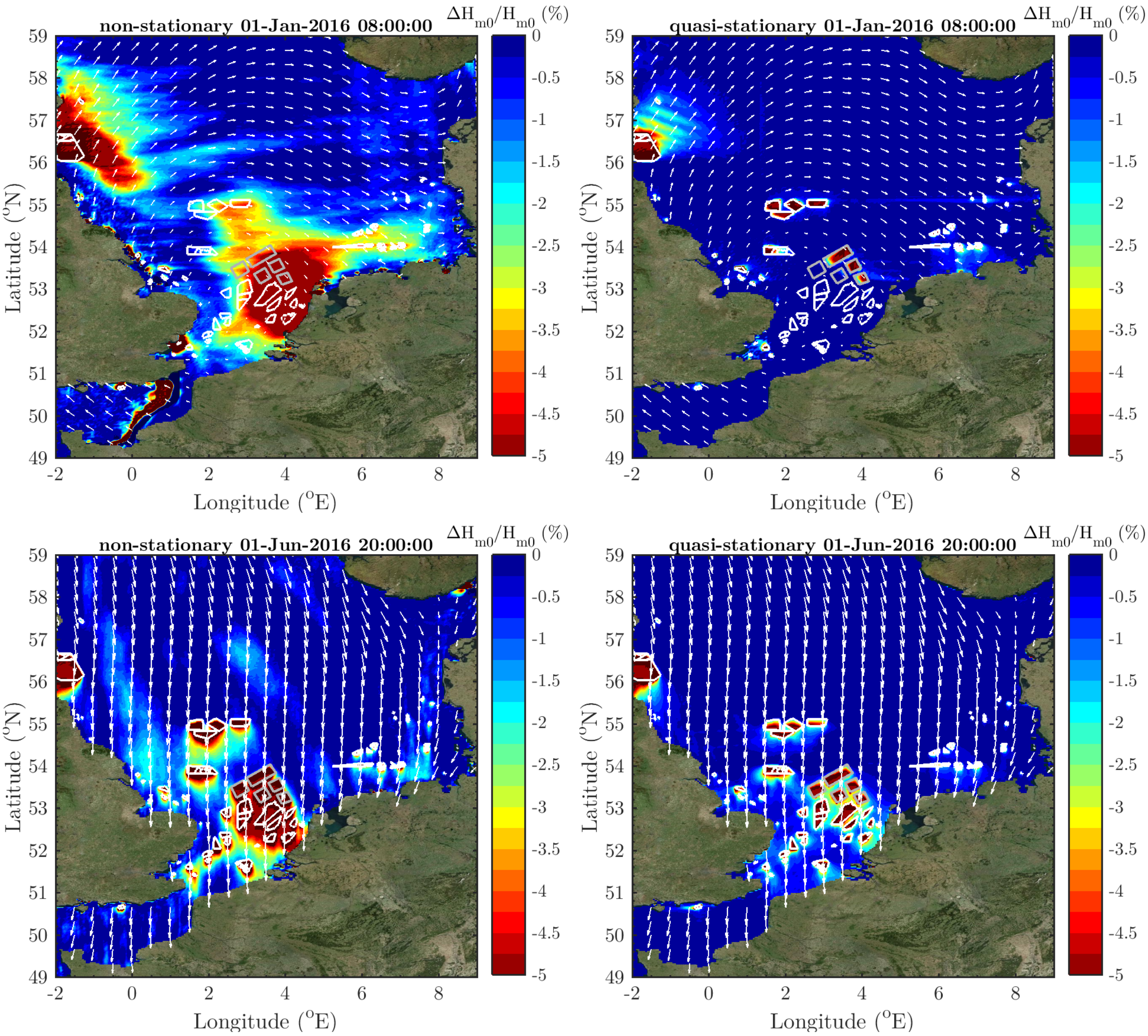

Figure 4.3: Relative wave height change in SWAN-DCSM for non-stationary (left column) and quasi-stationary (right-column) computations considering OWFs in 2050. Upper row: January 1st 2016 08:00:00 UTC. Lower row: June 1st 2016 20:00:00 UTC. White arrows indicate the wind direction. The arrow length is proportional to the wind speed magnitude.

INIT DEF

where yyyy, mm, dd and hh are the notations for year, month, day and hour and INIT DEF uses the 2^{nd} generation mode to create an initial condition for the next stationary computation.

Model output

In SWAN-DCSM two-dimensional wave spectra are requested at 55 nesting points around the boundaries of SWAN-HCWD. Using these spectra as boundary conditions SWAN-HCWD computes spatial fields of significant wave height (H_{m0}) and mean wave direction (ϕ) covering the entire SWAN-HCWD domain. In addition, the above wave parameters together with the peak wave period (T_p) are retrieved close to the Dutch coast, at 112 locations along the -9 m NAP contour[2]. These parameters are used as input for coastline modeling. The time interval of the output is 1 hour.

Summarized settings

The setup of SWAN modeling discussed in the previous subsections is summarized in Table 4.2. In addition, Table 4.3 gives detailed characteristics of the SWAN-DCSM and SWAN-HCWD domains. Both tables are presented at the end of this chapter, in Section 4.3.

4.2. Unibest-CL+ coastline modelling

To study the effect of the (modified) wave climate on the coastline response the 1D coastline model Unibest-CL+ is applied. The model computes the wave driven alongshore sediment transport and the coastline changes due to spatial gradients in the transport. It assumes that the transport develops instantaneously so that the alongshore current has sufficient time and space to develop. This is the case for long coastal stretches such as the Dutch coast. However, Unibest-CL+ does not explicitly resolve the cross-shore sediment transport (but this can be included implicitly as a source/sink term in the alongshore sediment transport).

The wave driven alongshore sediment transport occurs close to the coast (in a zone of hundreds of meters from the shoreline). It is caused by an alongshore current generated by waves that approach the coast under an angle. The magnitude of the alongshore current depends on the wave characteristics, predominantly the significant wave height (H_{m0}) and the mean wave direction with respect to the coast, also called angle of incidence (ϕ_{coast}). The alongshore sediment transport can also be influenced by water level fluctuations, such as tidal forcing. The wave and tidal conditions are provided to the model in a schematized way.

Schematized coastline

The Dutch coast is located in the central part of the Netherlands and has a length of 118.5 km. It is bounded in the North by the Marsdiep tidal inlet near Den Helder and in the South by a long jetty near Hoek van Holland, which is part of the approach channel to the Port of Rotterdam. Two

[2]Normaal Amsterdams Peil: a local datum approximately equal to the mean sea level (MSL).

openings are observed along the Dutch coast. One near IJmuiden, which is the entrance to the Port of Amsterdam and another one at the small harbor of Scheveningen, 16 km north of Hoek van Holland. The schematized Dutch coastline is displayed in Figure 4.4.

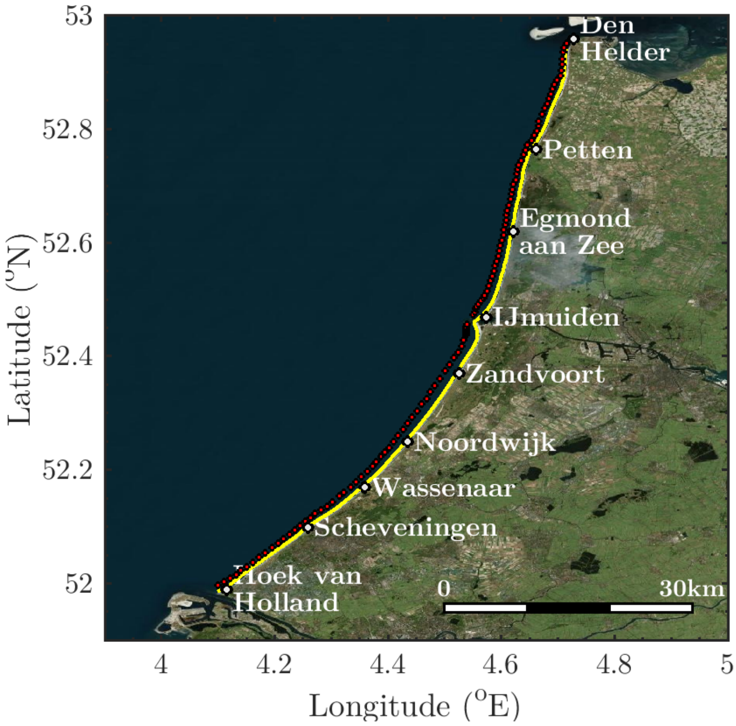

Figure 4.4: Dutch coastline schematized in Unibest-CL+ (in yellow). The red dots indicate the 112 locations at the -9 m NAP contour from where the SWAN wave output is supplied to Unibest-CL+.

The schematized coastline is set up in the RD coordinate system (Rijksdriehoekscoördinaten) for which data is used from approximately 450 measured cross-shore profiles. The coastline points are determined at the MKL[3] position of each cross-shore profile. The profiles are derived from the JARKUS database of year 2005. This source might be quite outdated however this is not expected to affect the final result since the aim is to assess the potential impact of OWFs on the Dutch coast.

Boundary conditions

At the southern boundary of the model, near Hoek van Holland, a zero sediment transport is assumed. This is reasonable since the long jetty of the Port of Rotterdam completely blocks the alongshore sediment transport. At the northern boundary, where the coastline meets the Marsdiep tidal inlet, an assumption of constant coastline orientation seems more reasonable. At the 112 locations along the -9 m NAP contour (red dots in Figure 4.4) the annual wave climate from SWAN-HCWD is forced into Unibest-CL+, schematized into clusters. More specifically, the annual timeseries of significant wave height (H_{m0}) and mean wave direction (ϕ) are schematized

[3]Momentary Coastline Position: derived from integrating the volume of sand in the nearshore zone. It is located approximately between MSL + 3 m (dune foot) and MSL -5 m (Stronkhorst, Huisman, Giardino, Santinelli, & Santos, 2018).

into 40 wave height classes and 36 directional sectors. Table 4.1 presents this in more detail. The resulting wave conditions are approximately 240 per boundary location. This is a quite detailed schematization but it is chosen nevertheless because the resulting computational time is acceptable. The peak wave period is excluded from the schematization since its influence in coastline dynamics is of less importance compared to wave height and direction. An additional reason though is the fact that SWAN is very sensitive in computing this quantity. Tide is also not included in the computations for simplicity, assuming it is of secondary importance compared to the wave action.

Table 4.1: Unibest-CL+ wave climate schematization.

parameter	H_{m0} (m)	ϕ (°N)
number of classes	40	36
minimum value	0	0
maximum value	4	360
class size	0.10	10

Using the schematized wave climate as boundary condition and the initial coastline orientation, an $S-\phi$ curve is computed at each one of the 112 locations, that gives the net sediment transport as function of the wave approach angle (ϕ_{coast}). This computation is carried out in the Longshore Transport module (LT) of Unibest-CL+.

Cross-shore profiles

A cross-shore profile is derived at each one of the 112 boundary locations, based on JARKUS data. The active height of each profile is set at 10 meters. Figure 4.5 shows the resulting cross-shore bathymetry and coastline orientation along the Dutch coast.

Sediment characteristics

For sediment transport computations the formula of Van Rijn (2004) is applied. The sediment has a median grain diameter (D_{50}) of 200 μm and percentile values of 120 μm (D_{10}) and 300 μm (D_{90}) respectively. These values are typical for the Dutch coast (Stronkhorst et al., 2018; Wijnberg, 2002).

Sediment bypass at harbor jetties

Near the harbor jetties at Scheveningen and IJmuiden the alongshore sediment transport is completely blocked. In such cases it is common practice to perform annual bypassing, something that is considered in this study. For IJmuiden a bypassing of 120,000 m^3/year is applied, while a bypassing of 90,000 m^3/year is considered at Scheveningen. These values are based on knowledge from previous studies but do not represent the actual nourishment volumes that are currently deployed.

It should also be noted that the sediment transport near the harbor jetties of IJmuiden and Scheveningen is not representative, since the sheltering of waves is not taken into account. How-

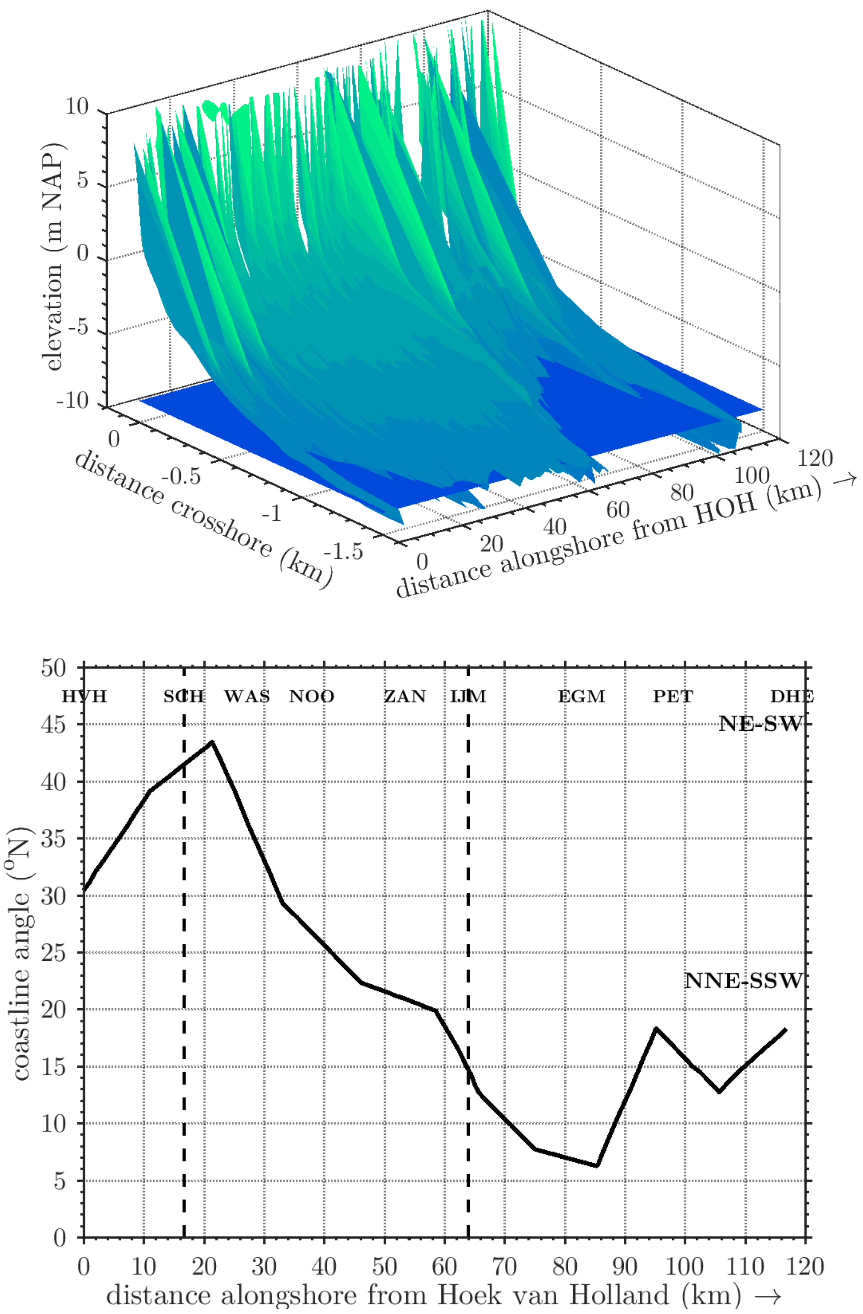

Figure 4.5: Cross-shore bathymetry (upper image) and coastline orientation (lower image) along the Dutch coast. The coastline orientation is measured clockwise starting from North. Locations along the Dutch coast are abbreviated as follows: HVH (Hoek van Holland), SCH (Scheveningen), WAS (Wassenaar), NOO (Noordwijk), ZAN (Zandvoort), IJM (IJmuiden), EGM (Egmond aan Zee), PET (Petten) and DHE (Den Helder).

ever, the width of the shadow zone due to sheltering is considered negligible when studying the alongshore morphology of the entire Dutch coast[4].

Additionally, results in the area close to Den Helder are not representative because the influence of the Marsdiep tidal inlet is not taken into account. The sediment transport there is highly influenced by the complex geometry and corresponding tidal currents in the flood and ebb channels. This area is indicated with a gray strip in relevant graphs depicted in Chapter 5.

4.3. Summarized settings of SWAN modeling

The following tables summarize the SWAN model settings as well as details of the used grids. More information regarding the pre-processing of both SWAN and Unibest-CL+ models can be found in Appendix E.

Table 4.2: Overview of SWAN model settings.

<table>
<tr><th></th><th colspan="2">SWAN-DCSM</th><th>SWAN-HCWD</th></tr>
<tr><td>Mode</td><td>non-stationary</td><td>quasi-stationary</td><td>quasi-stationary</td></tr>
<tr><td>f (Δf) (Hz)</td><td colspan="3">0.03 – 0.6 (0.1f)</td></tr>
<tr><td>θ ($\Delta\theta$) (°)</td><td colspan="3">0° – 360° (8°)</td></tr>
<tr><td>water level</td><td colspan="3">no</td></tr>
<tr><td>currents</td><td colspan="3">no</td></tr>
<tr><td>3rd generation mode</td><td colspan="3">Komen (1984)</td></tr>
<tr><td>whitecapping</td><td colspan="3">Komen (1984), $\delta = 1$</td></tr>
<tr><td>triads</td><td colspan="2">no</td><td>itriad = 1, trfac = 0.8, cutfr = 2.5</td></tr>
<tr><td>C_{fric} $(m^2 s^{-3})$</td><td colspan="3">0.038</td></tr>
<tr><td>breaking</td><td colspan="3">$\gamma = 0.73$, $\alpha = 1$</td></tr>
<tr><td>quadruplets</td><td colspan="3">iquad = 2</td></tr>
<tr><td>Δt</td><td colspan="3">1 hr</td></tr>
<tr><td>numerical criterion</td><td colspan="3">STOPC</td></tr>
<tr><td>points converged (%)</td><td colspan="3">99</td></tr>
<tr><td>max. iterations</td><td colspan="3">50</td></tr>
<tr><td>α</td><td>0</td><td colspan="2">0.01</td></tr>
<tr><td>γ</td><td colspan="3">0.1</td></tr>
</table>

[4]The width of the shadow zone has approximately the same order of magnitude with the length of the jetties. This is approximately 2.5 km and 0.5 km (for IJmuiden and Scheveningen respectively). This is two orders of magnitude smaller compared to the length of the entire Dutch coast(119 km).

Table 4.3: Overview of SWAN-DCSM and SWAN-HCWD domain characteristics.

Name	**Shape**	**ΔX**	**ΔY**	**number of cells (active grid points)**	**X_{min};X_{max}**	**Y_{min};Y_{max}**
SWAN-DCSM grid	rectangular	0.05° ≈ 2.4 km to 3.7 km	0.03° ≈ 3.3 km	420 × 480 (137,068)	-12° ; +9° ≈ 1500 km	+48° ; +64° ≈ 1700 km
SWAN-HCWD grid	curvilinear	50 m to 1200 m	35 m to 2600 m	78 × 175 (12,934)	+3.6° ; +4.8° ≈ 100 km	+51.9° ; +53.1° ≈ 100 km
SWAN-DCSM bathymetry	rectangular	0.025° ≈ 1.2 km to 2 km	0.0167° ≈ 1.8 km	1120 × 1260	-15° ; +13° ≈ 2300 km	+43° ; +63.9° ≈ 2300 km
SWAN-HCWD bathymetry	curvilinear	50 m to 1200 m	35 m to 2600 m	78 × 175	+3.6° ; +4.8° ≈ 100 km	+51.9° ; +53.1° ≈ 100 km
Original wind grid	rectangular	0.3° ≈ 14.5 km to 24.4 km	0.3° ≈ 33.4 km	94 x 71	-15° ; +13.2° ≈ 2300 km	+42.9° ; +64.2° ≈ 2300 km
Refined wind grid	rectangular	0.05° ≈ 2.4 km to 4.1 km	0.05° ≈ 5.6 km	564 x 426	-15° ; +13.2° ≈ 2300 km	+42.9° ; +64.2° ≈ 2300 km

5

Results

This chapter elaborates on modeling results. The wave climate is investigated by looking at the significant wave height (H_{m0}) and the mean wave direction (ϕ) within the finer computational domain and along the -9 m NAP contour, defined as the nearshore margin. The effect of OWFs or an island is depicted by computing the annual mean change in wave height and direction in relation to a baseline situation, where no OWFs are present. The change in wave height is expressed as a percentage relative to the baseline case (no OWFs). The change in wave direction is computed in absolute terms, expressed in degrees. Results are shown for OWF development stages defined in Section 3.3. Regarding coastline modeling the computed quantities are the net annual sediment transport (Q_s) and the coastline change with respect to 2018 (Y). The effect of OWFs or an island is computed as the change of the above quantities with respect to the baseline situation (no OWFs). Results are shown in absolute terms, for years 2023, 2030 and 2050 (corresponding to the transition between development stages). Positive gradients of the change in net sediment transport due to OWFs or an island indicate net erosion in the already evolving coastline. This is expressed in nourishment need and is compared with historical nourishment volumes along the Dutch coast. It is found that the greatest nourishment need (located north of Zandvoort and Petten) can only reach 1% of past nourishment volumes.

5.1. Definitions

Wave parameters are presented as annual mean quantities. The annual mean significant wave height and direction are denoted by ${H_{m0}}^{\text{mean}}$ and ϕ^{mean} respectively. Furthermore, the effect of OWFs and an island on wave height is expressed with the annual mean relative change:

$$\frac{\Delta H_{m0}}{H_{m0,\text{baseline}}}^{\text{mean}} = \left(\frac{H_{m0,\text{effect}} - H_{m0,\text{baseline}}}{H_{m0,\text{baseline}}}\right)^{\text{mean}} \tag{5.1}$$

whereas the effect on wave direction is expressed with the annual mean absolute change:

$$\Delta\phi^{\text{mean}} = (\phi_{\text{effect}} - \phi_{\text{baseline}})^{\text{mean}} \tag{5.2}$$

In the above expressions the subscript "effect" corresponds to a simulation accounting for OWFs or an island and the subscript "baseline" to the baseline case (no OWFs or island).

The above quantities show the cumulative effect. This is the effect of OWFs in the current development stage together with OWFs of previous stages. The cumulative effect does not clearly indicate the development stage that mostly affects the nearshore wave climate. To better understand the net contribution of each development stage, the following term is computed:

$$\frac{\Delta H_{m0}}{H_{m0,\text{effect1}}}^{\text{mean}} = \left(\frac{H_{m0,\text{effect2}} - H_{m0,\text{effect1}}}{H_{m0,\text{effect1}}}\right)^{\text{mean}} \tag{5.3}$$

for the significant wave height and

$$\Delta\phi^{\text{mean}} = (\phi_{\text{effect2}} - \phi_{\text{effect1}})^{\text{mean}} \tag{5.4}$$

for the mean wave direction. In the above expressions the subscript "effect2" corresponds to a simulation accounting for OWFs at a certain development stage and the subscript "effect1" to a simulation accounting for OWFs of the previous development stage.

The change in wave direction is also referred to as "wave direction turning" or simply "turning".

Regarding coastline modeling, the effect of OWF developments and an island is expressed with the absolute change:

$$\Delta A^{\text{t}} = {A^{\text{t}}}_{\text{effect}} - {A^{\text{t}}}_{\text{baseline}} \tag{5.5}$$

where A is either the net annual sediment transport (Q_s) or the coastline change with respect to 2018 (Y), both in year t, while the subscripts "effect" and "baseline" have the same meaning as explained above.

5.2. Wave modeling results

The effect on waves is presented for each development stage summarized in images consisting of four subfigures. The upper subfigures show the geographical distribution of the annual mean quantities in the SWAN-HCWD domain. The left image refers to wave height and the right one to wave direction. The images directly below show the distribution of the same quantities at the -9 m NAP contour, defined as the nearshore margin. More specifically, the latter images show the annual mean value (red line) as well as the 1st and 3rd quartiles[1] (dashed blue and dotted blue lines respectively). The quartiles give an indication of the range of values computed in the 1-year wave simulation. The -9 m NAP contour is also indicated with a red line in every map plot, for easy reference.

Undisturbed wave height and direction

The annual mean wave height and wave direction in the baseline case are depicted in Figure 5.1.

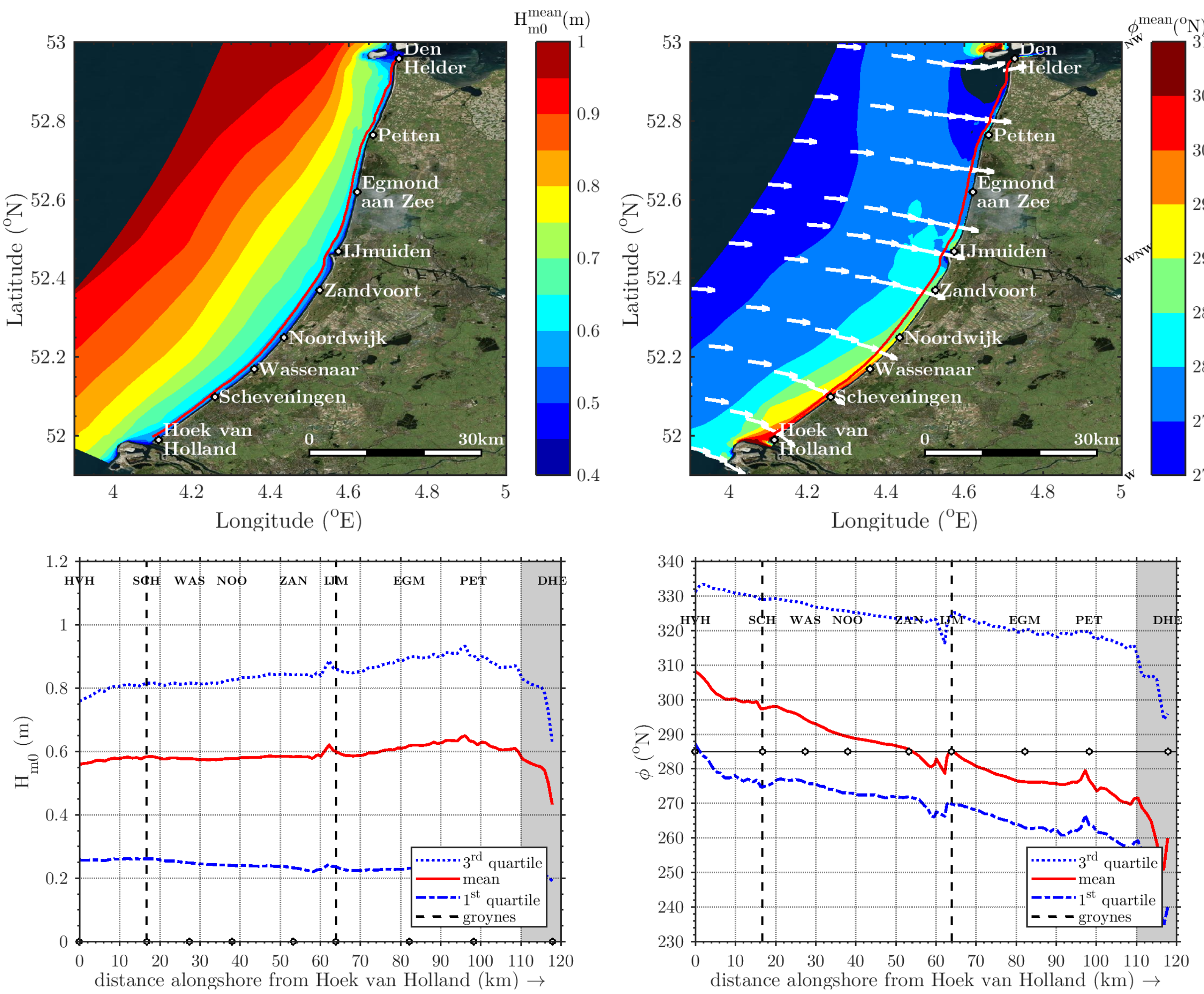

Figure 5.1: Undisturbed annual mean wave height and direction in the SWAN-HCWD domain.

[1] 1st quartile: middle value between the minimum and the median of a dataset; 3rd quartile: middle value between the median and the maximum of a dataset.

At the northern edge of the domain the mean wave height is equal to 1 m and declines to 0.9 m in the southwest. Along the -9 m NAP contour it is approximately 0.6 m. At Hoek van Holland ($x = 0$ km) H_{m0} is around 0.56 m while south of Petten ($x = 96$ km) a maximum value of 0.65 m is observed. Waves propagate on average from the West. They turn clockwise reaching the southern part of the Dutch coast and counterclockwise in the northern part. The resulting direction is weighted with the wave energy (proportional to H_{m0}^2) to make sure it is the most dominant[2]. At the -9 m NAP contour the mean wave direction is between 310°N and 250°N, decreasing northward in magnitude .

OWF effect

Regarding OWFs the interest is only focused on significant changes in wave climate. These are changes greater than 1% for wave height and greater than 0.5° for wave direction. Figure 5.2 shows the effect in 2018.

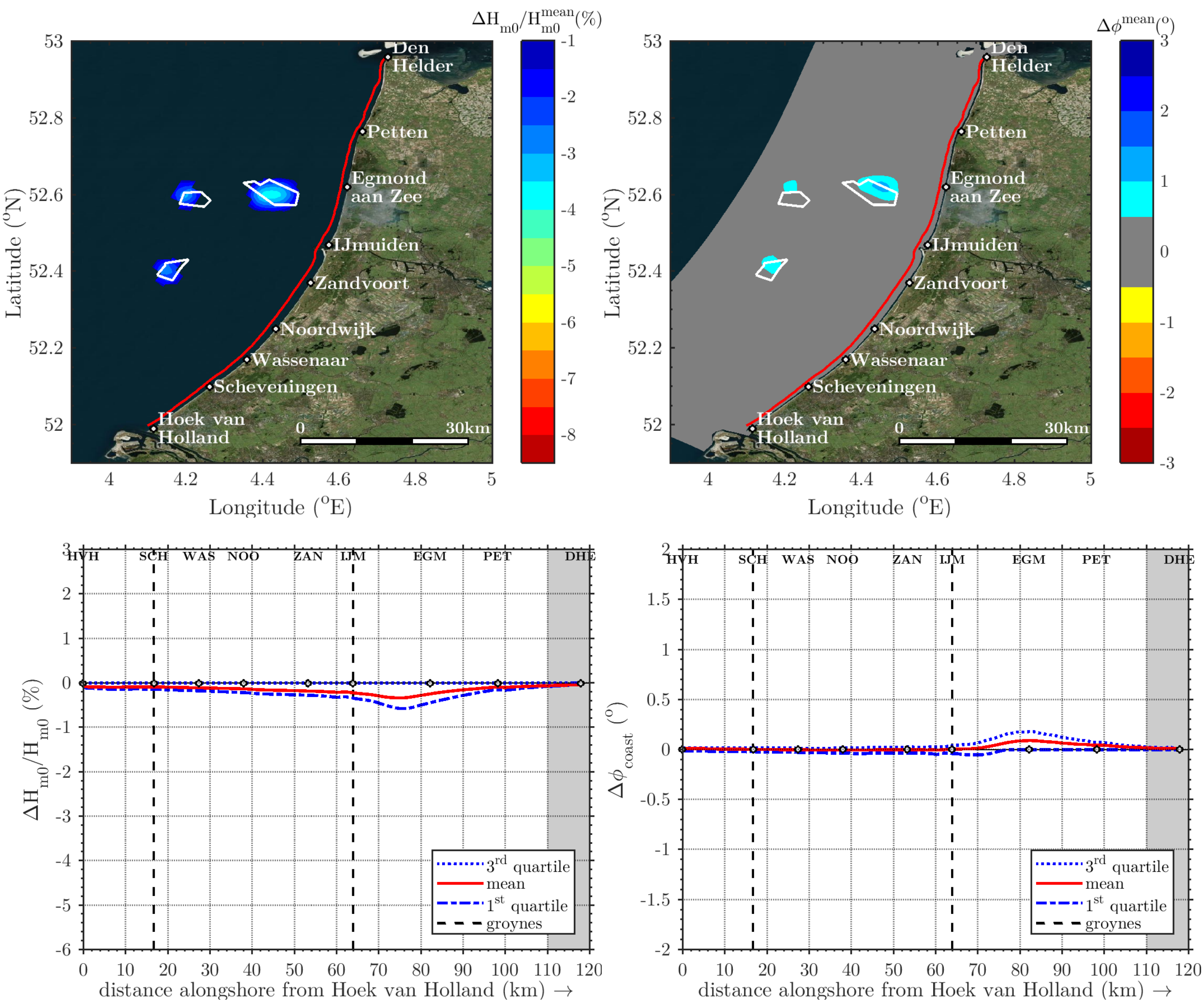

Figure 5.2: Cumulative effect of OWFs in 2018 on wave height and direction.

[2]The idea is to give more weight to more energetic components, since these contribute more towards generating an alongshore sediment transport in the nearshore.

In 2018 the effect is only significant inside the OWF areas. Wave height is reduced by a mean value of 4% within Egmond aan Zee OWF (OWEZ) and by around 2% at the rest OWFs (Princess Amalia on the West and Luchterduinen in the South). The effect at the -9 m NAP contour is insignificant. The mean wave height decrease shows a peak of 0.3% south of Egmond ($x = 76$ km) caused mainly by OWEZ. This is because OWEZ is located closer and has a bigger size compared to the rest OWFs of 2018. Regarding wave direction, a mean clockwise turning of 1° is observed within the northeastern flank of every OWF. At the the -9 m NAP contour the clockwise turning decreases significantly having a maximum of only 0.1°, north of Egmond ($x = 84$ km).

Moving to year 2023 the resulting effect is significantly stronger. Results are shown in Figure 5.3.

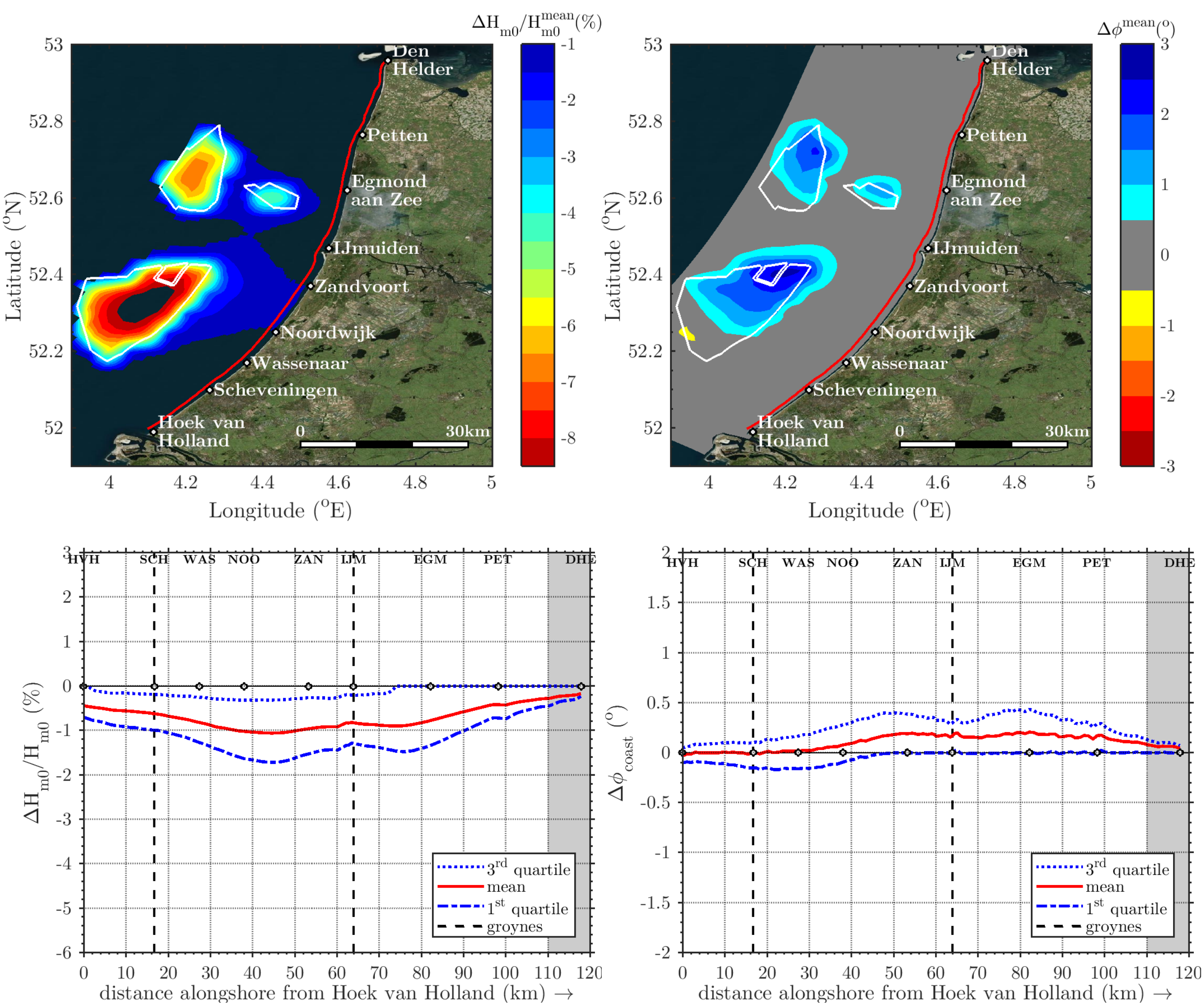

Figure 5.3: Cumulative effect of OWFs in 2023 on wave height and direction.

Within Hollandse Kust Zuid (HKZ) a mean wave height decrease of 8.5% occurs. Inside Hollandse Kust Noord (HKN) the wave height decrease is 7% and in Egmond aan Zee it is around 4.5%. It is obvious that the bigger the OWF area, the greater the wave height decrease. The affected area downwind of HKZ reaches the Dutch coast. At the -9 m NAP contour the peak in mean wave height decrease is observed in between Noordwijk and Zandvoort and is equal to 1% (x = 45 km). Moving northward, the decrease in wave height is slightly smaller but remains close to 1%, as far as Egmond (x = 78 km). Regarding wave direction, a mean clockwise turning of 2.5° is observed within the northeast area of HKZ, while a value of 2° occurs northeast of HKN and northeast of Egmond aan Zee. At the -9 m NAP contour the mean clockwise turning significantly decreases, having a maximum of 0.2° at Zandvoort (x = 53 km) and retaining a value of around 0.1° all the way to the northern boundary (x = 118.5 km). The turning is always clockwise northward of Noordwijk (x = 45 km). On the other hand, occasions of counterclockwise turning are observed in the south (see the 1st quartile in Figure 5.3).

The additional effect in year 2023 is extremely superior compared to the effect in 2018. This can be seen in Figure 5.4 that shows the net effect in 2023.

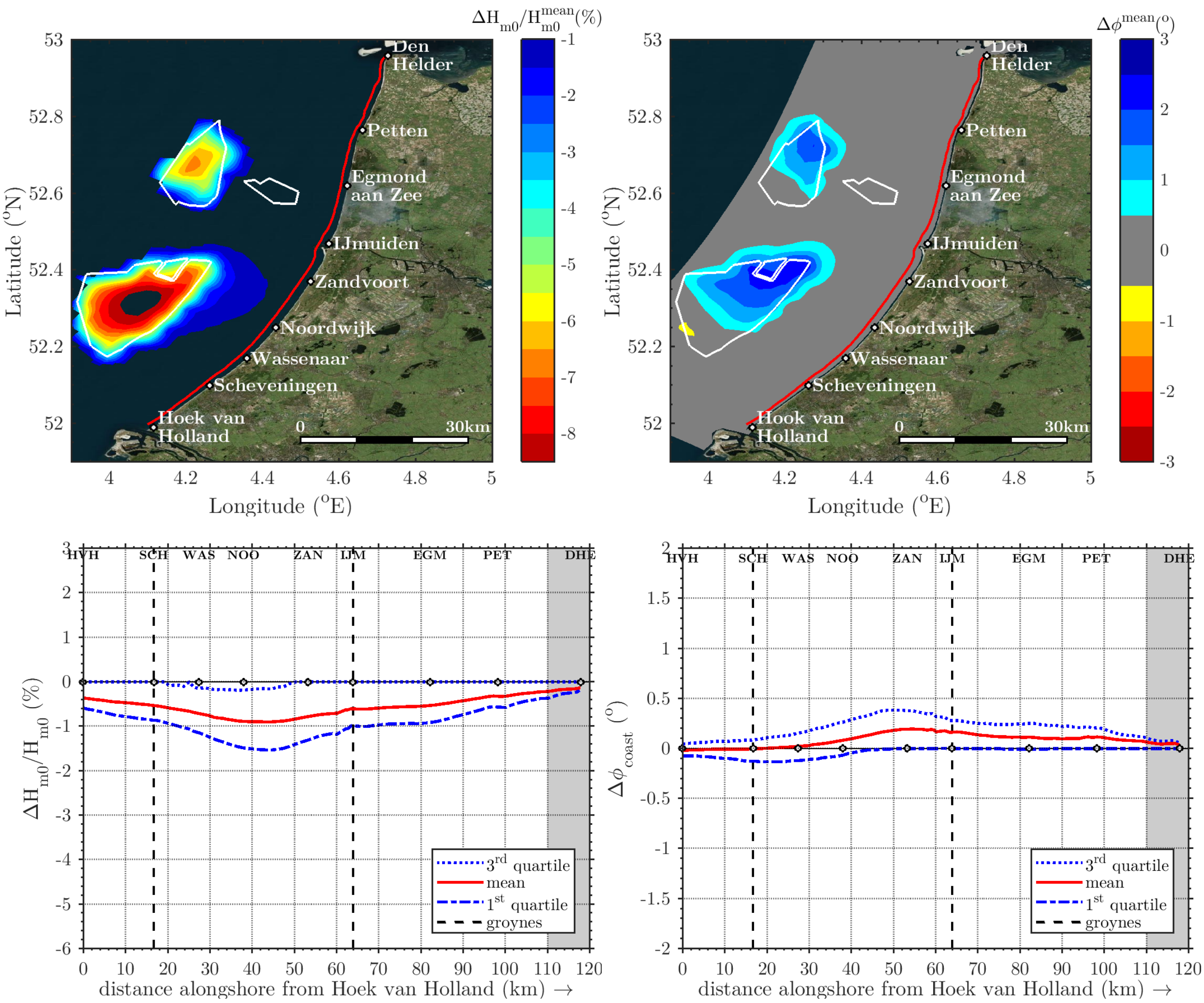

Figure 5.4: Net effect of OWFs in 2023 on wave height and direction.

Almost the entire contribution originates from OWFs developed in 2023, which add more than double the effect on the wave height decrease in the nearshore, compared to 2018. The only significant contribution in 2018 comes from Egmond aan Zee OWF.

In year 2030 the effect in the nearshore is significantly intensified. The cumulative effect is depicted in Figure 5.5.

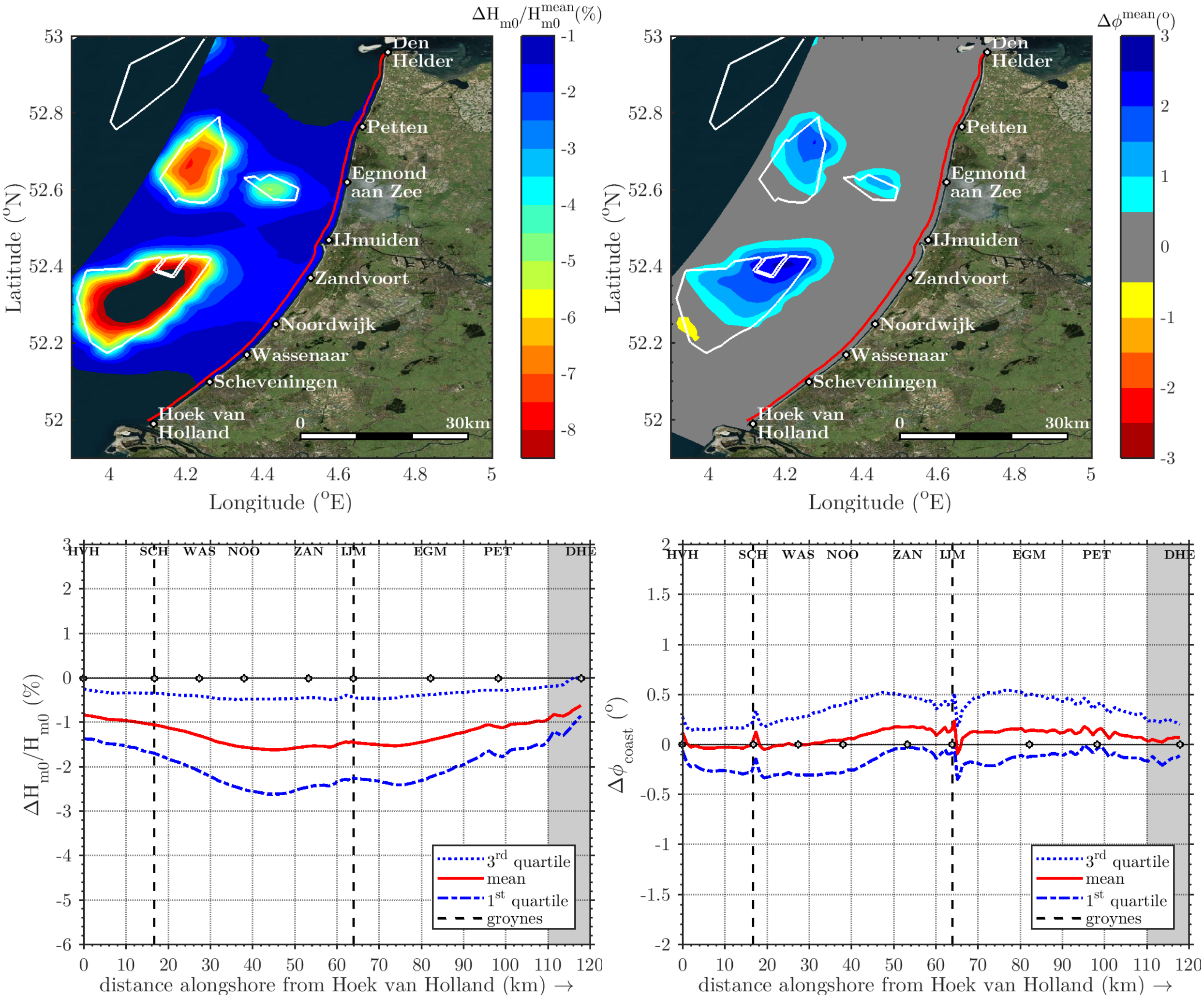

Figure 5.5: Cumulative effect of OWFs in 2030 on wave height and direction.

Significant wave height decrease can be observed at the greatest part of the Dutch coast and more specifically from Scheveningen to Petten ($x = 16 - 98$ km). The effect becomes stronger in between Noordwijk and Zandvoort ($x = 38 - 53$ km), where a peak of 1.5% in mean wave height decrease is observed ($x = 45$ km). Same as in 2023, the wave height decrease is close to the peak value as far as Egmond ($x = 78$ km). Also, similar to 2023, a peak value of 0.2° in mean clockwise turning can be seen at Zandvoort ($x = 53$ km). The change is zero in IJmuiden and retains clockwise values all the way to the North. Contrary to 2023 though, occasions of counterclockwise turning are observed along the entire Dutch coast (negative values of 1$^{\text{st}}$ quartile).

OWFs in 2030 add a significant contribution to the nearshore effect observed in 2023. The net effect is depicted in Figure 5.6.

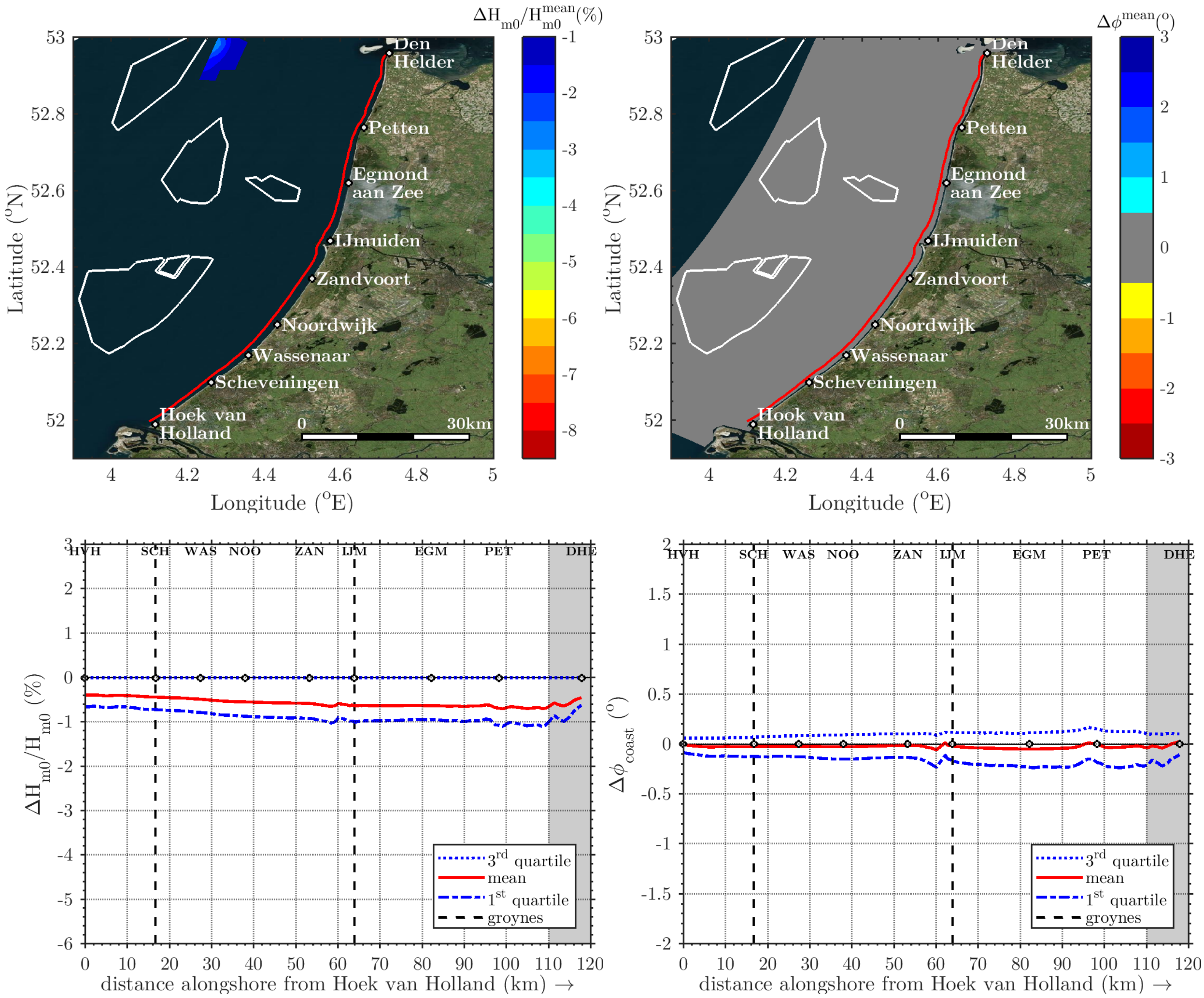

Figure 5.6: Net effect of OWFs in 2030 on wave height and direction.

At the -9 m NAP contour a mean wave height decrease of 0.5% is computed. It slightly increases northward, reaching a peak of 0.7% at Petten ($x = 98$ km). This is reasonable, since Petten is closer to the shadow zone of IJmuiden Ver OWF and the rest OWFs to be realized in 2030 (mainly HKW, HKNW and HKZW, see Figure 3.3). This indicates that, even though these OWFs are away from the Dutch coast, they have such a big size that their effect can be felt in the nearshore. In general, the net effect on wave height indicates a 50% additional decrease compared to 2023, thus making the contribution of 2030 significant. The additional effect on wave direction however is zero, indicating that the direction turning is mainly affected by OWFs developed closer to the Dutch coast.

The hypothetical OWFs in 2050 are located further offshore. Their contribution in the nearshore is found to be zero. This is shown in Appendix C, which presents the net effect of development stages 2050 and 2050A. Based on this finding, it can be stated that OWFs developed within a moderate spatial footprint[3], located away from the Dutch coast, are not expected to add a significant contribution on the effect in the nearshore.

Island effect

Apart from OWFs the effect of an energy island is investigated. In the selected scenario, the island has a size of 5 km^2 and is located approximately 30 km offshore. First, the effect of the island alone is depicted in Figure 5.7.

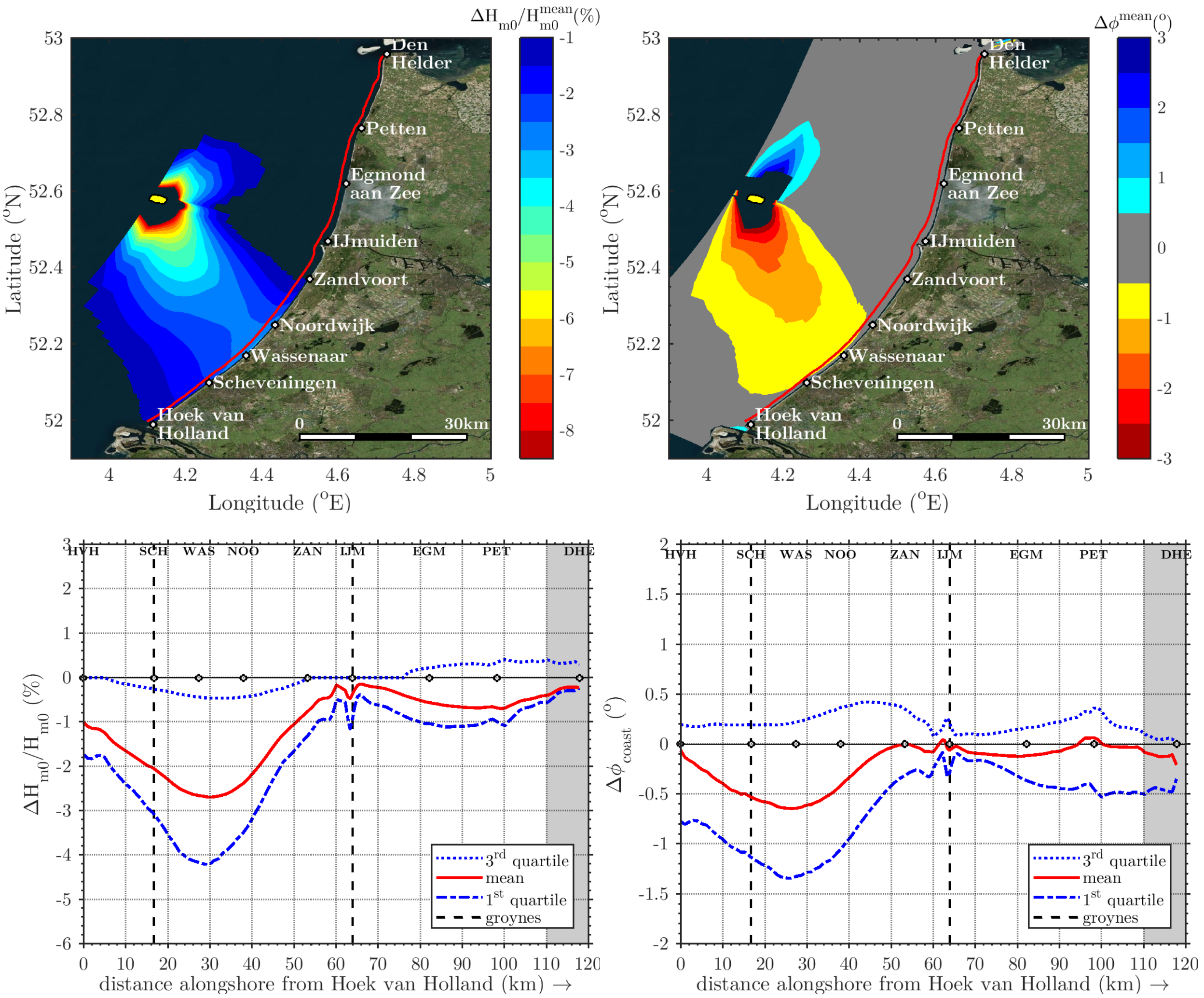

Figure 5.7: Net effect of 5 km^2 island located around 30 km offshore, on wave height and direction.

The energy island greatly affects the wave climate. The area of significant wave height decrease covers the region between Hoek van Holland and Zandvoort ($x = 0 - 53$ km), reaching a peak of 2.6% north of Wassenaar ($x = 30$ km). This is around 1.6 times greater than the value computed for the OWF effect in 2030 (decrease of 1.5%). Regarding wave direction, a mean counterclockwise rotation of 0.65° is observed at Wassenaar ($x = 28$ km). This is 3.2 times big-

[3]A moderate spatial footprint is defined as an area with a dimension significantly smaller than the fetch length for wave generation in the North Sea.

ger than the maximum value computed for OWFs in 2030 (clockwise rotation of 0.2°). In the region of North Holland ($x = 64 - 118.5$ km) the mean wave height decrease is less than 1%, with a value of 0.8% at Petten ($x = 98$ km). The mean change in wave direction has a negative small value, indicating counterclockwise turning. Exception is the region around Petten ($x = 98$ km), where a small positive value is observed.

OWF and Island effect

The previous subsection presented the effect of OWFs and an energy island separately. OWFs affect a greater part of the Dutch coast, however the intensity of the effect is significantly lower compared with the impact of a 5 km^2 island located 30 km offshore. Developing the energy island together with OWFs will yield the effect shown in Figure 5.8.

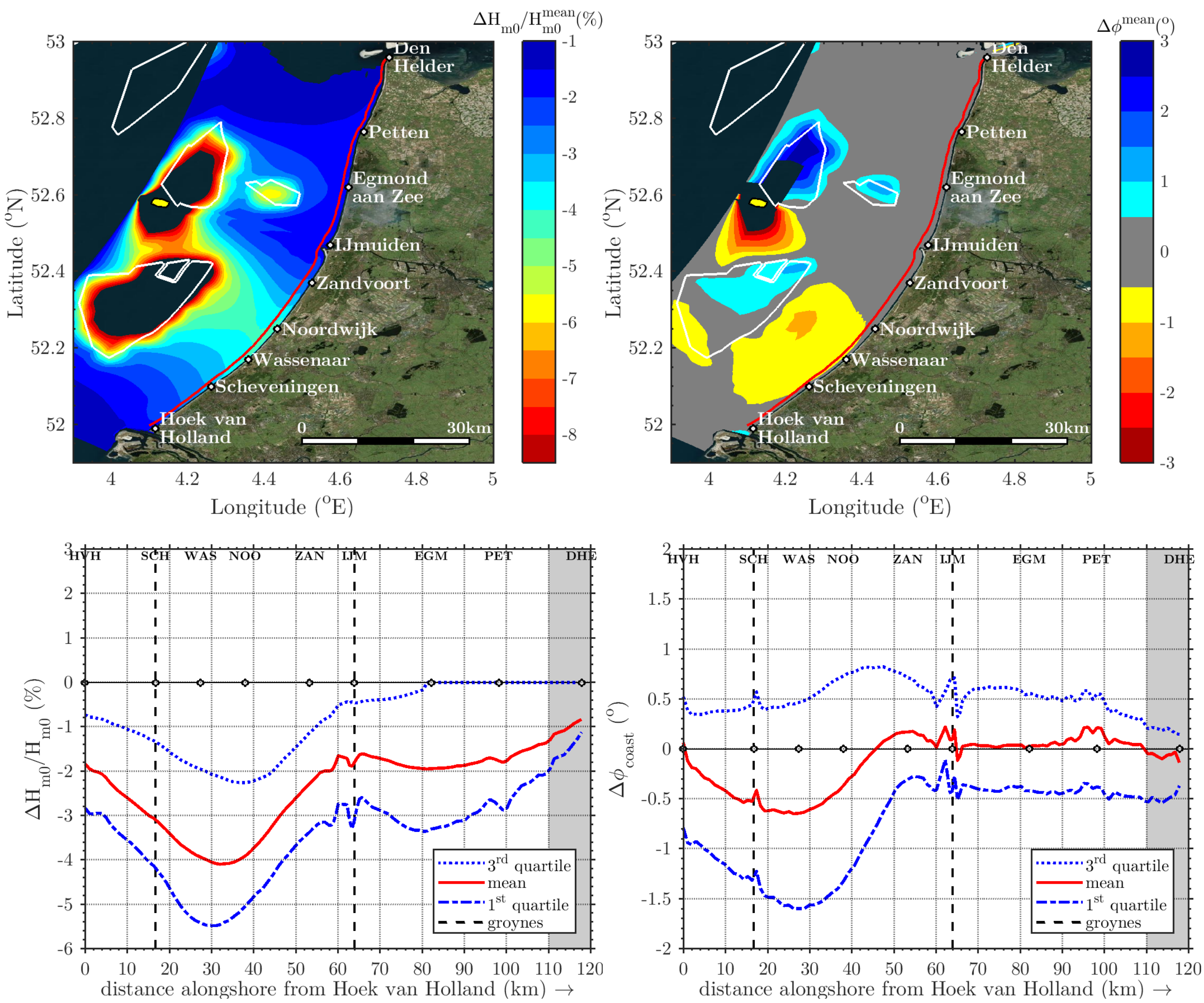

Figure 5.8: Cumulative effect of OWFs in 2030 and 5 km^2 island located around 30 km offshore, on wave height and direction.

Both interventions have the same influence on wave height, which decreases along the entire Dutch coast. At Hoek van Holland, a value of 2% in mean wave height decrease is observed. This reaches a peak of around 4% north of Wassenaar ($x = 34$ km). Moving northward the mean wave height decrease drops to 2% at Zandvoort ($x = 53$ km) and maintains that value as far as Petten ($x = 98$ km). Reaching Den Helder, the decrease steadily drops to 1%.

On the other hand, the interventions show an opposite effect on wave direction. As seen in previous images, at the -9 m NAP contour the mean change in wave direction is predominantly clockwise due to OWFs and counterclockwise due to the energy island. However, the island effect is stronger close to the coast, leading to a peak of 0.65° in counterclockwise turning at Wassenaar ($x = 28$ km). The mean change in wave direction at the rest of the Dutch coast is predominantly zero. At Zandvoort ($x = 53$ km), IJmuiden ($x = 64$ km) and Petten ($x = 98$ km) however, a mean clockwise turning of around 0.3° is observed. This is because the direction turning due to the island is zero and all the contribution originates from OWFs.

The following table summarizes the peak values in mean wave height and direction change observed at the -9 m NAP contour, as discussed in this section:

Table 5.1: Peak values of annual mean change in wave height and direction along the Dutch coast. The first value of distance corresponds to wave height change and the second one to wave direction change.

Intervention	$\Delta H_{m0}/H_{m0}{}^{\text{mean}}$ (%)	$\Delta\phi_{\text{coast}}{}^{\text{mean}}$ (°)	**Distance alongshore from Hoek van Holland (km)**
OWFs 2018	-0.3	+0.1	76, 82
OWFs 2023	-1	+0.2	44, 53
OWFs 2030	-1.5	+0.2	45, 54
Island	-2.6	-0.65	30, 28
OWFs 2030 + Island	-4	-0.65	34, 28

5.3. Coastline modeling results

This section presents the results of coastline modeling. These are the annual net sediment transport along the Dutch coast and the coastline position with respect to 2018. The effect of OWFs and an island is shown as the net change in the above quantities. The Dutch coast is divided into sections of 2 km where the results are averaged, to remove small scale fluctuations. Results are shown in years 2023, 2030 and 2050.

Locations shown in map plots of Section 5.2 are also depicted here along the horizontal axis of each image. In addition, the locations of groynes at IJmuiden and Scheveningen are indicated with dashed black lines.

To expresses the nourishment need for counteracting the effect of OWFs and an island, the gradient of the change in net sediment transport is computed. This is realized in sections of 2 km of coastline. The results are also expressed in monetary values and compared with past nourishment volumes along the Dutch coast, which took place in between March 2006 and October 2016.

Undisturbed net sediment transport and coastline change

The net sediment transport and the coastline change in the baseline case (no OWFs) are shown in Figure 5.9.

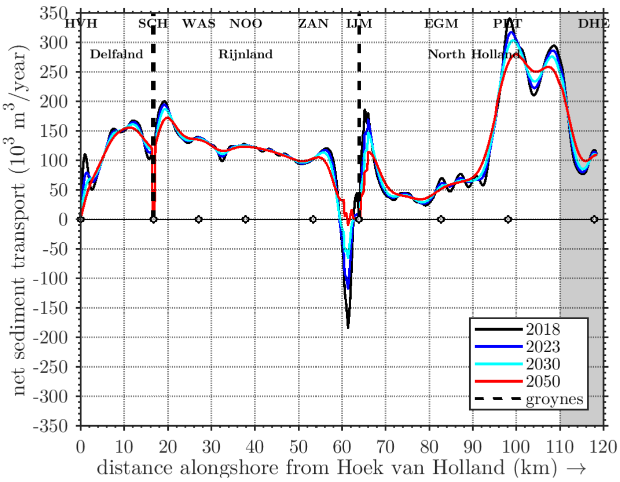

Figure 5.9: Undisturbed net sediment transport (left) and coastline change with respect to 2018 (right) along the Dutch coast.

The net sediment transport is northward directed (positive values) except for a 3 km stretch south of IJmuiden. This can be explained by looking at the initial alongshore morphology (Figure 4.4) and the dominant wave direction (Figure 5.1) in that region. Initially, the dominant wave direction is clockwise with respect to the shore normal. This results in a southward directed sediment transport (negative values). However, the positive gradient in sediment transport progressively leads to erosion and clockwise rotation of the coastal orientation. This decreases the wave approach angle with respect to the shore normal and thus the magnitude of the sediment transport. Eventually, the dominant wave direction turns counterclockwise with respect to the shore normal, resulting in a northward directed sediment transport (see the positive values in 2050).

The maximum sediment transport occurs north of Petten ($x = 100$ km) and in 2018 is equal to 340,000 m^3/year, dropping to 260,000 m^3/year by 2050. Near the groynes of IJmuiden and Scheveningen the transport is zero, since no sediment is allowed to pass through. However, bypassing is assumed near the groynes. A volume of 120,000 m^3/year is transported north of Scheveningen and a volume of 90,000 m^3/year north of IJmuiden. In the latter case, the sediment is transported from 3 locations updrift to 3 locations downdrift. This can be seen from the steps in the net sediment transport curve (indicated more clearly in year 2050, see left image in Figure 5.9). Coastline change is directly related to the gradient in net sediment transport. Positive gradients indicate erosion, negative gradients indicate accretion and changes in curvature indicate maximum erosion/accretion.

The Dutch coast is divided into three coastal cells in which sediment is predominantly redistributed. The coastal cells are divided by the groynes of Scheveningen and IJmuiden. The large jetty south of Hoek van Holland and the groyne of Scheveningen identify Delfland. The region in between Scheveningen and IJmuiden is Rijnland. Finally, IJmuiden and Den Helder define North Holland. The change in net sediment transport due to OWFs or an island is independent in each coastal cell, since sediment bypassing in the model occurs both in the baseline (no OWFs) as well as the effect situation (accounting for the effect of OWFs or an island).

OWF effect

The effect of OWFs on coastal morphology is presented in Figure 5.10. The net change in coastline is depicted with solid black bars, whereas the net change in sediment transport is presented with empty bars in blue outline.

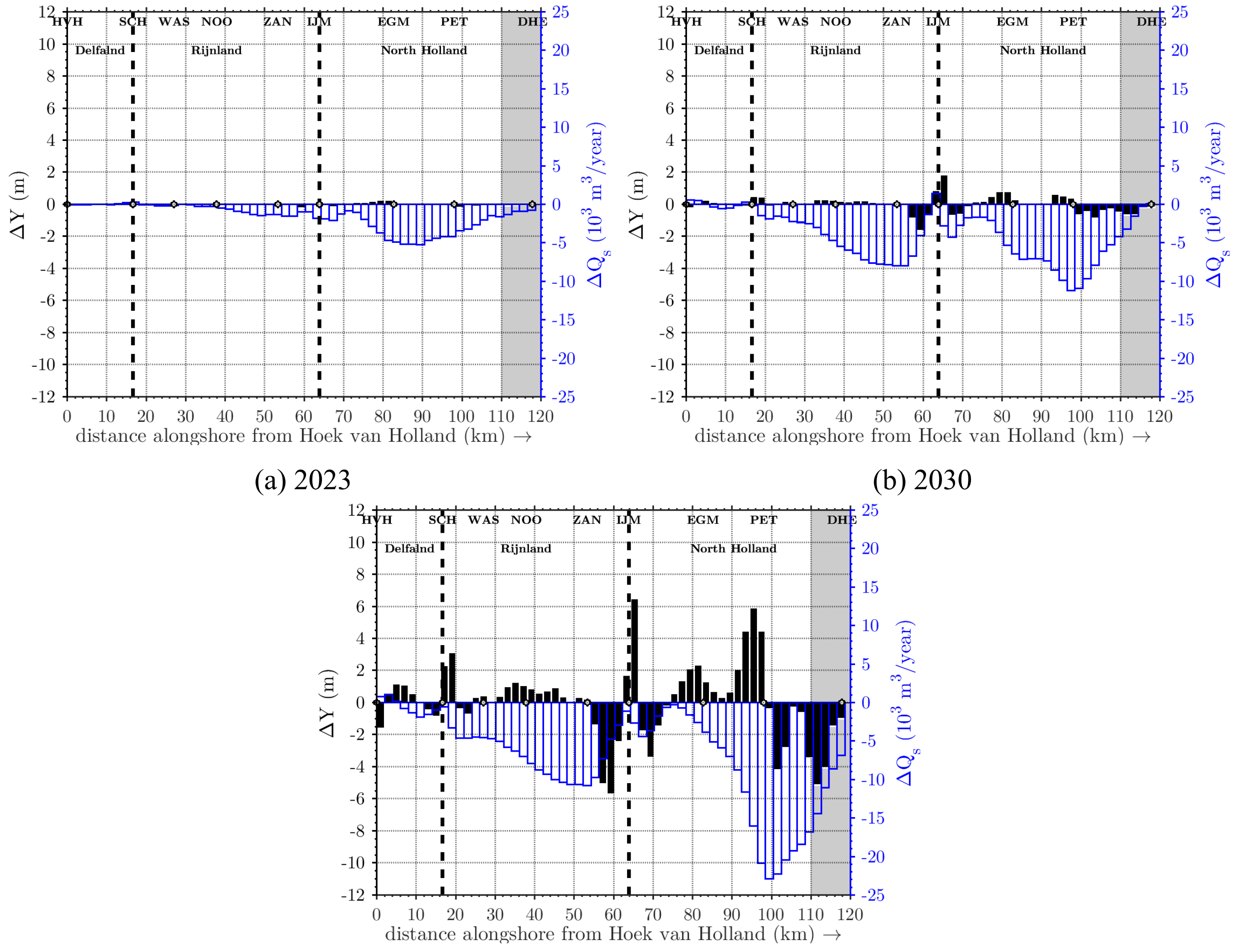

(c) 2050

Figure 5.10: Effect of OWFs on net sediment transport and coastline change along the Dutch coast. Effect in (a) 2023, (b) 2030 and (c) 2050.

The above subfigures show the change in net sediment transport and the resulting effect on coastline position in years 2023, 2030 and 2050. As previously explained, the effect in period 2018 – 2023 originates from OWFs in 2018 whereas the effect in periods 2023 – 2030 and 2030 – 2050 is due to OWFs in 2023 and 2030, respectively.

The change in net sediment transport and coastline is directly linked to the effect on wave climate. In year 2023, it is only Rijnland and North Holland that experience a decrease in net sediment transport. The greatest decrease is located south of Petten ($x = 90$ km) with a value of 5,000 m^3/year. In 2030, the effect on Rijnland is intensified due to the construction of Hollandse Kust Zuid. At that region, the greatest decrease in net sediment transport is 8,000 m^3/year, located at Zandvoort ($x = 53$ km). At North Holland the location with the greatest decrease is Petten ($x = 98$ km), with a value of 11,000 m^3/year. It is interesting to note that Petten is not the location of greatest wave height decrease (see Figure 5.3) yet it shows the greatest decrease in net sediment transport. This becomes more clear in 2050. At that moment, the greatest decrease in sediment transport is observed at the same locations as in year 2030. At Zandvoort ($x = 53$ km) it is equal to 11,000 m^3/year while at Petter it reaches a value of 23,000 m^3/year.

Island effect with and without OWFs

The effect of an energy island on coastline morphology, including and excluding OWFs, is depicted in Figure 5.11. It is reminded that the island has a size of 5 km^2 and is located approximately 30 km offshore, southwest of HKN.

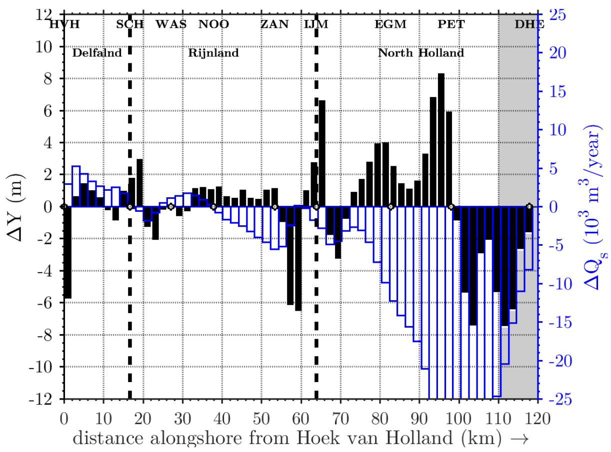

(a) 2050 Island and OWFs

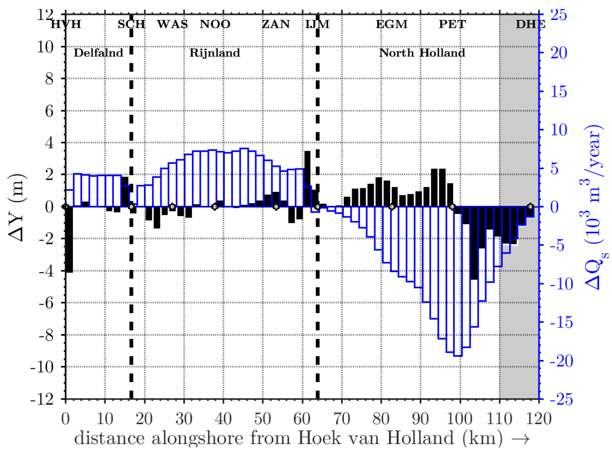

(b) 2050 only Island

Figure 5.11: Effect of 5 km^2 island located around 30 km offshore on net sediment transport and coastline change, including OWFs (left) and excluding OWFs (right).

Contrary to OWFs that show little effect in Delfland in 2050, an increase in sediment transport is observed due to the island. The net increase continues northward, all the way within the Rijnland region, with a peak value of 7,500 m^3/year in between Wassenaar and Zandvoort ($x = 45$ km). The net increase in the region of Delfland and Rijnland indicates that the mean counterclockwise change in wave direction (0.65°) is more dominant than the mean wave height decrease (2.6%), both resulting from the island alone. On the other hand, in the North Holland region, a net decrease in sediment transport is computed, which means that the mean decrease in wave height dominates over the (almost zero) mean change in wave direction (see Figure 5.7). The greatest decrease in net sediment transport is computed at Petten ($x = 98$ km) and is equal to 19,000 m^3/year. Note that, since the net effect of the island is considered, the results for coastline change refer to a duration relative to 2030, which is the moment when the island is assumed to be realized. Therefore, when referring to 2050 the time horizon is 20 years and not 32 (as is the case with OWFs).

The increase in net sediment transport in Delfland and in the southern part of Rijnland is still visible when combining the island with OWFs. It is clear however that the increase is lower compared with the island alone, since OWFs result in an additional decrease in wave height, which counteracts the increase in net sediment transport due to the island alone. In Delfland, the greatest increase in sediment transport is located north of Hoek van Holland ($x = 3$ km) and is equal to 5,000 m^3/year. In Rijnland, the greatest increase is located in between Wassenaar and Noordwijk ($x = 32$ km) and amounts to 2,000 m^3/year, while the greatest decrease is located at Zandvoort ($x = 53$ km) and is equal to 5,000 m^3/year. The peak value of decrease in net sediment transport is located at North Holland, where the contribution from both the OWFs and the island has the same sign. In 2050, the peak decrease is more than 25,000 m^3/year, located at Petten ($x = 98$ km).

The following table summarizes the information regarding the locations of maximum increase or decrease in net sediment transport, as discussed in this section.

Table 5.2: Peak values of change in net sediment transport along the Dutch coast due to OWFs or an island. Distance is indicated with respect to Hoek van Holland.

Year - Intervention	**Peak increase (m^3/year)**	**Alongshore distance (km)**	**Peak decrease (m^3/year)**	**Alongshore distance (km)**
2023 - OWFs	–	–	5,000	90
2030 - OWFs	–	–	8,000 ; 11,000	53 ; 98
2050 - OWFs	–	–	11,000 ; 23,000	53 ; 98
2050 - Island	7,500	45	19,000	98
2050 - OWFs + Island	5,000	3	5,000 ; > 25,000	53 ; 98

Nourishment need

To get an estimate of the necessary nourishment volumes along the Dutch coast for counteracting the effect of OWFs and an island, the gradients of the change in net sediment transport are computed. These are shown with black bars in Figure 5.12.

In addition, the nourishment need is expressed in monetary values, assuming a price of 8 €/m^3 [4]. The equivalent cost is depicted on the right hand side of every image. Positive gradients are associated with net erosion, indicating nourishment need. Therefore, only these are shown in the images below.

In 2023, OWFs result in a maximum nourishment need of 0.4 m^3/m north of IJmuiden ($x = 68$ km) and at Petten ($x = 98$ km). In addition, smaller nourishment volumes of around 0.25 – 0.3 m^3/m are computed north and south of Petten ($x = 71$ km and $x = 58$ km). In 2030, the areas

[4] The price is just an indication. The aim is not to show exact values but rather define an order of magnitude.

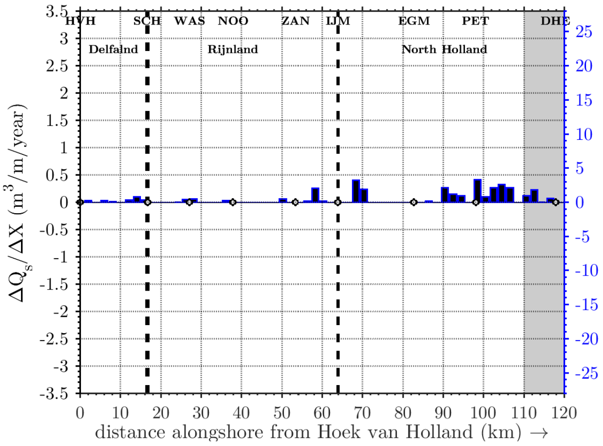

(a) 2023

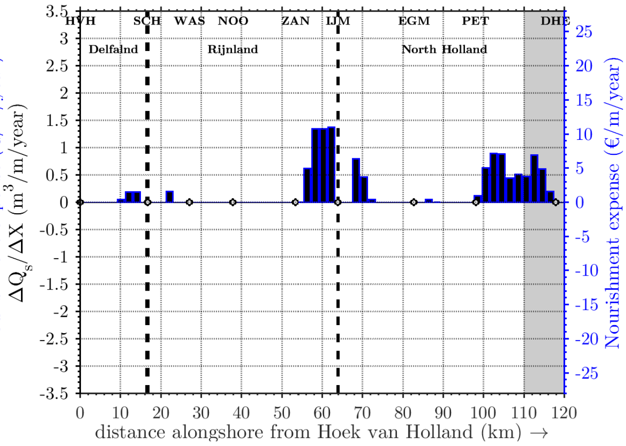

(b) 2030

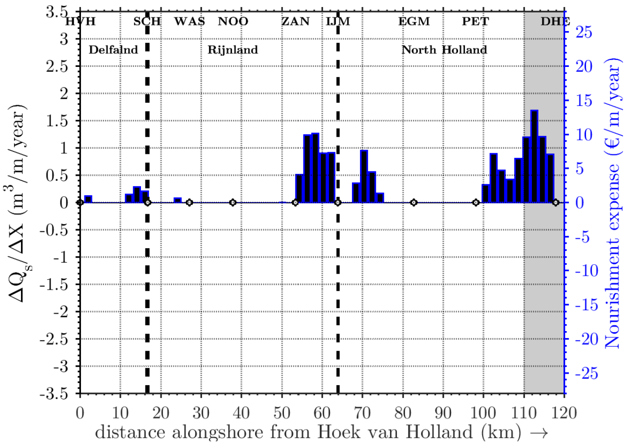

(c) 2050

Figure 5.12: Nourishment volumes along the Dutch coast for counteracting the effect of OWFs. Negative gradients (indicating net accretion) are excluded from the images.

between Zandvoort and IJmuiden ($x = 55 - 64$ km) as well as the region between Petten and Den Helder ($x = 98 - 118.5$ km) need to be supplied with a volume of 1.3 m^3/m and 0.8 m^3/m respectively. In addition, local nourishment volumes of 0.2 m^3/m need to be provided north and south of Scheveningen ($x = 23$ km and $x = 14$ km) and 0.75 m^3/m should be supplied north of IJmuiden ($x = 68$ km). In 2050, the maximum nourishment volumes slightly decrease to 1.25 m^3/m in between Zandvoort and IJmuiden ($x = 55 - 64$ km) while in the region between Petten and Den Helder ($x = 98 - 118.5$ km) the nourishment volume increases, with a maximum of 1.7 m^3/m at $x = 114$ km.

From the results it becomes obvious that the areas that need attention are the northern parts of Rijnland and North Holland ($x = 55 - 64$ km and $x = 98 - 118.5$ km) as well as the area north of IJmuiden ($x = 68 - 76$ km). Within these regions the greatest nourishment volumes are found near Zandvoort and Petten ($x = 58$ km and $x = 114$ km respectively). These are characterized as hot-spots resulting from the cumulative effect of OWFs.

The effect of an energy island in 2050, including and excluding OWFs, is shown in Figure 5.13.

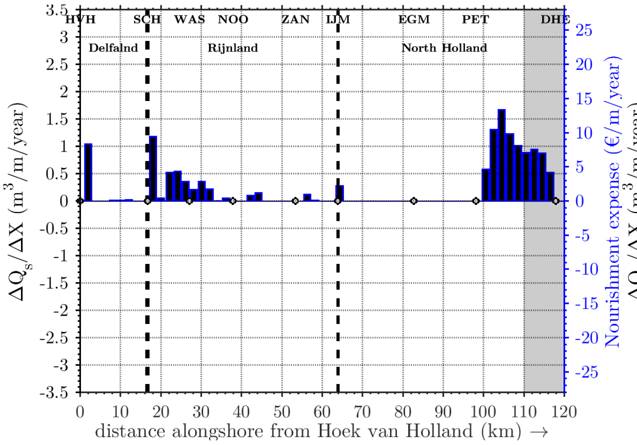

(a) 2050 only island

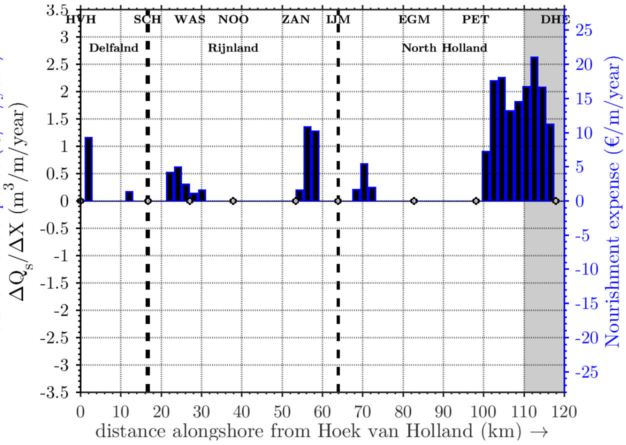

(b) 2050 island and OWFs

Figure 5.13: Nourishment volumes along the Dutch coast for counteracting the effect of a 5 km^2 island located 33 km offshore. Situation with (right) and without (left) OWFs. Negative gradients (indicating net accretion) are excluded from the images.

For the island alone in 2050, 1 m^3/m of nourishment is needed north of Hoek van Holland (x = 2 km) and north of Scheveningen (x = 15 km). In addition, sediment should be supplied in the coastal stretch between Scheveningen and Noordwijk ($x = 22 - 33$ km), with a maximum volume of 0.5 m^3/m, while sediment should be provided in between Petten and Hoek van Holland ($x = 100 - 118.5$ km), with a maximum of 1.7 m^3/m. Including the OWFs counteracts the nourishment need north of Scheveningen, shifting the effect close to IJmuiden, with volumes of up to 1.35 m^3/m at $x = 58$ km and 0.7 m^3/m at $x = 70$ km. The nourishment volumes in between Petten and Den Helder ($x = 100 - 118.5$ km) increase significantly, reaching a maximum of 2.6 m^3/m at $x = 113$ km.

Looking again at the nourishment need when including an island, it becomes clear that the effect is counteracted at Rijnland and Delfland, while it is intensified at North Holland. This is in accordance with the effect on wave climate as seen in Figure 5.8.

To understand the significance of the computed nourishment need, this is compared with past nourishment volumes along the Dutch coast, which took place in the period between March 2006 and October 2016. These are shown in Figure 5.14. It can be seen that past volumes are two orders of magnitude greater than the computed nourishment need. In the worst case scenario (comparing the maximum nourishment need of 2.6 m^3/m with the minimum nourishment volume of 235 m^3/m) an additional 1.1% of additional nourishment volume needs to be accounted, to counteract the effect of OWF developments and a 5 km^2 island located around 30 km offshore.

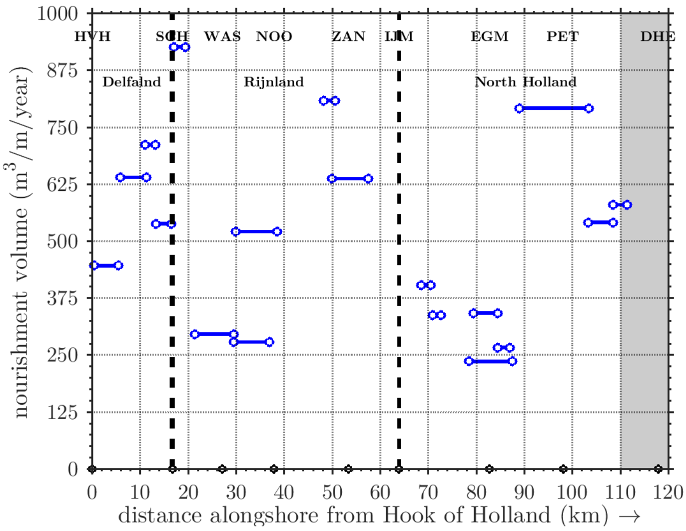

Figure 5.14: Nourishment volumes at the Dutch coast in between March 2006 and October 2016 (Rijkswaterstaat, 2017).

6

Discussion

This chapter discusses the results presented in Chapter 5. It is divided into two sections dealing with wave and coastline modeling respectively. The goal is to understand the reasons behind the effect of OWFs and an island on wave climate and coastal response. The obtained knowledge aims at determining a framework for identifying the chain of effects due to future large-scale OWFs and suggesting alternative OWF designs for the benefit of the Dutch coast. Ultimately, this chapter prepares the ground for answering the research questions defined in Chapter 1.

6.1. Effect on wave climate

OWF effect

In this study, existing and future designated OWFs in the North Sea are categorized into development stages, accounting for years 2018, 2023 and 2030, with a distance from the Dutch coast approximately equal to 10 – 20 km, 20 km and 40 – 80 km and an average OWF size equal to 20 km^2, 300 km^2 and 500 km^2, respectively. In addition, hypothetical OWF scenarios are considered for year 2050, located around 80 – 100 km offshore, with an average size of 700 km^2.

In 2018 the effect is insignificant. The greatest influence is found in the shadow of OWEZ, in the region between IJmuiden and Egmond, with a mean wave height decrease of 0.3% and a mean change in wave direction equal to 0.1° (Figure 5.2). The effect is significantly intensified in 2023. The greatest influence is shifted to the region between Noordwijk and Zandvoort, with a mean wave height decrease of 1% and a mean change in wave direction equal to 0.2° (Figure 5.3), mainly caused by the HKZ wind farm. In general, the additional effect on wave height in 2023 is more than two times greater compared to 2018, thus making the influence of wind farms in 2023 extremely superior compared to 2018. OWFs in 2030 further intensify the influence on wave height, leading to a mean wave height decrease of 1.5% (Figure 5.5). This is an additional 50% on the wave height decrease in 2023, indicating that the effect of OWFs in 2030 (mainly IJmuiden Ver, HKW, HKNW and HKZW) on the nearshore wave climate is significant. However, the wind farms in 2030 do not show additional change in wave direction. This leads to the conclusion that the wave direction is mostly affected by OWFs developed closer to the coast. The hypothetical OWFs in 2050 do not add any significant contribution to the already existing effect (Figure C.1), showing that OWFs developed even further offshore will not affect the nearshore wave climate of the Netherlands.

The above results indicate that the mean tendency of existing and future OWFs in the North Sea is to decrease the wave height and cause a slight change in wave direction. The effect becomes stronger with time, with the construction of more and larger OWFs. Assuming a constant decrease in wind speed within the OWFs, it is found that a greater wind farm area causes a greater effect on the nearshore wave climate. The wave direction is only affected by OWFs developed until 2023, located around 20 km away from the Dutch coast. The effect on wave height continues to exist for OWFs constructed until 2030, located around 40 – 80 km offshore.

The added effect on the nearshore wave climate is less significant for OWFs developed further offshore. However, this statement might be only valid for OWFs developed within a moderate spatial footprint in the North Sea. This is demonstrated in Figure 6.1. The image shows two development zones that cover the same area and are both located more than 40 km away from the Dutch coast. In the first case (area A), OWFs are developed all the way across the entire North Sea, while in the second one (area B) OWFs are developed in the southern part of the North Sea, in what is called ”a moderate spatial footprint”. Even though both zones are located far away from the Dutch coast, such that the effect on the nearshore wave climate is insignificant, zone A could still result in a significant effect on waves approaching the Dutch coast. This is because waves that propagate within area A are affected over the greatest part of their fetch length. Different orientations of the areas depicted in the image could lead to an optimum spatial planning, which causes the least influence on the nearshore wave climate of the Netherlands.

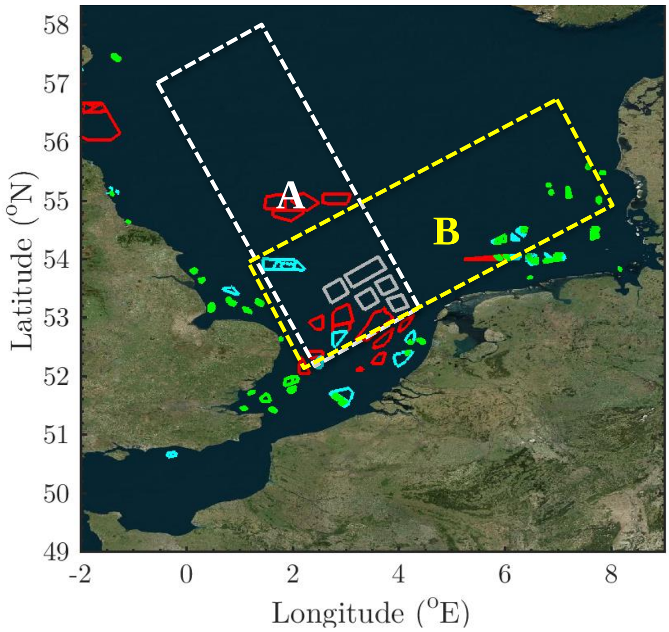

Figure 6.1: Possible scenarios of spatial planning for future OWF developments. Two areas are indicated (A and B), having the same size and located more than 40 km km away from the Dutch coast. Area A might result in a greater effect on the nearshore wave climate of the Netherlands, compared to area B.

Comparison of OWF effect with literature findings

Literature findings on the effect of a single OWF on wave climate were presented in Table 2.2. The interest in this section is mainly focused on the effect in the nearshore, which is expressed by the Far-Field effect (FF), referring to changes at least 2 km downwind of an OWF.

The results of the underlying study are within the same order of magnitude with what is addressed in literature. The rather small decrease of 0.1% to 0.3% computed by Beiboer and Cooper (2002) is accounted to the small OWF size (5 km^2) and the fact that no decrease in wind speed was assumed. The great decrease of 6.7% found by Rodriguez Gandara and Harris (2012) is due to the large OWF area (663 km^2 – comparable to IJmuiden Ver OWF, see Figure 1.3) in combination with the rather short OWF distance from the coast (12 km).

Results from Alari and Raudsepp (2012) and Christensen et al. (2013) are closer to the values computed in this thesis. The OWF areas of these studies are in between 20 km^2 and 40 km^2, smaller than most of the OWFs in the current work but located closer to the coast (5 – 20 km). In addition, contrary to the approach followed in this thesis, Alari and Raudsepp (2012) did not consider a change in wind speed and used an assumption of linear scaling to account for the dissipation due to turbine monopiles. On the other hand, the approach of Christensen et al. (2013) is more relevant to what was done in this thesis and it is quite satisfactory that the results (wave height decrease of 1%) are also closer to our findings.

It should be noted however that no study investigates the cumulative effect of large-scale OWF developments. All works consider a single OWF with an area smaller than the average size of future OWF developments in the North Sea. This means that such OWFs do not fall under the category of "large-scale OWF developments". Only Rodriguez Gandara and Harris (2012) study a rather big OWF, but this is located extremely close to the coast. Therefore, it is not relevant to make more detailed comparisons between the current work and literature references. Comparisons are only made on the order of magnitude of the effect on wave height. In that respect, the results are satisfactory.

Island effect

In addition to OWFs, a 5 km^2 energy island is modeled, located southwest of HKN, around 30 km away from the Dutch coast. The island alone affects a smaller region compared to OWFs. The greatest influence is found in between Wassenaar and Noordwijk with a mean wave height decrease of 2.6% and a mean change in wave direction equal to 0.65° (counterclockwise, see Figure 5.7). These values are 1.6 and 3.2 times greater than the effect of OWFs in 2030, indicating that the effect due to the schematized island is stronger, yet spread in a smaller region along the Dutch coast.

The fact that the island shows a greater influence compared to OWFs might not always be the case. The result found here is based on one specific island case. Different island shapes, sizes, locations and design criteria (type of protection against waves – e.g breakwater vs artificial shoreface; type of island foundation – e.g. landfill vs floating island etc.) should be tested, to derive more solid conclusions.

OWFs and Island effect

Combining OWFs with the island results in a much greater effect on the nearshore wave climate, leading to a value of 4% in mean wave height decrease, located in between Wassenaar and Noordwijk (Figure 5.8). The two interventions however give opposite contributions on the effect on wave direction. This can only be seen though in the northern part of the Dutch coast, since in the South the effect of the island is much stronger compared to OWFs; the change in wave direction is equal to 0.65° which is already caused by the island alone.

6.2. Mechanism of the effect on wave climate

As discussed above, OWFs and an island affect the wave climate by decreasing the significant wave height and by causing a slight change in wave direction (or a turning in energy propagation). To better understand this effect, idealized wave simulations were performed, assuming a moderate wind speed of 12 m/s, blowing from NNW above the entire SWAN-DCSM and SWAN-HCWD domains. This section points out the main findings, while extensive results are presented in Appendix D.

Regarding OWFs the decrease in wave height is directly caused by the less energy input due to wind within the OWF areas. As for the island, the decrease in wave height is due to shielding of wave energy in the shadow area, since the incoming wave energy is absorbed by the obstacle. Wave energy at each point in space consists of components traveling from multiple directions. Therefore, a directional space is identified at each location within the computational grid. For the idealized simulations, the directional space consists of the W – NE sector (270°N – 30°N). An example of the energy distribution within the directional space is given in Figure D.5. The resulting directional width is quite big compared to reality, but this could be attributed to the assumption of a rather low wind speed (12 m/s) above the entire computational domain.

The change in wave direction can be explained by the fact that directional components that travel over longer distances within the OWF areas are affected more than the other directional components. This is illustrated in Figure 6.2.

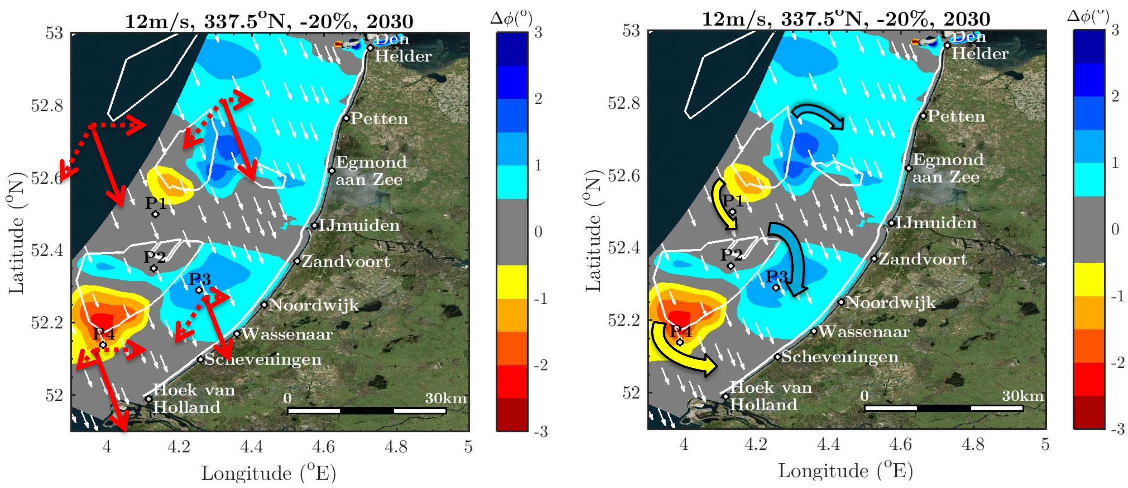

Figure 6.2: Mechanism of wave direction change due to OWFs. Left image: solid red arrows indicate the dominant direction of wave energy. Dashed red arrows define the directional width of the spectrum. The length of the arrows qualitatively indicates the magnitude of wave energy. Right image: yellow arrows indicate counterclockwise rotation and blue arrows clockwise rotation of wave direction.

The solid red arrows in the left image indicate the dominant energy directional component (containing the most energy) whereas the dashed arrows show the components defining the directional width of the spectrum. Looking at location P4, southwest of Hollandse Kust Zuid (HKZ), the NE component has traveled a greater distance within the OWF area compared to other components. In that case, the energy approaching P4 from that direction is significantly reduced. Therefore, the mean direction at P4 (taken as the average over all directions within the directional space) will turn counterclockwise with respect to the baseline situation (no OWF present). The opposite happens at location P3 at the eastern side of HKZ, since it is the western component that travels a greater distance within the OWF. At other locations the same reasoning applies. In regions surrounded by multiple OWFs, the cumulative effect is observed. This leads to a pattern of clockwise and counterclockwise turning in wave direction, as shown on the right image in Figure 6.2.

Regarding an island the same mechanism applies. This is illustrated in Figure 6.3.

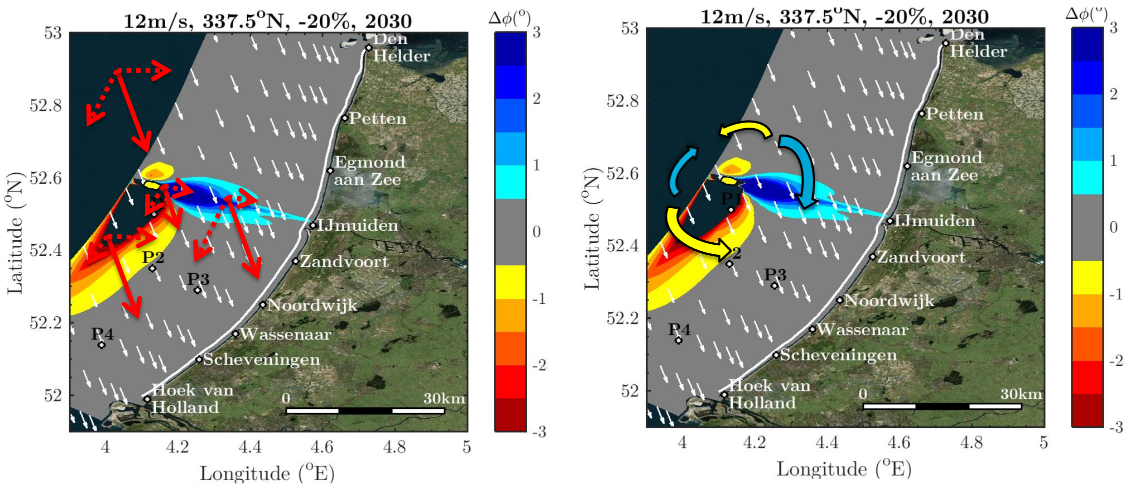

Figure 6.3: Mechanism of wave direction turning due to an island. Left image: solid red arrows indicate the dominant direction of wave energy. Dashed red arrows define the directional width of the spectrum. The length of the arrows qualitatively indicates the magnitude of wave energy. Right image: yellow arrows indicate counterclockwise rotation and blue arrows clockwise rotation of wave direction.

Immediately downwind of the island, along the dominant directional component (indicated with the solid red arrow) the turning is zero because energy from every direction is equally absorbed by the obstacle. Moving away from the dominant energy direction (to the NE or to the SW, looking at the specific example in Figure 6.3) a turning in wave direction is observed. In addition, north of the island, regions of counterclockwise and clockwise[1] turning are observed because wave energy is partially reflected. This leads to the rotation pattern of wave direction, displayed on the right image in Figure 6.3.

6.3. Effect on coastal morphology

Changes in net sediment transport are directly linked to the effect on wave climate. Regarding OWFs, the effect is a decrease in net sediment transport along the entire Dutch coast (see Figure 5.10). For the energy island two situations are identified. In case the decrease in wave height is accompanied by rather small changes in wave direction, a decrease in net sediment transport is observed. This happens in the northern part of the Dutch coat. When the decrease in wave height happens together with a big a counterclockwise change (indicating an increase in the angle

[1]The region of clockwise turning upwind of the island cannot be seen in Figure 6.3, because it is located outside the boundaries of the computational domain. However, this has been confirmed by looking at results in the SWAN-DCSM domain.

of approach with respect to the coast), the net sediment transport increases. This happens in the southern part of the Dutch coast (see right panel in Figure 5.11).

More specifically, the Dutch coast is divided into three coastal cells, namely Delfland, Rijnland and North Holland. Changes in net sediment transport are insignificant in Delfland compared to the other coastal cells. Considering OWF developments, in 2023 the decrease in net sediment transport shows a peak of 5,000 m^3/year near Egmond. In 2030, the region of Rijnland experiences a decrease of 8,000 m^3/year, located at Zandvoort, while in North Holland a decrease of 11,000 m^3/year is observed at Petten. The same locations experience a decrease of 11,000 m^3/year and 23,000 m^3/year respectively, in 2050.

An island results in an increase of 7,500 m^3/year in Rijnland, located in between Wassenaar and Zandvoort and a decrease of 19,000 m^3/year in North Holland and more specifically at Petten. Combining OWFs with an island reduces the effect in Rijnland and intensifies the impact in North Holland where a decrease of more than 25,000 m^3/year is observed at Petten.

Upon initial inspection, the maximum decrease in net sediment transport observed at Petten is counter-intuitive, since the wave height decrease is greater at Zandvoort, while the change in wave direction is nearly the same at both locations.

However, when drawing results on the effect on the alongshore sediment transport, it is important to consider the change in angle of approach and the change in sediment transport, reflecting on the baseline values. By qualitatively looking at the dominant wave direction at Zandvoort and Petten (see upper right image in Figure 5.1), it can be concluded that the angle of approach with respect to the coast is slightly smaller at Zandvoort compared to Petten. Also, based on the left image in Figure 5.9, the baseline value of the net sediment transport at Petten is bigger compared to Zandvoort. This indicates that, for the same effect on the wave climate, the change in net sediment transport will be bigger in Petten compared to Zandvoort. To better illustrate this, the $S - \phi$ curves at Zandvoort and Petten, for both the baseline case as well as the OWF and an island cases, are presented in Figure 6.4.

It can be seen that the magnitude of net sediment transport for different wave approach angles with respect to the coast is smaller at Zandvoort compared to Petten. In addition, the current wave approach angle with respect to the coast is bigger at Petten compared to Zandvoort. Therefore, even thought the wave height decrease is smaller at Petten, the above factors result in a greater decrease in net sediment transport compared to Zandvoort.

Nourishment need

To determine the nourishment need for counteracting the effect of OWFs and an island, the gradients of the change in net sediment transport were computed. Positive gradients are only shown, since these indicate net erosion of the already evolving coastline. It was found that the regions north of Zandvoort and north of Petten need the greatest nourishment volumes. In addition, to identify the significance of nourishment need, this was compared with past nourishment volumes

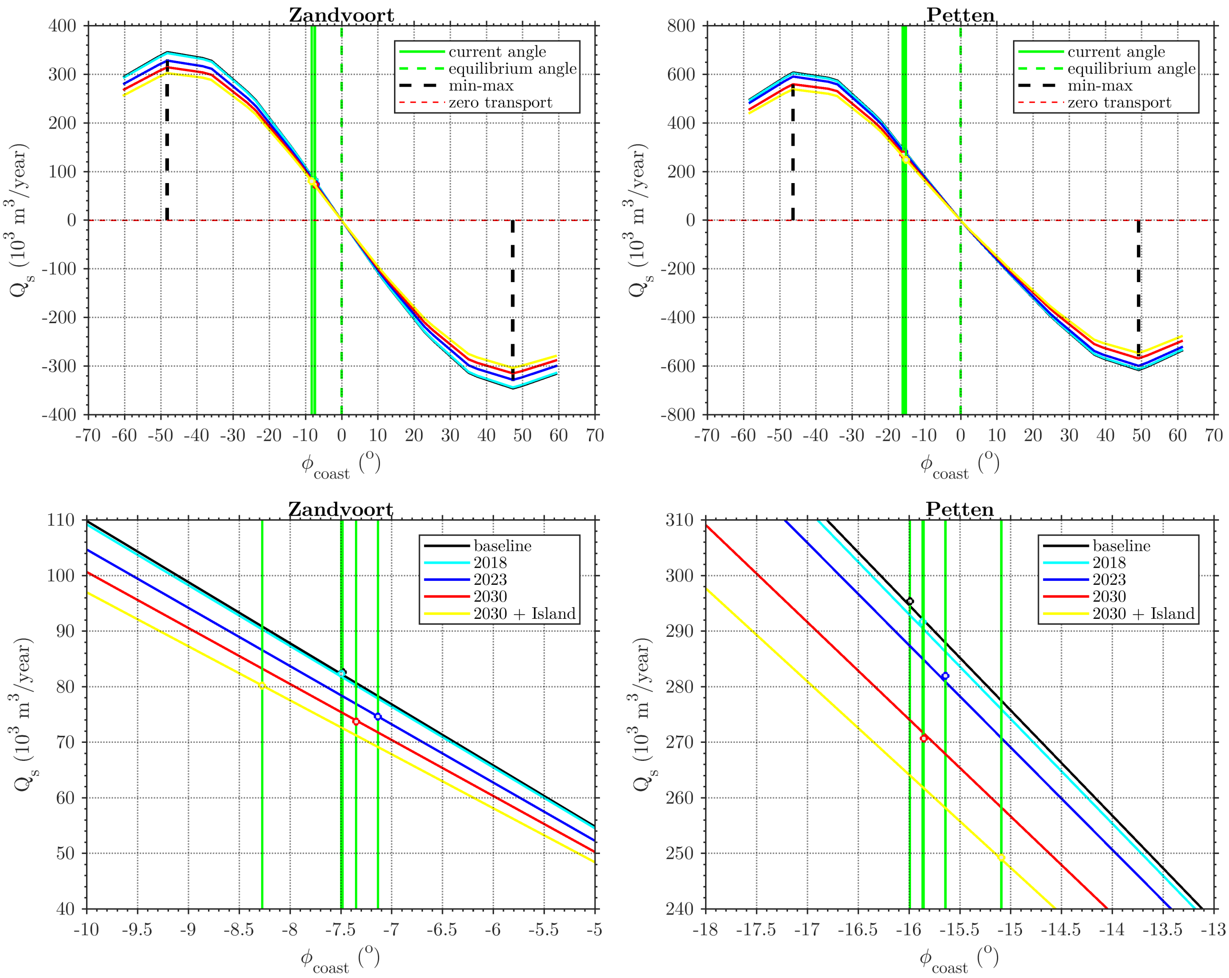

Figure 6.4: $S-\phi$ curves at Zandvoort (upper left) and Petten (upper right) for the undisturbed situation (black line) and the effect of OWFs in 2018 (cyan line), 2023 (blue line), 2030 (red line) and 2030 including an energy island (yellow line). The images below are zoomed areas close the current wave approach angle with respect to the coast, at Zandvoort (lower left) and Petten (lower right).

at the Dutch coast. It was found that, in the worst case scenario, only 1.1% of additional volume needs to be accounted for counteracting the effect of OWF developments together with an island in the future.

An alternative approach however could be to redesign or relocate the OWF areas, such that the effect on coastal morphology is diminished. To reach a final decision though, an analysis on the potential cost of different OWF designs in relation to the additional nourishment expense should be carried out.

Incorporating findings on Dutch coastal maintenance policy

The effect of OWF developments on the coastline response of the Dutch coast was found to be an order of 5,000 – 25,000 m^3/year decrease in net sediment transport. Looking back at the baseline values in Figure 5.9 this is around 10% of the baseline rates. The significance of that result can be studied in many ways one of which is comparing the nourishment need with current nourishment volumes along the Dutch coast. Since the nourishment need was found to be just 1.1% of additional volume, in case the change in sediment transport is less than 10% of the baseline rates, it is questionable to what extent the offshore developments can be used to support the coastline maintenance strategy.

7

Conclusions and recommendations

Conclusions

- The change in wave climate due to OWFs can be attributed to the location, orientation, shape and size of the individual wind farm areas.
- Future, large-scale OWFs in the North Sea affect the nearshore wave climate of the Dutch coast by causing a mean change in significant wave height in the order of 1 – 2 % and a slight rotation in wave direction.
- The combined contribution of future OWFs and a 5 km^2 energy island located around 30 km away from the Dutch coast results in a mean change in significant wave height in the order of 4% and a mean change in wave direction of around 0.60° in the nearshore.
- The decrease in wave height due to OWFs with respect to a baseline situation (no OWFs present) is caused by the less energy input inside the wind farm areas (assuming wind speed decrease). Moreover, the decrease in wave energy is greater for components that travel a longer distance within the OWF areas. This means that the components approaching a location near a wind farm are not equally affected by the OWF itself. Therefore, when looking at the directional domain of the spectrum at such locations, a slight rotation in mean wave energy direction (computed as the average direction within the directional domain of the spectrum) is observed. A similar mechanism applies to an island, since it absorbs the incoming energy.
- The effect on net sediment transport is an additional 1% of nourishment volume to the already applied annual volumes along the Dutch coast.

- The effect on the alongshore sediment transport due to the changing wave climate depends on the baseline values in sediment transport and wave approach angle.
- The location, shape and size of future offshore wind farms in the North Sea are parameters the could influence the coastline dynamics of the Dutch coast.

Recommendations for further research

- Define a cumulative layout for large-scale OWF developments in the North Sea (width, orientation) so that the effect on the nearshore wave climate works for the benefit of the Dutch coast.
- Explore OWF design parameters in relation to the effect on the Dutch coast.
- Investigate hot-spots on a smaller spatial scale.
- Study the effect of OWFs in relation to other long-term effects (such as sea level rise)
- Study the effect of OWFs on the vertical motion of the ocean and the coastal upwelling-downwelling.

7.1. Conclusions

Conclusions from this work are directly drawn by answering the research questions, stated in Section 1.5.

1. **What is the effect on the nearshore wave climate along the Dutch coast resulting from various OWF development stages in the North Sea?**

   Given the currently available roadmap for offshore wind development until 2050, this study has demonstrated that future, large-scale offshore wind farm developments in the North Sea have an effect on the nearshore wave climate of the Dutch coast. The effect was found to be a mean change in significant wave height in the order of 1 – 2 %. Also, slight changes in wave direction were observed.

   The relatively small OWFs in 2018, at an approximate distance of 10 – 20 km from the Dutch coast, hardly affect the nearshore wave climate, while OWFs in 2023, located around 20 km offshore and having an average size of 200 km^2, add more than two times the effect on wave height in the nearshore, compared to 2018. OWFs developed around 2030, located around 40 – 80 km offshore and having an average size of 500 km^2, result in a 50% additional decrease in wave height in the nearshore compared to 2023, but add no further effect on wave direction.

   The combined contribution of OWFs in 2030 together with a 5 km^2 energy island west of HKZ, located around 30 km away from the Dutch coast, further intensifies the effect one the nearshore wave climate, leading to a mean wave height decrease in the order of 4% and a change in wave direction in the order of 0.6° (rotating counterclockwise).

   (a) **How can we explain these phenomena?**

   The change in wave climate can be attributed to the location, orientation, shape and size of the individual wind farm areas. Bigger wind farm sizes result in greater change in wave height and direction. Also, an OWF located further from the coast shows less impact on the nearshore wave climate.

   The decrease in wave height due to OWFs is caused from the less energy input by wind inside the OWF areas. The study also revealed that the slight change in wave direction is attributed to directional components that travel longer distances within the OWFs, which therefore lose more energy compared to other directional components. As a result, the mean wave direction, which is computed as the average direction over the whole directional domain, shows a slight rotation compared to the undisturbed case (no OWFs). A similar mechanism applies to an island, which directly absorbs the incoming wave energy.

2. **What is the change in net sediment transport along the Dutch coast resulting from various OWF development stages in the North Sea?**

   This study has demonstrated the effect of the changing wave climate on the alongshore morphology of the Dutch coast. This is a decrease in net sediment transport in the range of 5,000 – 25,000 m^3/year. Including an island together with OWFs intensifies the decrease to more than 25,000 m^3/year. The locations experiencing the greatest effect are Zandvoort and Petten.

   (a) **How is this change related to the effect on wave climate?**

   Regarding wave climate, the alongshore sediment transport depends mainly on two variables in the nearshore: the wave height and the wave angle of approach with respect to the coast. A decrease in wave height and/or a decrease in the wave angle of approach with respect to the coast results in a decrease in net sediment transport. The magnitude of the decrease however depends on the baseline value of the above variables.

3. **Can we plan the development of large-scale OWFs in the North Sea, for the benefit of the Dutch coast?**

   This study draws results considering only the future designated OWF areas in the North Sea. From the general findings it can be concluded that the location, shape and size of the OWFs affects the wave climate (wave height and direction) in the nearshore. Therefore, these parameters could influence the coastal dynamics of the Netherlands.

   (a) **How close to the Dutch coast is the effect from existing and future OWFs significant for affecting the alongshore morphology?**

   It has been found that the hypothetical OWF developments in 2050, at an approximate distance of 80 – 100 km from the Dutch coast, are not expected to influence the alongshore morphology. On the other hand, OWFs developed in 2023 and 2030, located in between 20 – 80 km away from the Dutch coast are expected to significantly affect the wave climate. The above findings suggest that the region of insignificant OWF influence lies in between 80 km – 100 km offshore. In addition, results showed that an energy island of 10's of km^2 is not expected to have an effect on the nearshore wave climate, as long as it is located 70 km away from the Dutch coast.

   (b) **Can we identify locations (hot-spots) of significant erosion and thus nourishment need?**

   The study identifies locations of greatest nourishment need immediately north of Zandvoort and north of Petten. These areas require nourishment volumes in the order of 1 – 1.5 m^3/m. Adding an island together with OWFs increases the nourishment need at

Petten to around 2.5 m^3/m. These volumes account for just 1% of currently applied nourishment at the Dutch coast.

(c) **What knowledge have we acquired on future design of OWFs?**

Even thought the effect of future OWFs on the wave climate and alongshore sediment transport is marginal, the study approach has proved to be effective in quantifying the chain of effects of OWFs and made it possible to identify potential hot-spots along the Dutch coast. Therefore, the knowledge acquired from these effects can be used to optimize future wind farm planning in relation to coastline maintenance policies.

7.2. Recommendations

The work presented in this thesis is an exploratory study to understand the effect of OWFs on the nearshore wave climate and the coastal response of the Dutch coast. In that respect, it is believed that the current work can be supported by many follow-up studies. Recommendations for further research are presented below.

Recommendations for technical improvements of current work

- **Wind effect schematization**

  This study assumed a constant wind speed decrease of 20% inside the OWF areas, taken as an average of maximum values observed in literature. Additional parameters, such as the influence of a wind farm wake that can extend for many kilometers downwind, has not been considered here. In addition, the characteristics of the individual turbines (hub height, rotor diameter) are expected to further influence the 10-m wind speed. Taller and larger wind turbines will harvest more wind energy thus further reducing the wind speed at hub height. It is questionable however whether this will lead to a decrease in wind speed 10 m above the water surface, since the extraction of wind energy will take place at an even greater height. Nevertheless, it has been found that the high turbulence in the vertical might cause an increase in 10-m wind speed. In any case, schematizing the wind climate including more physics on the effect of OWFs on wind is highly recommended. However, it should be taken into account that there is still lot of knowledge to be obtained in this field.

- **Domains of interest**

  It is also recommended to decrease the domain of interest and more specifically the wind input grid. In this study a wind field covering the whole North Sea was used, where the wind speed was reduced inside the OWF areas. This resulted in a lot of pre-processing time for generating the modified wind input files (1 year of wind input corresponded to a size of approximately 30 gigabytes). Using a smaller domain for wind input neglects the effect caused by OWFs further offshore, but it has already been found that these add an insignificant contribution to the nearshore wave climate.

An alternative solution could be to consider a smaller representative duration for computations or even schematize the wind input into climates. By introducing scenarios of different wind speed magnitude and direction instead of a full hindcast of varying wind speed in space and time, will tremendously decrease the post-processing time. The approach to do so however, should make sure that the schematized wind climate properly represents the long-term wind speed statistics at the entire North Sea.

- **Wave modeling**

  It has been found that non-stationary computations show inconsistencies regarding the relative change in wave height. However, a non-stationary run is more ideal when large areas are modeled. Therefore, it is recommended to explore the potential for performing non-stationary computations.

  It is also advised to consider currents, at least in the domain close to the coast, since the wave-current interaction is significant in the nearshore and also affects coastal morphology. The same applies to water level fluctuations, such as tidal motion.

  In addition, if a more detailed modeling approach is needed, it is recommended to include the wind turbine monopiles. If the domain resolution is bigger than the turbine diameter it, is advised to use an approach of linear scaling similar to Alari and Raudsepp (2012).

- **Coastline modeling**

  Regarding coastline modeling it is suggested to obtain more representative JARKUS data. In the current work the profiles and the initial coastline position were based on period 2003 – 2005 while the wave hindcast was carried out for 2016. This difference is merely accounted by assuming a spin-up period of 5 years in coastline modeling, so that the initial coastline represents the situation in 2008 – 2010. However, it is important to realize the objective of the research. The current work does not aim at forecasting the coastline response at a specific moment in the future but rather explores the effect on waves and coastline dynamics by schematizing the time-dependent OWF developments into stages.

  It is also important to note that in general the depth of closure should be more properly defined. Here it was assumed to be located at the -9 m NAP contour. This was found to be satisfactory in this work but this might not always be the case. The depth of closure depends on the timescale of the period investigated. For larger timescales the depth of closure increases. An increasing depth of closure means that, for the coastline model to properly compute the sediment transport, the output from the wave model should be retrieved at deeper water. Nevertheless, the depth of closure directly depends on the wind climate used as an input. Therefore, such a climate should also account for extreme conditions, observed on larger time-scales.

Recommendations for further research

- **Large-scale cumulative OWF layout**

  Looking at the entire North Sea region, it is recommended to identify the spatial footprint within which developing OWFs is not expected to influence the nearshore wave climate and the along-shore morphology of the surrounding coastal regions. Different orientations or layouts can lead to an optimum situation for the benefit of the Dutch coast. This was introduced in Section 6.1 of the Discussion chapter.

- **Explore offshore wind farm design parameters**

  To derive design criteria for future OWF developments for the benefit of the Dutch coast, it is recommended to explore alternative OWF layouts, sizes, locations and orientations. Also, in the context of offshore wind development, it is advised to test different island shapes, sizes and construction methods (sandfill, floating island, caisson structure etc.).

- **Investigate hot-spots on a smaller spatial scale**

  Based on the already identified hot-spots, it is recommended to explore whether they pose an immediate threat to nearby areas (natural habitats, touristic resorts, nearby living areas, popular beaches) and study them in more detail, using a higher resolution approach.

- **Study the effect of OWFs in relation to other long-term effects**

  It is know that not only OWFs are expected to affect the nearby coastal areas. There are also other factors such as the sea-level rise that has been found to influence the alongshore morphology. It is therefore recommended to determine the significance of the OWF effect in relation to such long-term effects.

- **Study the effect of OWFs on the vertical motion of the ocean ocean and the coastal upwelling-downwelling**

  It has been found that OWFs can also alter the vertical motion of the ocean and therefore the coastal upwelling and downwelling (Paskyabi, 2015; Segtnan & Christakos, 2015). Since water levels affect the alongshore morphology, it is recommended to study the potential effect of OWFs in the North Sea on coastal stratification and upwelling, using an approach similar to this thesis.

References

4C Offshore. (2018). *Global offshore renewable map.* Retrieved 2018-03-10, from https://www.4coffshore.com/offshorewind/

Ainslie, J. F. (1988). Calculating the flowfield in the wake of wind turbines. *Journal of Wind Engineering and Industrial Aerodynamics*, *27*(1–3), 213–224. doi: 10.1016/0167-6105(88)90037-2

Alari, V., & Raudsepp, U. (2012). Simulation of wave damping near coast due to offshore wind farms. *Journal of Coastal Research*, *28*(1), 143–148. doi: 10.2112/JCOASTRES-D-10-00054.1

Beiboer, F., & Cooper, B. (2002, January). *Potential effects of offshore wind developments on coastal processes* (Tech. Rep. No. ETSU W/35/00596/00/REP). Retrieved 2018-08-01, from https://tethys.pnnl.gov/publications/potential-effects-offshore-wind-developments-coastal-processes

Christensen, E. D., Johnson, M., Sørensen, O. R., Hasager, C. B., Badger, M., & Larsen, S. E. (2013). Transmission of wave energy through an offshore wind turbine farm. *Coastal Engineering*, *82*, 25–46. doi: 10.1016/j.coastaleng.2013.08.004

Christensen, E. D., Kristensen, S. E., & Deigaard, R. (2014). Impact of an offshore wind farm on wave conditions and shoreline development. *Coastal Engineering Proceedings*, *1*(34), 87. doi: 10.9753/icce.v34.sediment.87

Christiansen, M. B., & Hasager, C. B. (2005). Wake effects of large offshore wind farms identified from satellite SAR. *Remote Sensing of Environment*, *98*(2–3), 251–268. doi: 10.1016/j.rse.2005.07.009

Clark, S., Schroeder, F., & Baschek, B. (2014, December). *The influence of large offshore wind farms on the North Sea and Baltic Sea - a comprehensive literature review* (Tech. Rep. No. HZG Report 2014-6). Retrieved 2018-08-01, from https://tethys.pnnl.gov/publications/influence-large-offshore-wind-farms-north-sea-and-baltic-sea-comprehensive-literature

Cui, Y., Li, L., Liu, Y., & Gao, L. (2015). Wind turbine wake vertical distributions considering different inflow shear indices. *International Conference on Renewable Power Generation (RPG 2015)*, 1–6. doi: 10.1049/cp.2015.0490

Dörenkämper, M., Witha, B., Steinfeld, G., Heinemann, D., & Kühn, M. (2015). The impact of stable atmospheric boundary layers on wind-turbine wakes within offshore wind farms. *Journal of Wind Engineering and Industrial Aerodynamics*, *144*, 146–153. doi: 10.1016/j.jweia.2014.12.011

EC. (2011). *Communication from the Commission to the European Parliament, the Council, the European Economic and Social Committee and the Committee of the regions: A Roadmap for moving to a competitive low carbon economy in 2050.* Retrieved 2018-02-20, from https://eur-lex.europa.eu/legal-content/EN/ALL/?uri=CELEX:52011DC0112

EC. (2015). *Paris agreement.* Retrieved 2018-02-20, from https://ec.europa.eu/clima/policies/international/negotiations/paris_en

EC. (2016). *EU reference scenario 2016: Energy, transport and GHG emissions trends to 2050.* Retrieved 2018-03-20, from https://ec.europa.eu/energy/en/data-analysis/energy-modelling

ECMWF. (2018). *ERA5 data documentation.* Retrieved 2018-08-01, from https://confluence.ecmwf.int/display/CKB/ERA5+data+documentation

EMODnet. (2018). *EMODnet marine wind farm interactive map of Europe.* EMODnet human activities. Retrieved 2018-03-10, from http://www.emodnet-humanactivities.eu/view-data.php

Frandsen, S., Barthelmie, R., Pryor, S., Rathmann, O., Larsen, S., Højstrup, J., & Thøgersen, M. (2006). Analytical modelling of wind speed deficit in large offshore wind farms. *Wind Energy*, *9*(1–2), 39–53. doi: 10.1002/we.189

Gautier, C., & Caires, S. (2015, June). *Operational wave forecasts in the southern North Sea.* The Hague, the Netherlands: 36th IAHR World Congress. Retrieved from https://www.researchgate.net/publication/290440200_OPERATIONAL_WAVE_FORECASTS_IN_THE_SOUTHERN_NORTH_SEA

González-Longatt, F., Wall, P., & Terzija, V. (2012). Wake effect in wind farm performance: Steady-state and dynamic behavior. *Renewable Energy*, *39*(1), 329–338. doi: 10.1016/j.renene.2011.08.053

GWEC. (2017). *Global wind report 2016 – annual market update 2016* (Tech. Rep.). Retrieved from http://gwec.net/publications/global-wind-report-2/global-wind-report-2016/

Hasager, C. B. (2014). Offshore winds mapped from satellite remote sensing. *Wiley Interdisciplinary Reviews: Energy and Environment*, *3*(6), 594–603. doi: 10.1002/wene.123

Hasager, C. B., Nygaard, N., Volker, P., Karagali, I., Andersen, S., & Badger, J. (2017). Wind farm wake: The 2016 Horns Rev photo case. *Energies*, *10*(3), 317. doi: 10.3390/en10030317

Hasager, C. B., Rasmussen, L., Peña, A., Jensen, L. E., & Réthoré, P.-E. (2013). Wind farm wake: The Horns Rev photo case. *Energies*, *6*(2), 696–716. doi: 10.3390/en6020696

Hasager, C. B., Vincent, P., Badger, J., Badger, M., Di Bella, A., Peña, A., … Volker, J. H. P. (2015). Using satellite SAR to characterize the wind flow around offshore wind farms. *Energies*, *8*(6), 5413–5439. doi: 10.3390/en8065413

Holthuijsen, L. H., Booij, N., & Ris, R. C. (1993). A spectral wave model for the coastal zone. In *Ocean wave measurement and analysis* (p. 630-641). ASCE. Retrieved from http://

cedb.asce.org/CEDBsearch/record.jsp?dockey=0087343

Jensen, N. O. (1983). A note on wind generator interaction. Risø National Laboratory for Sustainable Energy, Technical University of Denmark, Frederiksborgvej 399, P.O. 49, 4000, Roskilde, Denmark. Retrieved from http://orbit.dtu.dk/en/publications/a-note-on-wind-generator-interaction(2ac0aed9-af5e-4a3e-94f0-6ca825631180).html

Jongbloed, R. H., van der Wal, J. T., & Lindeboom, H. J. (2014). Identifying space for offshore wind energy in the North Sea. Consequences of scenario calculations for interactions with other marine uses. *Energy Policy*, *68*, 320–333. doi: 10.1016/j.enpol.2014.01.042

Komen, G. J., Cavaleri, L., Donelan, M., Hasselmann, K., Hasselmann, S., & Janssen, P. A. E. M. (1994). *Dynamics and modelling of ocean waves*. Cambridge University Press. doi: 10.1017/CBO9780511628955

Li, X., & Lehner, S. (2013). Observation of TerraSAR-X for studies on offshore wind turbine wake in near and far fields. *IEEE Journal of Selected Topics in Applied Earth Observations and Remote Sensing*, *6*(3), 1757–1768. doi: 10.1109/JSTARS.2013.2263577

Mittelmeier, N., Allin, J., Blodau, T., Trabucchi, D., Steinfeld, G., Rott, A., & Kühn, M. (2017). An analysis of offshore wind farm SCADA measurements to identify key parameters influencing the magnitude of wake effects. *Wind Energy Science*, *2*, 477–490. doi: 10.5194/wes-2-477-2017

Müller, M., Haesen, E., Ramaekers, L., & Verkaik, N. (2017, July). *Translate COP21: 2045 outlook and implications for offshore wind in the North Seas* (Tech. Rep. No. ESMNL17412). Retrieved 2018-08-01, from https://www.ecofys.com/en/publications/translate-cop21/

Noordzeeloket. (2018). *Routekaart windenergie op zee 2030.* Retrieved 2018-23-08, from https://www.noordzeeloket.nl/functies-en-gebruik/windenergie/vervolgroutekaart/ (in Dutch)

Paskyabi, M. B. (2015). Offshore wind farm wake effect on stratification and coastal upwelling. *Energy Procedia*, *80*(21), 131–140. doi: 10.1016/j.egypro.2015.11.415

Platis, A., Siedersleben, S. K., Bange, J., Lampert, A., Bärfuss, K., Hankers, R., … Emeis, S. (2018). First in situ evidence of wakes in the far field behind offshore wind farms. *Scientific Reports*, *8*(2163). doi: 10.1038/s41598-018-20389-y

Rajewski, D. A., Takle, E. S., Lundquist, J. K., Oncley, S., Prueger, J. H., Horst, T. W., … Doorenbos, R. K. (2013). Crop wind energy experiment (CWEX): Observations of surface-layer, boundary layer, and mesoscale interactions with a wind farm. *Bulletin of the American Meteorological Society*, *94*, 655–672. doi: 10.1175/BAMS-D-11-00240.1

Rijkswaterstaat. (2017). *Database of sand nourishments at the Dutch coast.* (for in-house Deltares use)

Ris, R. C., Holthuijsen, L. H., & Booij, N. (1994). A spectral model for waves in the near shore zone. In *Coastal engineering 1994* (Vol. 1). Retrieved from https://icce-ojs-tamu.tdl.org/icce/index.php/icce/article/view/4946/4626

Rodriguez Gandara, R., & Harris, J. (2012). Nearshore wave damping due to the effect on winds in response to offshore wind farms. *Coastal Engineering Proceedings*, *1*(33), 55. doi: 10.9753/icce.v33.waves.55

Roeland, H., & Piet, R. (1995). Dynamic preservation of the coastline in the Netherlands. *Journal of Coastal Conservation*, *1*(1), 17–28. doi: 10.1007/BF02835558

Sarlak, H., Nishino, T., Martínez-Tossas, L. A., Meneveau, C., & Sørensen, J. N. (2016). Assessment of blockage effects on the wake characteristics and power of wind turbines. *Renewable Energy*, *93*, 340–352. doi: 10.1016/j.renene.2016.01.101

Segtnan, O. H., & Christakos, K. (2015). Effect of offshore wind farm design on the vertical motion of the ocean. *Energy Procedia*, *80*, 213–222. doi: 10.1016/j.egypro.2015.11.424

Sijmons, D. (2014). *Landscape and energy: Designing transition* (D. Sijmons, J. Hugtenberg, F. Feddes, & A. van Hoorn, Eds.). nai010 publishers.

Stronkhorst, J., Huisman, B., Giardino, A., Santinelli, G., & Santos, F. D. (2018). Sand nourishment strategies to mitigate coastal erosion and sea level rise at the coasts of Holland (The Netherlands) and Aveiro (Portugal) in the 21st century. *Ocean & Coastal Management*, *156*, 266–276. doi: 10.1016/j.ocecoaman.2017.11.017

SWAN team. (2018a). *SWAN scientific and technical documentation.* Retrieved from http://swanmodel.sourceforge.net/online_doc/swantech/swantech.html

SWAN team. (2018b). *SWAN user manual.* Retrieved from http://swanmodel.sourceforge.net/online_doc/swanuse/swanuse.html

TenneT, Energinet, Gasunie, & Port of Rotterdam. (2018). *North Sea Wind Power Hub.* Retrieved 2018-23-08, from https://northseawindpowerhub.eu/

UN. (2015a). *COP21.* United Nations. Retrieved 2018-02-20, from https://unfccc.int/process-and-meetings/conferences/past-conferences/paris-climate-change-conference-november-2015/cop-21

UN. (2015b). *The Paris agreement.* United Nations. Retrieved 2018-02-20, from https://unfccc.int/process-and-meetings/the-paris-agreement/the-paris-agreement

UN. (2016). *Paris agreement - status of ratification.* United Nations. Retrieved 2018-02-20, from https://unfccc.int/process/the-paris-agreement/status-of-ratification

Van Koningsveld, M., & Mulder, J. P. M. (2004). Sustainable coastal policy developments in The Netherlands. A systematic approach revealed. *Journal of Coastal Research*, *20*(2), 375–385. doi: 10.2112/1551-5036(2004)020[0375:SCPDIT]2.0.CO;2

Wijnberg, K. M. (2002). Environmental controls on decadal morphologic behaviour of the Holland coast. *Marine Geology*, *189*(3–4), 227–247. doi: 10.1016/S0025-3227(02)00480-2

WindEurope. (2017a, September). *Wind energy in Europe: Outlook to 2020* (Tech. Rep.). Retrieved from https://windeurope.org/about-wind/reports/wind-energy-in-europe-outlook-to-2020/

WindEurope. (2017b, September). *Wind energy in Europe: Scenarios for 2030* (Tech. Rep.). Retrieved from https://windeurope.org/about-wind/reports/wind-energy-in-europe-scenarios-for-2030/

WindEurope. (2017c, February). *Wind in power: 2016 European statistics* (Tech. Rep.). Retrieved from https://windeurope.org/about-wind/statistics/european/wind-in-power-2016/

WindEurope. (2018a, February). *Wind in power 2017: Annual combined onshore and offshore wind energy statistics* (Tech. Rep.). Retrieved from https://windeurope.org/about-wind/statistics/european/wind-in-power-2017/

WindEurope. (2018b, February). *Offshore wind in Europe: key trends and statistics 2017* (Tech. Rep.). Retrieved from https://windeurope.org/about-wind/statistics/offshore/european-offshore-wind-industry-key-trends-statistics-2017/

WL|Delft Hydraulics. (1992, October). *Unibest, a software suite for simulation of sediment transport processes and related morphodynamics of beach profiles and coastline evolution. model description and validation* (Tech. Rep. No. H454.14). Delft, Netherlands: WL|Delft Hydraulics.

Zaghi, S., Muscari, R., & Di Mascio, A. (2016). Assessment of blockage effects in wind tunnel testing of wind turbines. *Journal of Wind Engineering and Industrial Aerodynamics*, *154*, 1–9. doi: 10.1016/j.jweia.2016.03.012

Zijlema, M., & van der Westhuysen, A. J. (2005). On convergence behaviour and numerical accuracy in stationary SWAN simulations of nearshore wind wave spectra. *Coastal Engineering*, *52*(3), 237–256. doi: 10.1016/j.coastaleng.2004.12.006

A

Measuring the OWF effect on 10-m wind speed

A.1. Remote sensing techniques for measuring 10-m wind speed

Usually, wind speed measurements near OWFs are derived with remote sensing techniques, which are less expensive compared to in situ measurements such as installing tall masts over the ocean (Li & Lehner, 2013). To capture the spatial variability of wind speed inside and downwind of an OWF the resolution of the measurements should be such than the OWF area is properly resolved. Traditional remote sensing techniques, such as passive microwave sensors or scatterometers, have a relatively low spatial resolution (25 km) and cannot be used for such a purpose (Hasager, 2014). At the moment, the predominant method that provides the accuracy needed, is analysis of Synthetic Aperture Radar (SAR) images. An alternative choice is Light Detection and Ranging (LIDAR) devices (Mittelmeier et al., 2017; Platis et al., 2018). By analyzing SAR or LIDAR images it is possible to map the wind speed 10 m above water surface, also called near-surface or 10-m wind speed (U_{10}). The 10-m wind speed is linked to wave generation in the open sea and is included in existing wave growth formulas (Komen et al., 1994).

Therefore, analysis of SAR and LIDAR images results in U_{10} maps containing information on wind speed magnitude and direction over a large spatial extent. This makes it possible to observe the effect of an OWF on the local wind climate. A 10-m wind speed map, retrieved from analysis of a SAR image, is presented in the following figure:

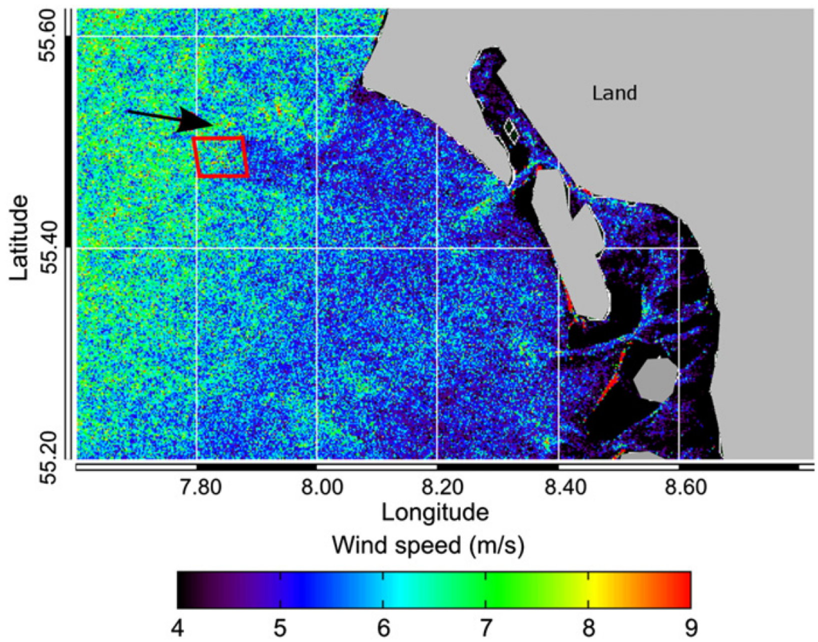

Figure A.1: 10-m wind speed map from analysis of a SAR image at Horns Rev 1 OWF in Denmark. The predominant wind direction is from west-northwest (Christensen et al., 2013).

A.2. Deriving 10-m wind speed maps from SAR and LIDAR

SAR and LIDAR images do not directly depict the 10-m wind speed but instead show bright and light regions. These indicate the backscatter of the radar signal that hits the sea surface. An example of such images is presented in Figure A.2.

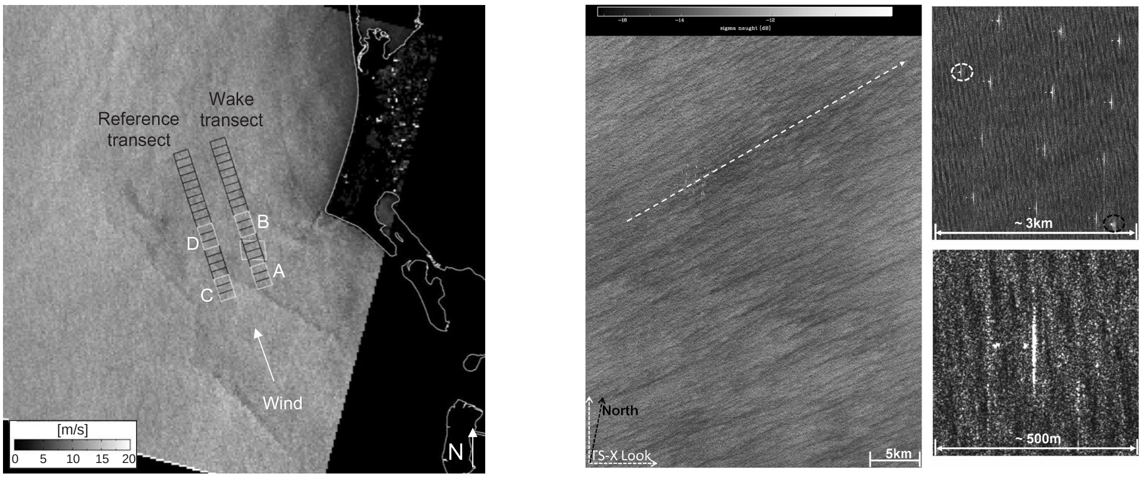

(a) (b)

Figure A.2: Definition of transects at (a) Horns Rev 1 OWF in Denmark (Christiansen & Hasager, 2005) and (b) Alpha Ventus OWF in Germany (Li & Lehner, 2013). The OWF in subfigure (a) is located in between sections A and B. In subfigure (b), the transect is the dashed line on the left image. The wind turbines of Alpha Ventus can be observed close to the southwestern edge of the transect. The upper right and lower right images depict zoomed areas within Alpha Ventus to demonstrate the accuracy of TerraSAR-X measurements.

The 10-m wind speed is a function of the shear stress exerted by wind on the sea surface. The latter can be linked to the backscatter signal. This dependence leads to U_{10} maps, already shown in Figure A.1.

Essentially, every pixel in the SAR or LIDAR image corresponds to a value of U_{10}. Such images however contain some an amount of noise that needs to be removed. This is realized by averaging the values within the pixels. To do so, a rectangular transect is defined on top of the image. The length of the transect runs along the OWF and extends both upwind and downwind – it should cover both the WFA as well as the WA (see Section 2.3 for definitions). In addition, the width of the transect should be big enough to include the OWF wake, which is constantly changing direction depending on wind (the transect width is equal to 3.2 km in the analysis of Christiansen and Hasager (2005) and 250 m in the work of Li and Lehner (2013), see Figure A.2. The noise is removed by averaging the 10-m wind speed along the width of the transect (averaging over 400 m in Christiansen and Hasager (2005) and over 250 m in Li and Lehner (2013)). It should be stressed that such a method results in loss of spatial resolution, making remote sensing techniques more appropriate for larger scale effects. Conclusively, the approach described above makes it possible to map the 10-m wind speed along the WFA and the WA, downwind of an OWF.

B

Wind data analysis

B.1. Wind statistics

As discussed in Section 3.2, a representative year is chosen for simulations that best describes the long-term wind climate of the North Sea. The goal is to avoid using a ”calm” year for simulations, in which case no significant storms would be present. This could result in underestimating the wave height in the nearshore and possibly drawing wrong conclusions on the effect of OWFs on waves in the long-run.

This section presents wind roses at the three characteristic locations defined in Section 3.2. The wind roses are depicted for every year as well as for the whole period 2010 – 2017. A wind rose is a schematic depiction of the joint probability distribution between the 10-m wind speed magnitude and direction at a specific location. The wind roses are presented in the following pages.

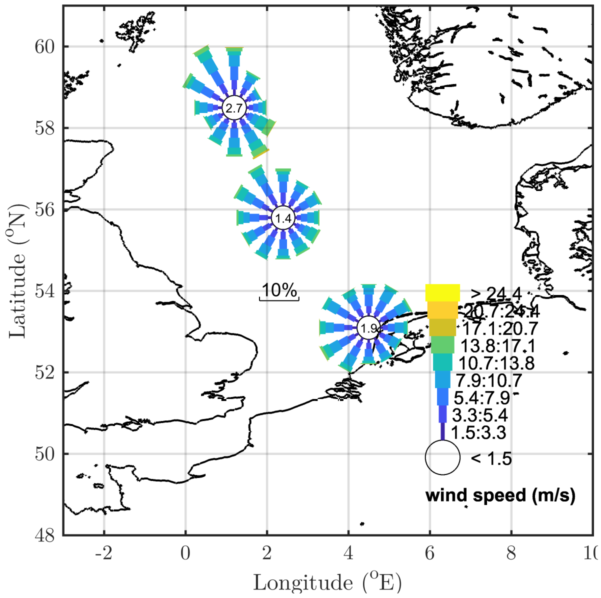

(a) 2010

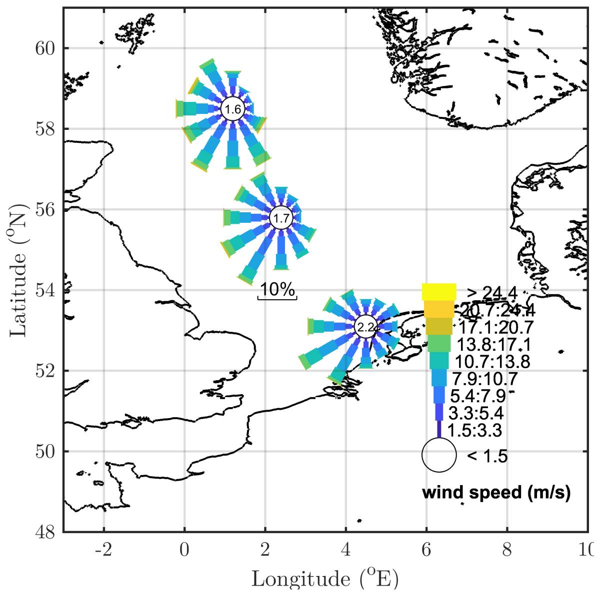

(b) 2011

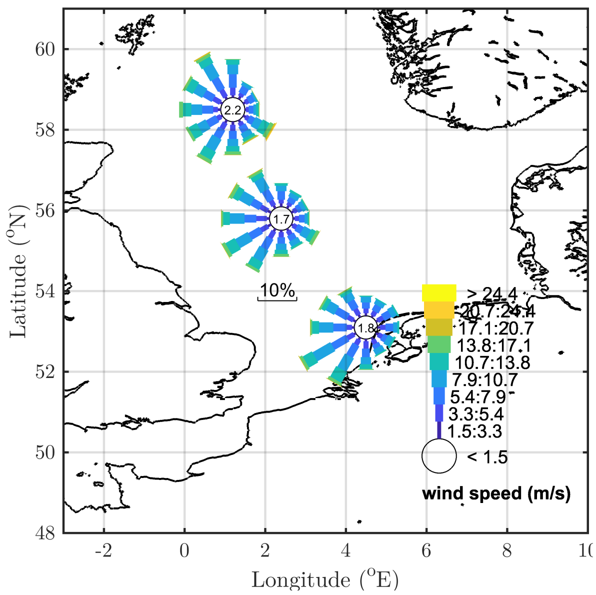

(c) 2012

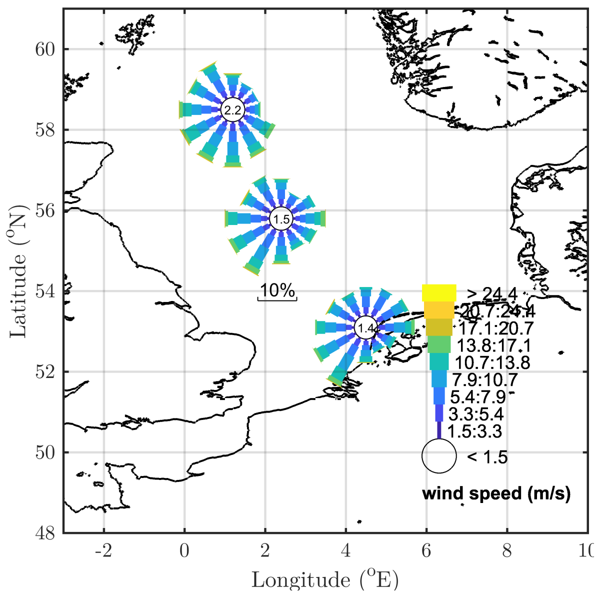

(d) 2013

Figure B.1: Annual wind roses for years 2010 till 2013.

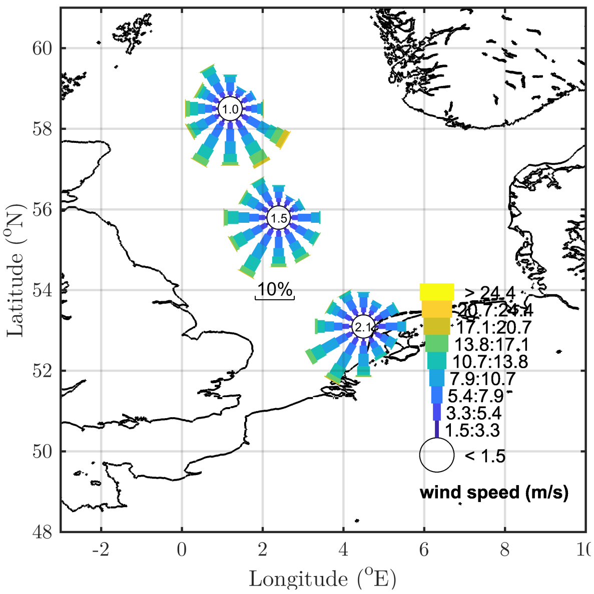

(a) 2014

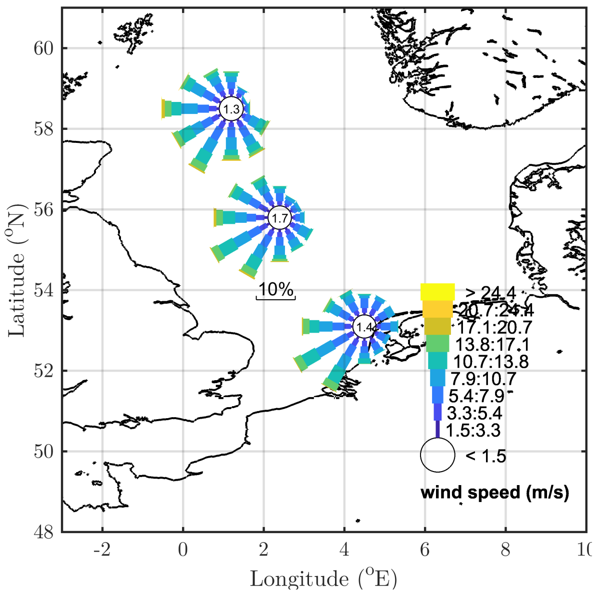

(b) 2015

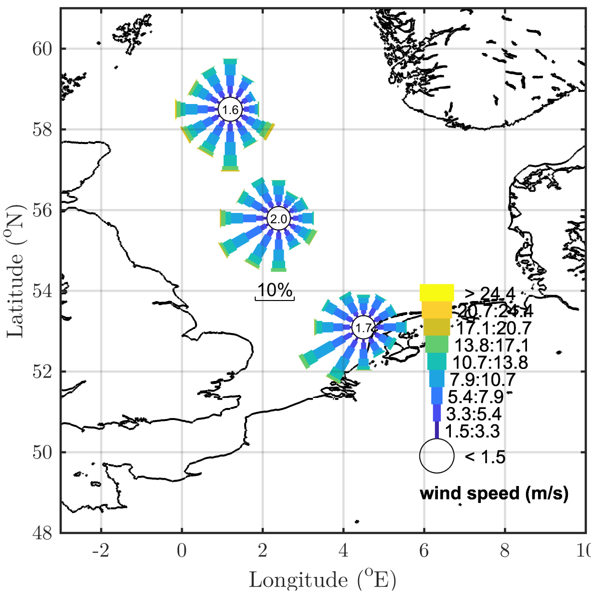

(c) 2016 (representative year)

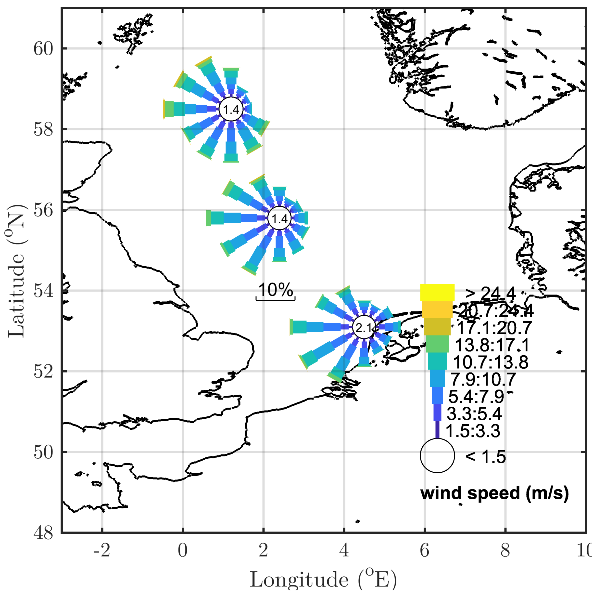

(d) 2017

Figure B.2: Annual wind roses for years 2014 till 2017.

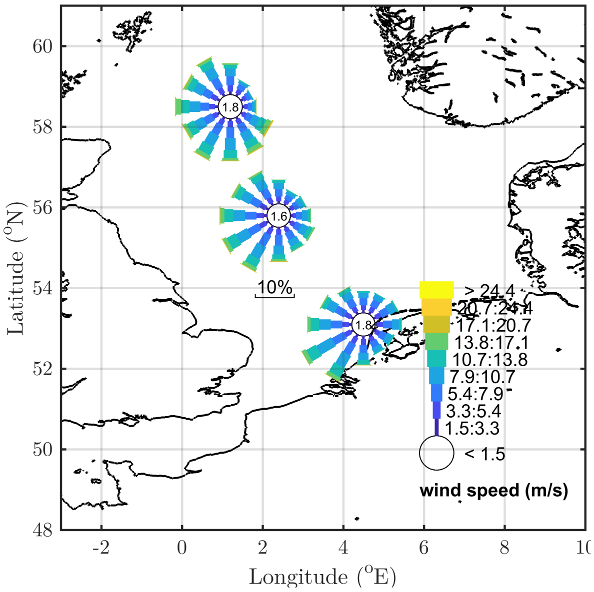

Figure B.3: Wind roses for period 2010 – 2017.

B.2. Wind grid refinement

To properly resolve the OWF areas, the original ERA5 wind grid is refined. This results in a grid with a 5-km ($\approx 0.05^\circ$) spatial resolution, 6 times less compared to the original one. The criterion for refining the grid is to properly capture most of the OWF areas using the biggest mesh size possible (the highest the spatial resolution of the grid the more computational time is needed for generating the wind input). Figure B.4 shows the OWF area resolution for various mesh sizes.

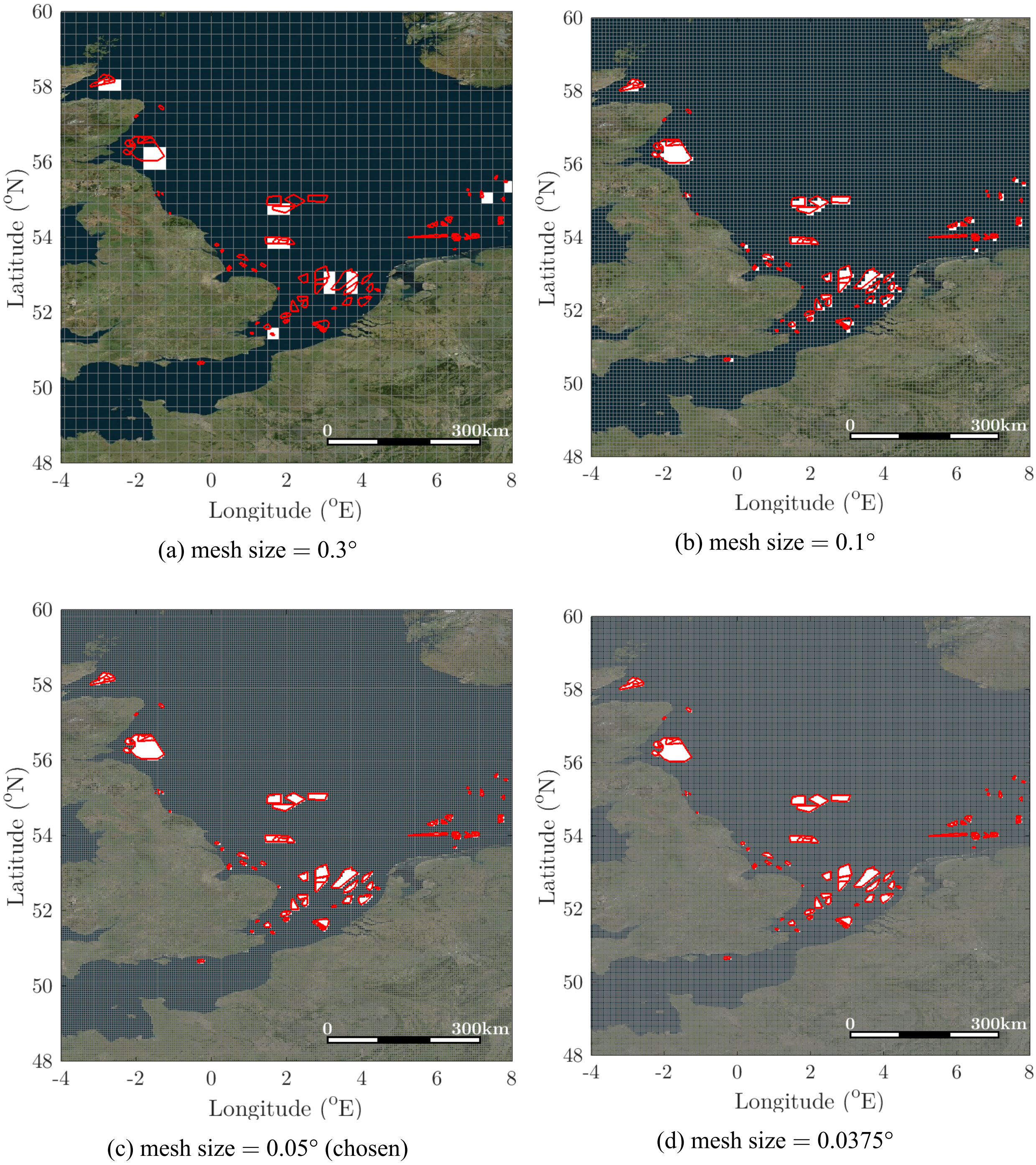

(a) mesh size = 0.3°

(b) mesh size = 0.1°

(c) mesh size = 0.05° (chosen)

(d) mesh size = 0.0375°

Figure B.4: OWF area resolution for different wind grid refinements.

C

Supplementary wave modeling results

This section contains additional results of wave modeling, showing the effect of OWFs or an island on the nearshore wave climate of the Netherlands. As explained in Chapter 5 the nearshore margin is the -9 m NAP contour, indicated with a red line in the map plots. The figures shown here are excluded from Chapter 5 since they refer to situations of zero or nearly zero influence or in development scenarios that are less probable to be realized in the context of OWF developments. They are included here instead, for the sake of completeness.

The net effect of OWFs in 2050 and 2050A on wave height and direction is depicted in Figure C.1. The effect in the nearshore is barely noticed. The mean wave height decrease reaches a maximum of 0.2% near Petten whereas the mean change in wave direction is no more than 0.1°.

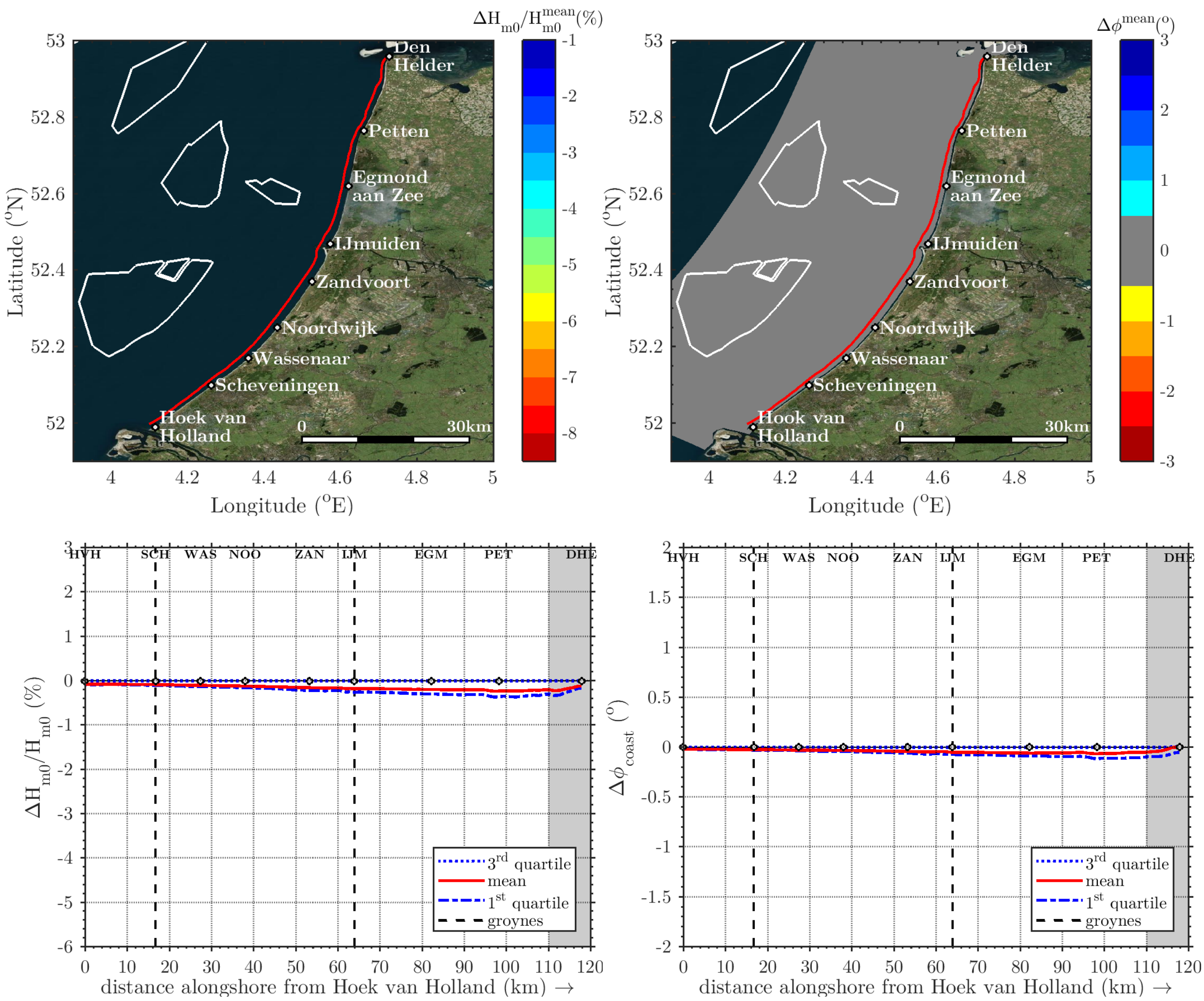

Figure C.1: Net effect of OWFs in 2050 and 2050A on wave height and direction.

A 20 km^2 island located 75 km or 95 km away from the Dutch coast does not show any influence on the nearshore wave climate of the Netherlands. The net effect is shown in (Figure C.2).

Positioning the 20 km^2 island around 30 km away from the Dutch coast is considered less probable to be realized in the far future. Such an island size is considered unrealistic in the context

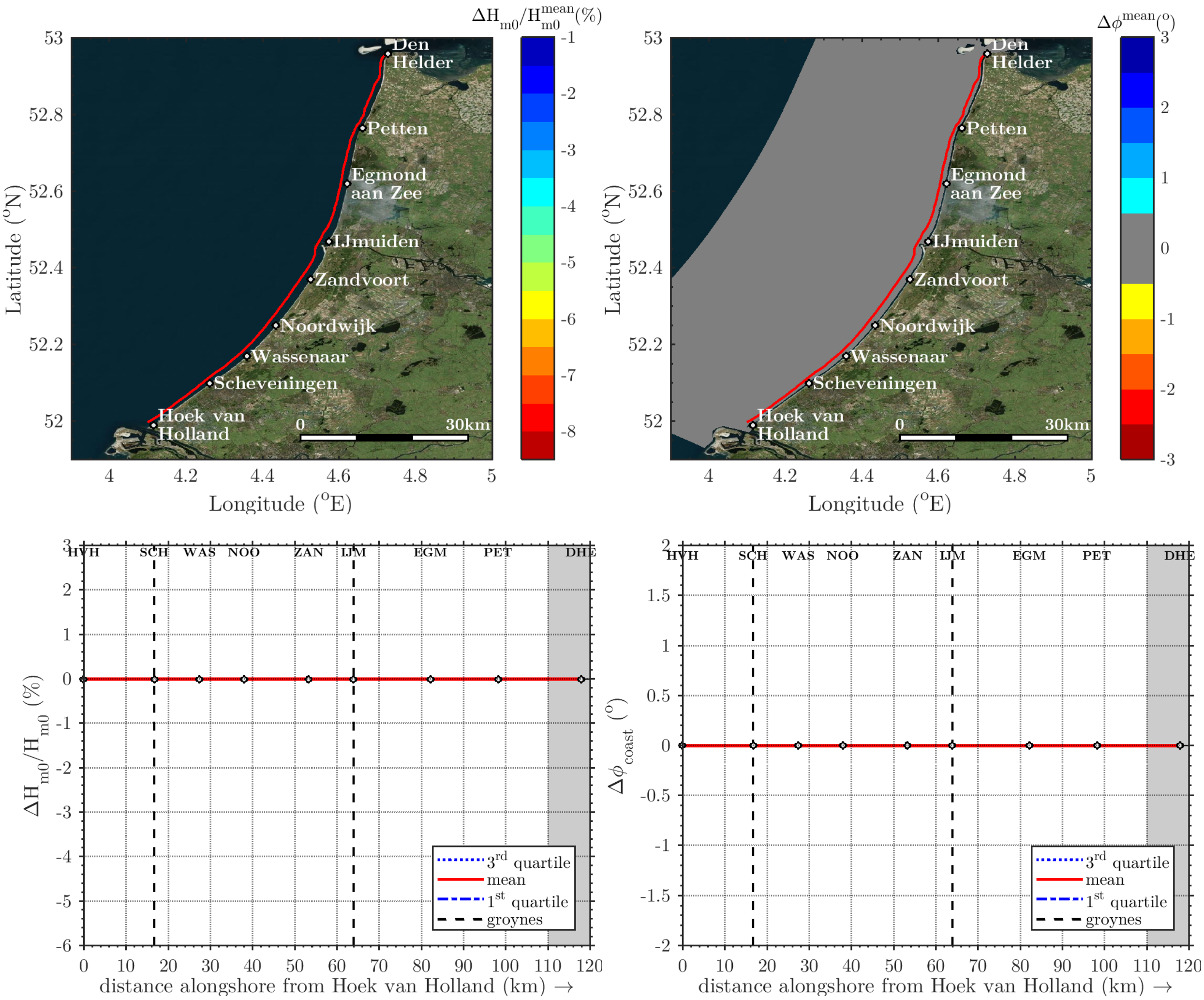

Figure C.2: Net effect of 20 km^2 islands 75 and 95 km offshore on wave height and direction.

of OWF developments. As discussed in Section 1.1 media reports an island of around 6 km^2 realized even further from the Dutch coast, at deeper water. However, an island of such a size could be the case for other projects (for example an offshore extension of the Amsterdam Schiphol airport).

The net effect of the island is shown in Figure C.3. The pattern of the effect is similar to the 5 km^2 island but the influence is more intense due to the greater island area. The greatest wave height decrease is found north of Wassenaar (x = 30 km) with a value of 3.5%. The influence is less in the North Holland region, where a peak 0.8% in mean wave height decrease is observed at Petten (x = 98 km). The mean change in wave direction results in a counterclockwise turning and reaches a peak of 0.85° at Wassenaar (x = 28 km). In North Holland the maximum is located south of Egmond (x = 78 km) with a value of 0.5°. Petten shows no change in wave direction.

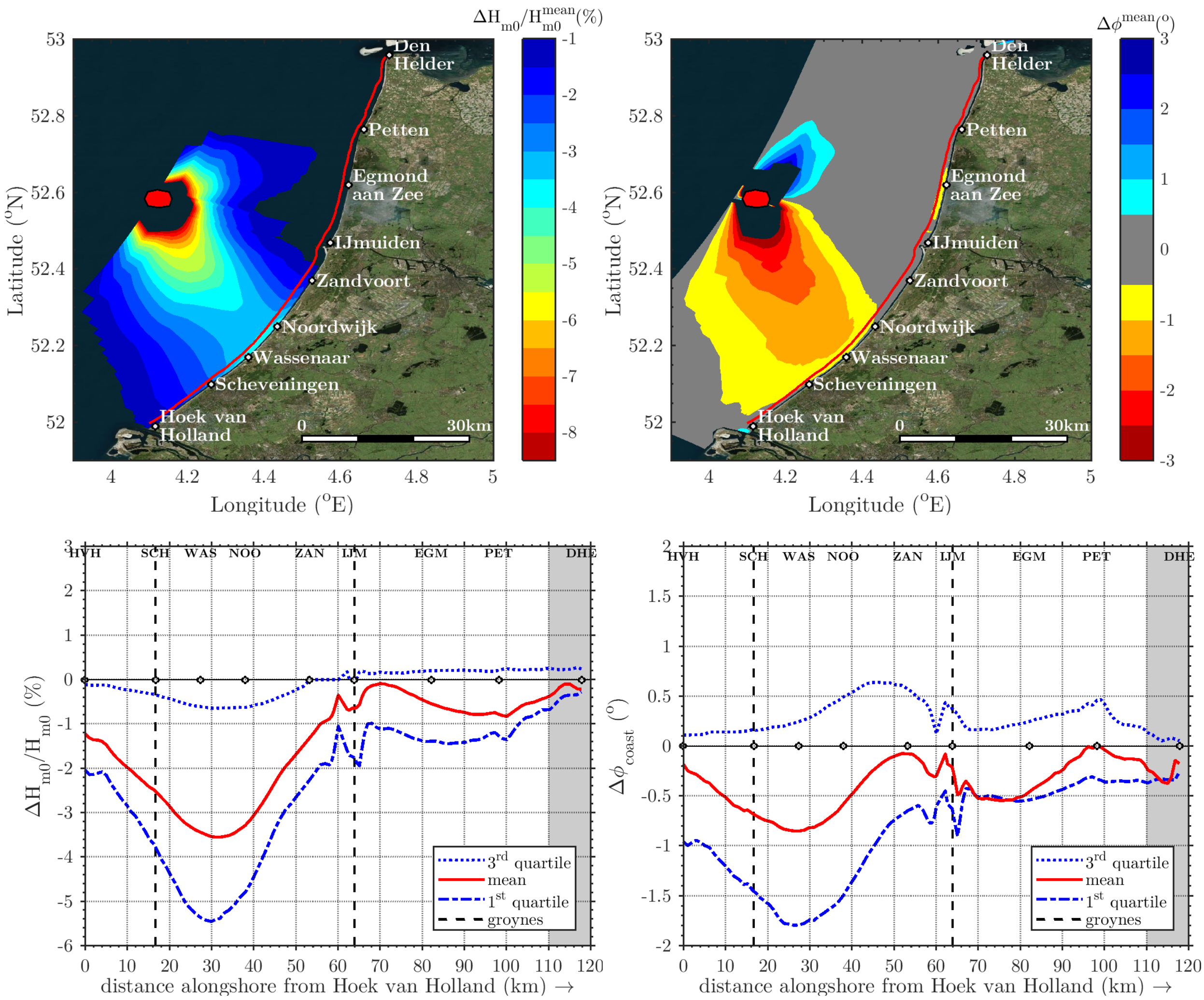

Figure C.3: Net effect of 20 km^2 island 33 km offshore on wave height and direction.

D

Understanding the effect of OWFs on wave climate

This section elaborates on the mechanism behind the effect of OWFs or an island on waves. This is realized by considering an idealized stationary case (solving a single time step) and presenting the geographical distribution of the spectral energy balance terms in the SWAN-HCWD domain. In addition, the change in wave height and direction resulting from the idealized case is compared with the annual mean change computed in Chapter 5. To obtain an even better understanding on the processes underlying the wave height decrease and the direction change, the energy change in the directional and frequency space resulting from OWFs or an island is computed.

D.1. The energy density balance

SWAN solves the energy balance equation. In a stationary situation, with no ambient currents and in nearshore applications the energy balance is given by:

$$\frac{\partial c_{g,x} E(\sigma,\theta;x,y,t)}{\partial x} + \frac{\partial c_{g,y} E(\sigma,\theta;x,y,t)}{\partial y} + \frac{\partial c_{\theta} E(\sigma,\theta;x,y,t)}{\partial \theta} = S(\sigma,\theta;x,y,t) \quad \text{(D.1)}$$

in which:

$$c_{g,x} = c_g \cos\theta \quad \text{(D.2)}$$

$$c_{g,y} = c_g \sin\theta \quad \text{(D.3)}$$

$$c_{\theta} = -\frac{1}{c}\frac{\partial c}{\partial m} \quad \text{(D.4)}$$

The first and second terms on the left hand side of Equation D.1 represent the energy propagation in geographic space (propagating with the depth-dependent velocities $c_{g,x}$ and $c_{g,y}$ respectively, see Equation D.2 and Equation D.3). These terms account for shoaling. The third term represents the propagation of energy in directional space (propagating with velocity c_{θ}). This term accounts for the depth-induced refraction.

The propagation velocity in directional space (θ) is expressed by Equation D.4. The expression shows a dependency on the velocity gradient perpendicular to the wave propagation direction (m).

The right hand side of Equation D.1 is the source term. At deep water it consists of wind input (S_{wind}), quadruplet wave-wave interactions (S_{nl4}) and white-capping (S_{wc}). In shallow water extra terms are added, consisting of triad wave-wave interactions (S_{nl3}), bottom friction (S_{fric}) and depth-induced wave breaking (S_{surf}). Therefore, the source term in the nearshore is formulated as follows:

$$S_{tot} = S_{wind} + S_{nl4} + S_{nl3} + S_{wc} + S_{fric} + S_{surf} \quad \text{(D.5)}$$

D.2. Idealized stationary simulations

To better understand the governing processes behind the effect of OWFs or an island on the nearshore wave climate, idealized stationary runs are performed using SWAN-DCSM and SWAN-HCWD. The 10-m wind speed has a constant magnitude of 12 m/s (a moderate value) and a direction NNW over the entire domain. The wind direction is shown with white arrows in all the following graphs. Furthermore, wave direction at the boundaries is aligned with wind. Simulations are carried out for the baseline situation as well as for OWFs in 2030 and the situation with the 5 km^2 island located around 30 km away from the Dutch coast.

First the geographical distribution of the three energy propagation terms (left hand side of Equation D.1) as well as the source, sink and redistribution terms (Equation D.5) are displayed in the SWAN-HCWD domain. The aim is to get an understanding on the significance of the processes in the nearshore. Results for OWFs in 2030 are shown in the left column of the following figures and results for the 5 km^2 island are shown in the right column. The energy is always expressed in m^2/s and the colorbar limits are kept constant to easily make comparisons between images. Values less than 1×10^{-5} m^2/s are considered insignificant and are excluded from the figures. In addition, the -9 m NAP contour is indicated with white color, for easy reference.

Propagation terms

The propagation terms consist of energy propagating in the geographical ($x - y$) and directional (θ) domains, accounting for shoaling and refraction respectively. The geographical distribution of these terms is depicted in Figure D.1.

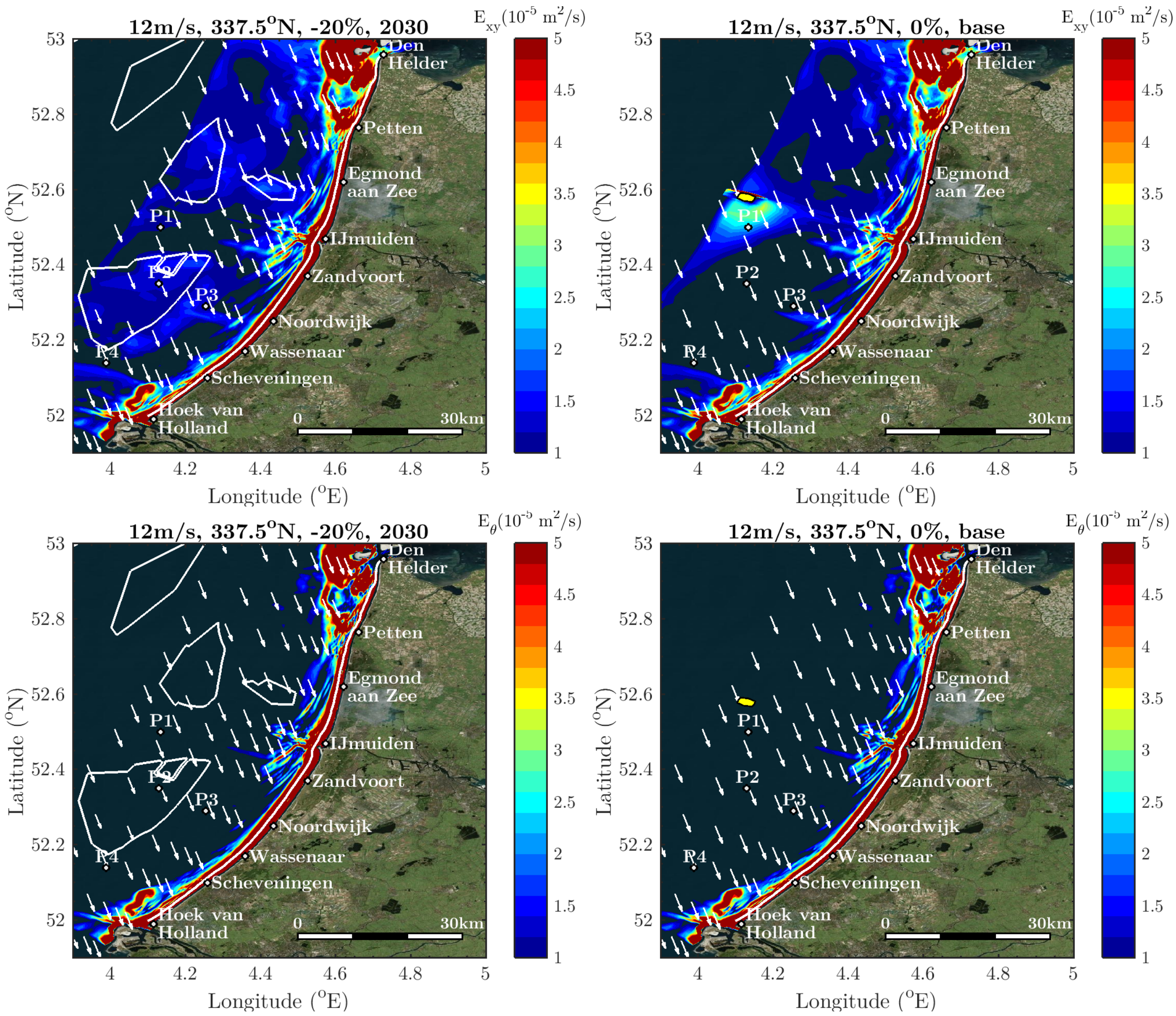

Figure D.1: Geographical distribution of energy propagation in $x - y$ (upper row) and θ space (lower row) in the SWAN-HCWD domain.

Energy propagation in the $x - y$ and θ space is greater in the nearshore. This is reasonable because refraction and shoaling are more intense in shallower water, where most waves ”feel” the bottom. Further offshore, the energy propagation in geographical space is more dominant than propagation in directional space. In addition, the energy propagation in geographical space significantly increases downwind of the energy island. The same occurs inside the OWF areas, however with a much lower intensity.

Source terms

The geographical distribution of energy input due to wind and the dissipation due to white-capping are presented in Figure D.2. Wind input is lower within the OWF areas, resulting from the assumed 20% decrease in wind speed. This directly affects wave generation, with waves having a smaller height. A smaller wave height results in less white-capping dissipation inside the OWFs. The same applies to the region downwind of the island, since the incoming energy is absorbed by the obstacle, resulting in smaller wave height in the shadow area.

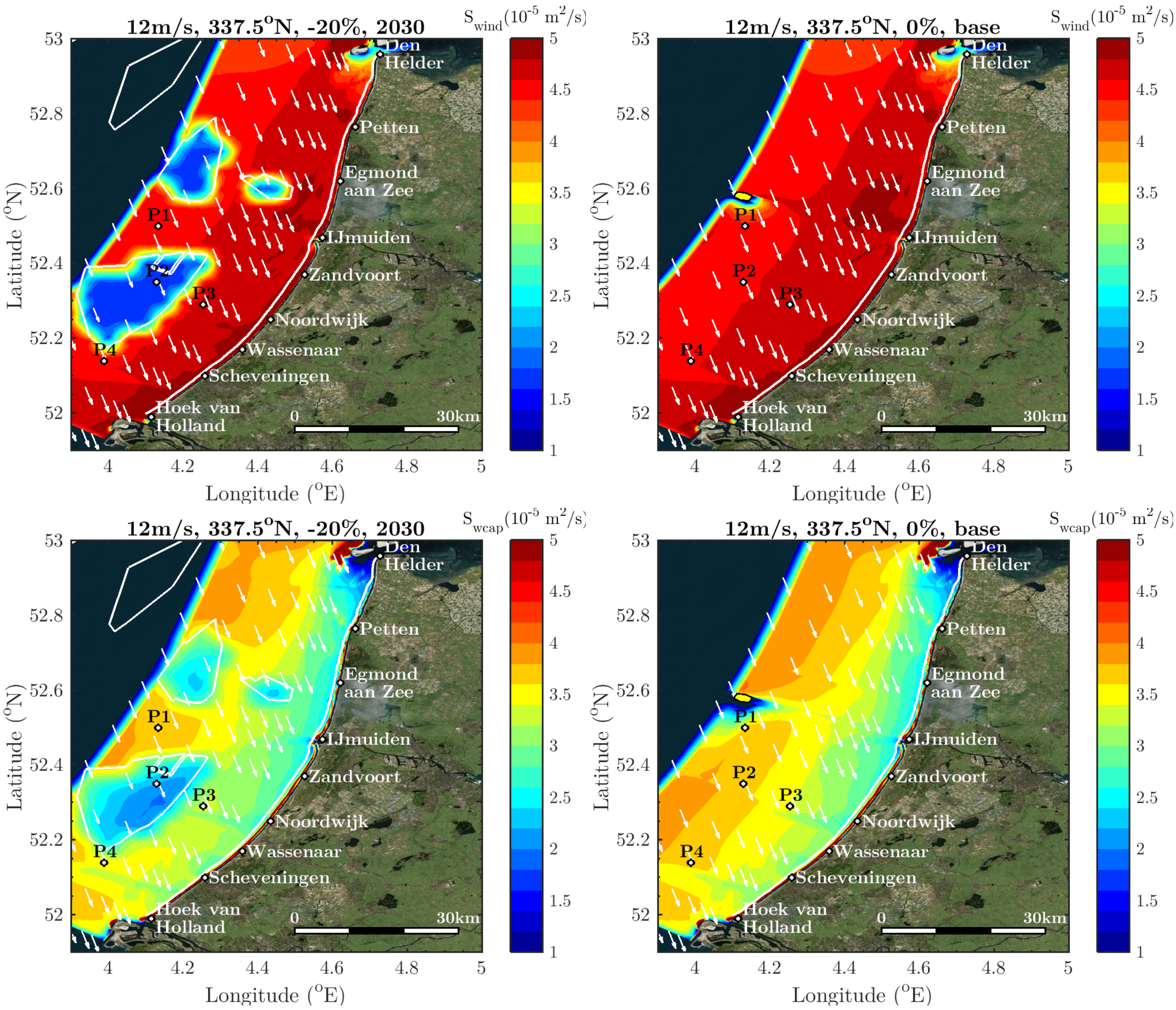

Figure D.2: Geographical distribution of energy generation due to wind (upper row) and dissipation due to white-capping (lower row) in the SWAN-HCWD domain.

The dissipation due to bottom friction and depth-induced wave breaking are presented in Figure D.3. These processes are significant only close to the coast. It is also important to note that for a moderate wind speed of 12 m/s, the dissipation due to bottom friction and depth-induced wave breaking predominantly occur at water depths shallower than 9 m. Therefore, choosing the -9 m NAP contour for extracting the SWAN output is considered satisfactory in this thesis. This is because the wave climate given as an input to Unibest-CL+ is not altered by bottom friction and depth-induced breaking.

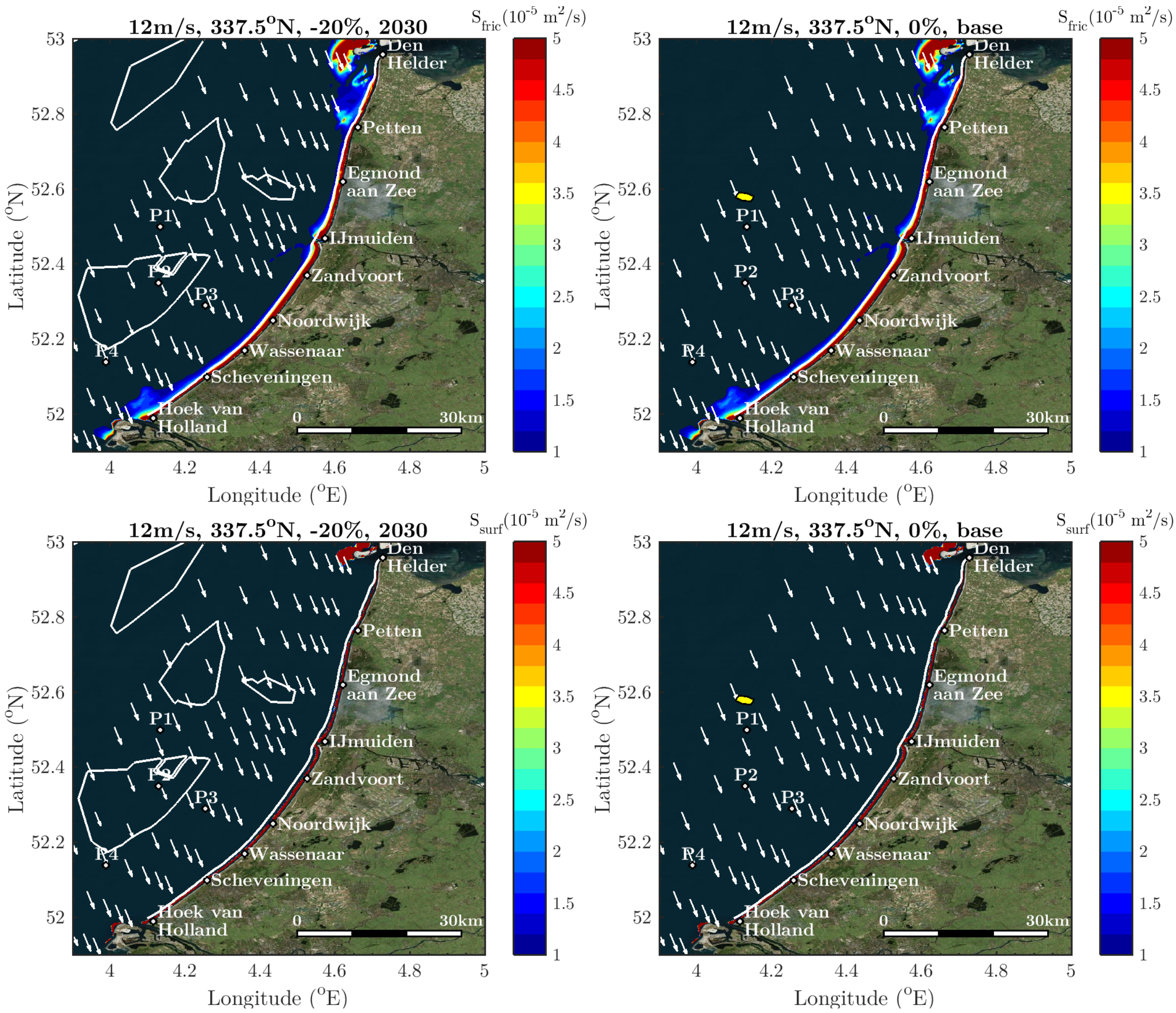

Figure D.3: Geographical distribution of energy dissipation due to bottom friction (upper row) and depth-induced wave breaking (lower row) in the SWAN-HCWD domain.

The energy redistribution due to quadruplet and triad wave-wave interactions is depicted in Figure D.4. As expected, the triad wave-wave interactions are only activated in shallow water and are of no significance close to the OWFs or the island. However, the quadruplet wave-wave interactions are significant in the offshore. Less energy is being redistributed within OWFs and downwind of the island, resulting from the smaller wave height in these regions.

It can be concluded that the dominant processes at the region where OWFs or an island are developed, are generation due to wind, dissipation due to white-capping and redistribution due to quadruplet wave-wave interactions. As explained above, these are the source terms activated in deep water.

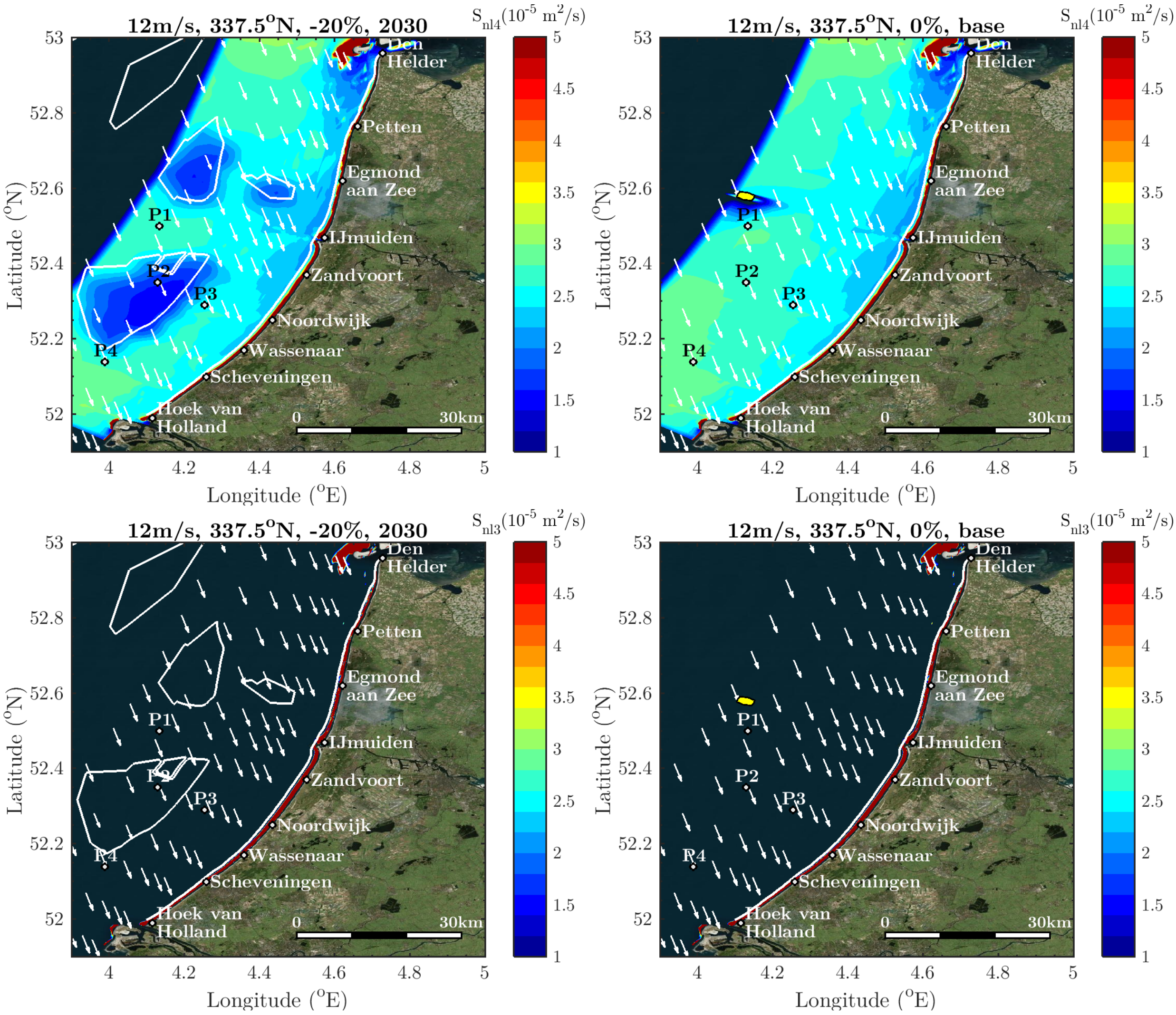

Figure D.4: Geographical distribution of energy redistribution due to quadruplet wave-wave interactions (upper row) and triad wave-wave interactions (lower row) in the SWAN-HCWD domain.

Effect on wave height and direction

To investigate the effect on wave height and direction, an approach similar to Chapter 5 is followed. In addition, the change of wave energy in frequency and directional space is computed at 4 locations. These are indicated by P1, P2, P3 and P4 and were already depicted in the previous images. For the undisturbed situation, the energy spectra are shown. To account for the effect of OWFs or an island, the change in energy density is depicted, expressed as a percentage relative to the total energy in the baseline case:

$$\Delta E = \frac{E_{\text{effect}} - E_{\text{baseline}}}{E_{\text{baseline}}^{\text{total}}} \tag{D.6}$$

where E_{effect} is the energy density in direction or frequency space in the OWF or island scenario, E_{baseline} is the energy density in direction or frequency space in the baseline case and $E_{\text{baseline}}^{\text{total}}$

is the total energy density in the baseline case.

The undisturbed values for wave height and direction, as well as the energy in frequency and directional space, are shown in Figure D.5. The energy at location P1 is greater compared to locations P2, P3 and P4, since P1 is located further offshore where the effect due to transformation processes is less and thus the wave height is greater. Location P3 contains the least amount of energy since it is closer to the coast. This can be seen in both frequency and directional space.

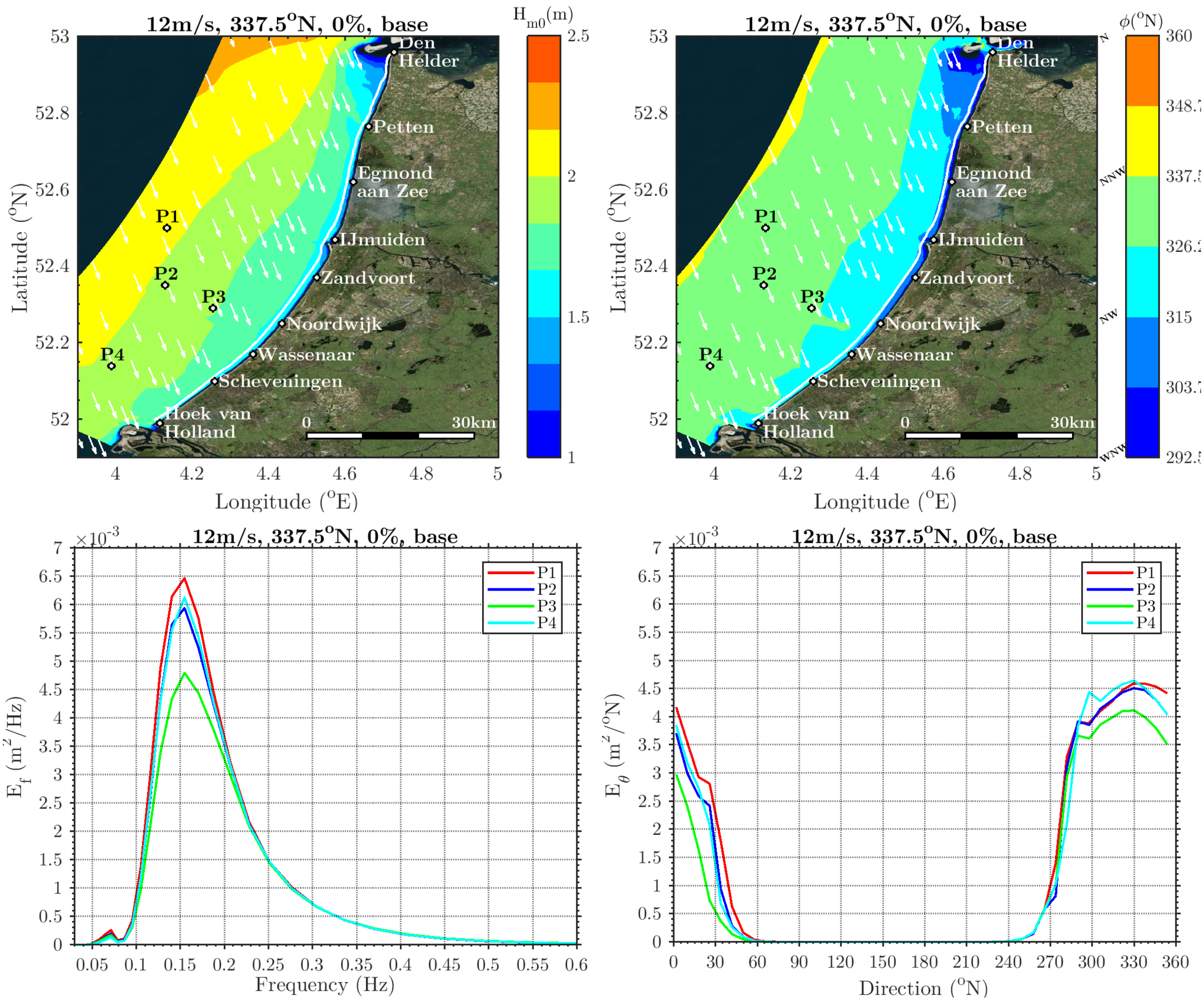

Figure D.5: Undisturbed wave height (upper left), wave direction (upper right) and energy density in frequency (lower left) and directional (lower right) space for a wind speed of 12 m/s blowing from NNW.

The effect of OWFs in 2030 is depicted in Figure D.6. In general, the results show a pattern similar to the annual mean quantities computed in Chapter 5. The wave height decrease becomes less with distance from the OWF areas. Also, for the specific case depicted in the image, wave direction shows a clockwise turning at the northeastern edge of the OWFs and a counterclockwise turning at the southwestern edge.

It should be reminded however that the results here originate from one stationary run. They are not averaged over time (as done in Chapter 5) making it easier to observe the effect for a single scenario of wind magnitude and direction. Looking at Chapter 5, values of counterclockwise rotation (negative values) are barely noticed, probably because averaging made them insignificant. This seems to depend on the wave climate in the nearshore and more importantly on the dominant wind direction as well as the shape and orientation of the OWFs.

Looking at the change in energy density, location P2 experiences the greatest decrease. This is reasonable since it is located closer to the OWF center compared to the other locations. Furthermore, at locations P2 and P3 wave direction rotates clockwise while at P1 and P4 it rotates counterclockwise. This can be explained by looking at the directional sector that loses the most energy. For points P2 and P3 it is the W – NNW sector (270° – 330°) that is mostly affected while for points P1 and P4 most of the energy is lost within the NNW – NE sector (330° – 30°).

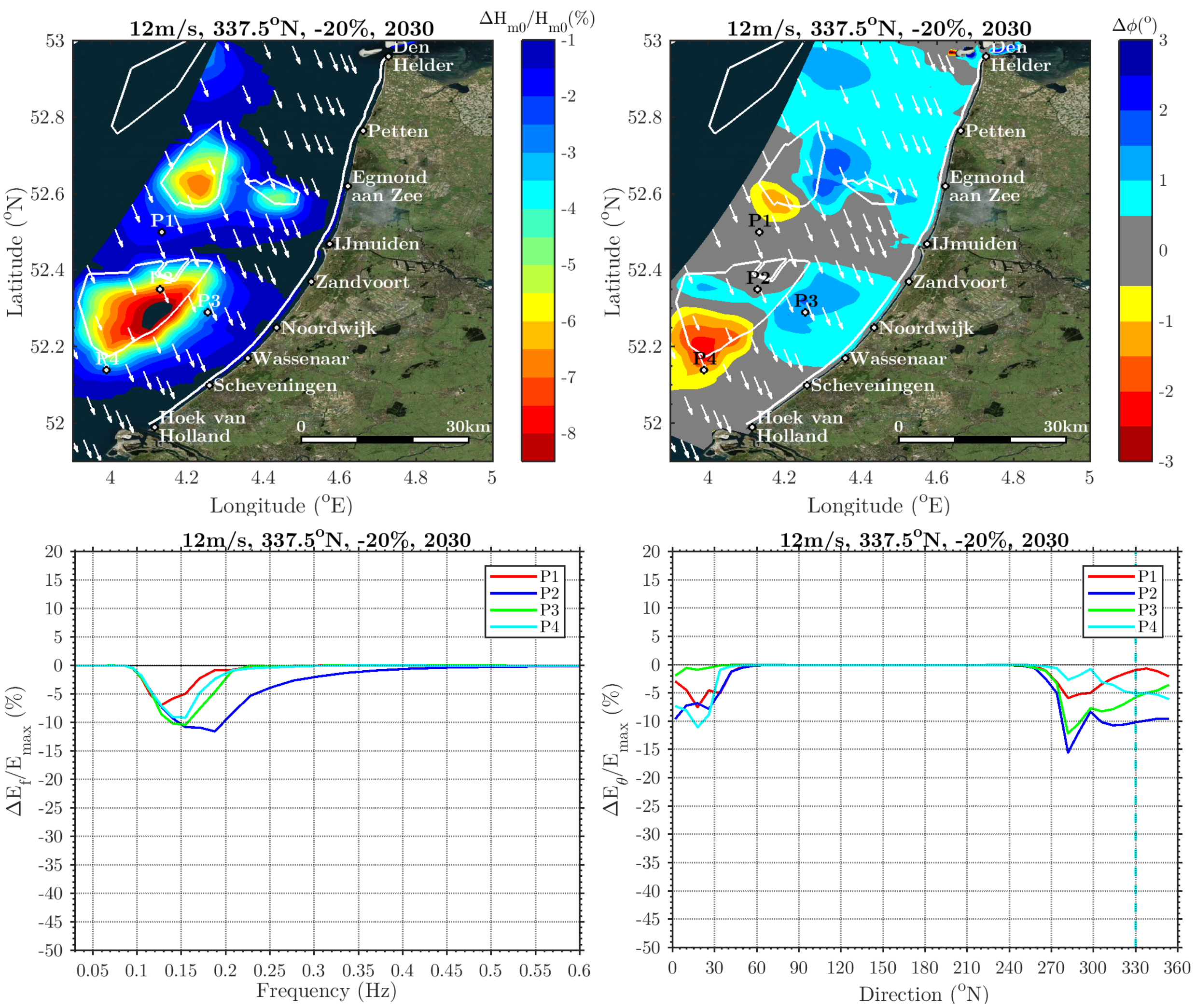

Figure D.6: Effect of development stage 2030 on wave height (upper left), wave direction (upper right) and energy density in frequency (lower left) and directional space (lower right) for a wind speed of 12 m/s blowing from NNW. The dashed line indicates the dominant energy propagation direction in the undisturbed situation.

The net effect of an island is shown in Figure D.7. The shielding of the area immediately downwind of the obstacle results in great loss of energy at location P1. The other locations experience a much smaller decrease, which is totally in line with the insignificant effect on wave height. Looking at the wave direction change, locations P1 and P2 show a counterclockwise turning since more energy is lost in the NNW – NE sector. At the rest locations the change in direction is less than 0.5° and is not shown in the map plot.

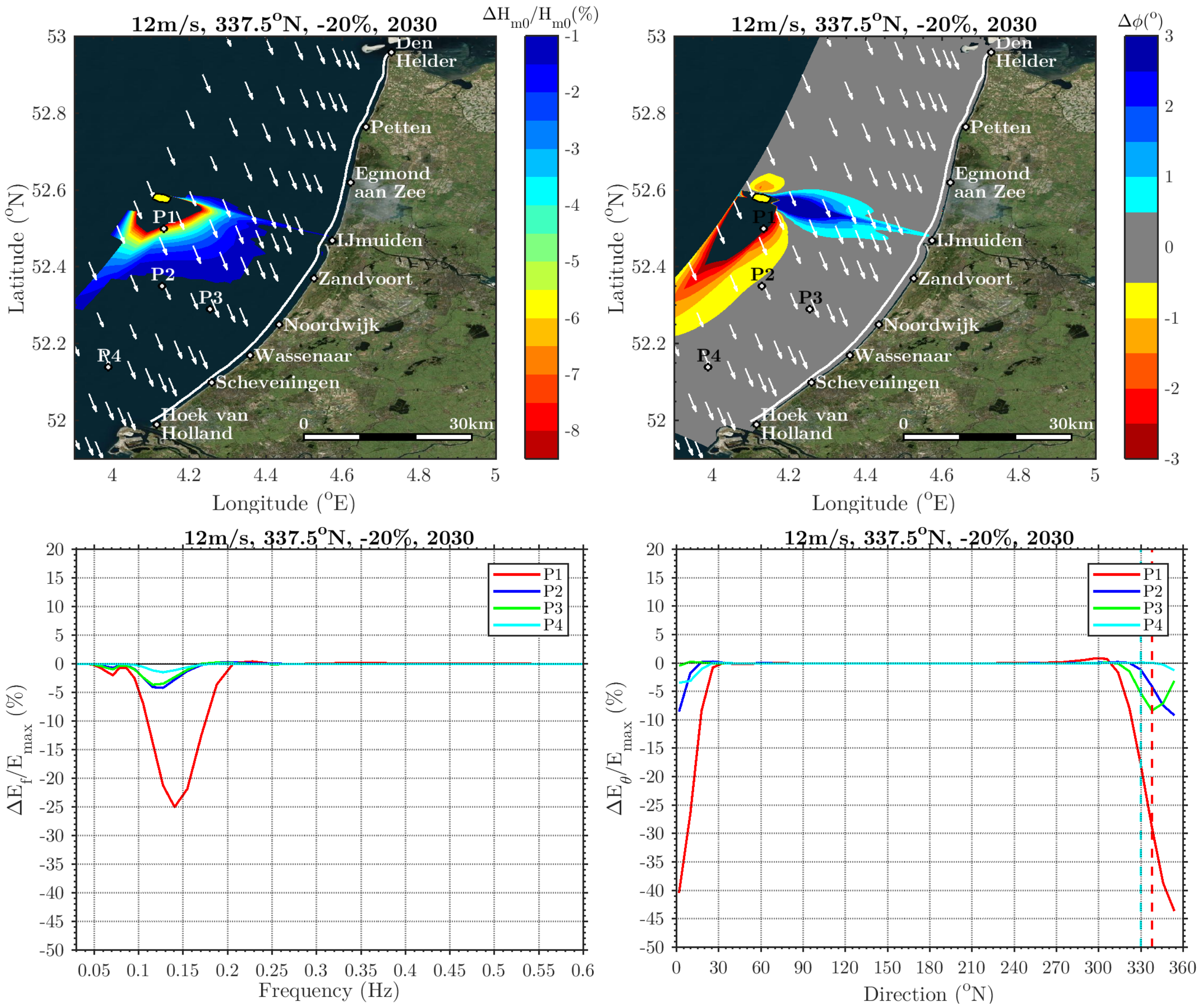

Figure D.7: Effect of an energy island on wave height (upper left), wave direction (upper right) and energy density in frequency (lower left) and directional space (lower right) for a wind speed of 12 m/s blowing from NNW. The dashed lines indicate the dominant energy propagation direction in the undisturbed situation.

In conclusion, wave height is found to decrease in the lee side of an OWF or an island while the wave direction slightly bends towards the shadow zone. The island effect seems to be stronger, but affects a smaller region compared to OWFs.

E

Model pre-processing

This section presents the flow chart of SWAN and Unibest-CL+ computations. In addition, the command files of SWAN and Unibest-CL+ runs are shown, accompanied by scripts created to execute the latter in batch mode.

E.1. SWAN simulations

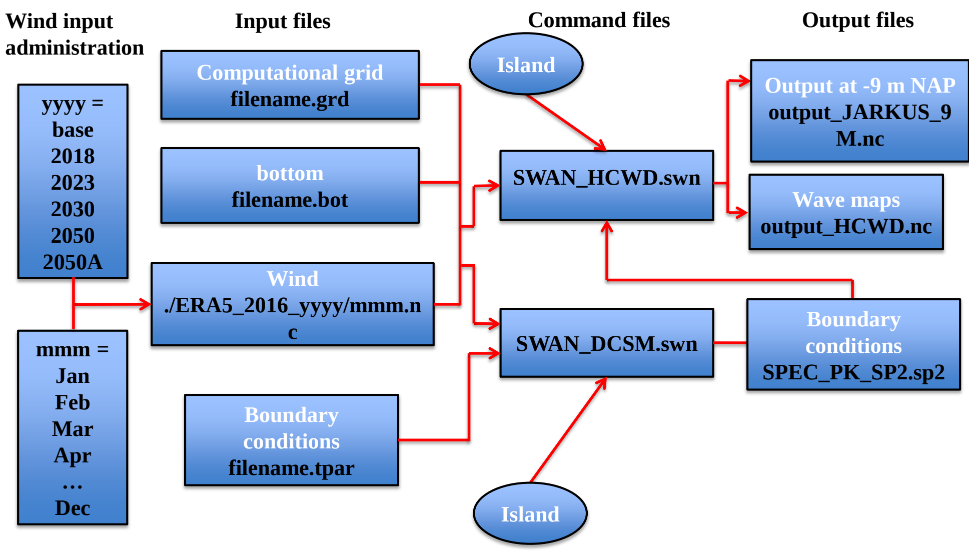

Figure E.1: Flow chart of SWAN simulations.

Example of SWAN-DCSM command file.

```
$** model version swan-dcsm-j15-v1 (june 2018)
$************************ HEADING ****************************************

PROJ 'OWFs_North_Sea' '001'

$************************ MODEL INPUT ************************************

SET NAUTICAL
SET LEVEL=0
MODE NONSTAT TWOD
COORDINATES SPHERICAL CCM

CGRID REGULAR -12. 48. 0. 21. 16. 420 480 CIRCLE 45 0.03 0.6

INPGRID BOTTOM REGULAR -15. 43. 0. 1120 1260 0.025 0.0166 EXC -9999.
READINP BOTTOM 1. '../../../../../bathymetry/swan-dcsm-j13-v1.BOT' 3 FREE

INPGRID WIND REGF '../../../../../ERA5/ERA5_2016_base/Jan.nc' &
NONSTAT 20160101.0000 1 HR 20160102.2300
READINP WIND 1.0 '../../../../../ERA5/ERA5_2016_base/Jan.nc'

```

```
$************************ BOUNDARY CONDITIONS *******************************

BOUND SHAPE    JONSWAP    3.30    PEAK DSPR POWER

BOUN   SEGM   XY 7.00 64.00 -12.00 64.00   VAR      FILE &
0.00  '/ERA5/DCSM_boundary_20150101_20170228/ERA5_63.90_6.90.tpar' 1 &
1.90  '../../../../../ERA5/DCSM_boundary/ERA5_63.90_5.10.tpar' 1 &
3.70  '../../../../../ERA5/DCSM_boundary/ERA5_63.90_3.30.tpar' 1 &
5.50  '../../../../../ERA5/DCSM_boundary/ERA5_63.90_1.50.tpar' 1 &
7.30  '../../../../../ERA5/DCSM_boundary/ERA5_63.90_-0.30.tpar' 1 &
9.10  '../../../../../ERA5/DCSM_boundary/ERA5_63.90_-2.10.tpar' 1 &
10.90  '../../../../../ERA5/DCSM_boundary/ERA5_63.90_-3.90.tpar' 1 &
12.70  '../../../../../ERA5/DCSM_boundary/ERA5_63.90_-5.70.tpar' 1 &
14.50  '../../../../../ERA5/DCSM_boundary/ERA5_63.90_-7.50.tpar' 1 &
16.30  '../../../../../ERA5/DCSM_boundary/ERA5_63.90_-9.30.tpar' 1 &
18.10  '../../../../../ERA5/DCSM_boundary/ERA5_63.90_-11.10.tpar' 1 &
19.00  '../../../../../ERA5/DCSM_boundary/ERA5_63.90_-12.00.tpar' 1

BOUN SEGM XY -12.00 64.00 -12.00 48.00 VAR FILE &
0.00  '../../../../../ERA5/DCSM_boundary/ERA5_63.90_-12.00_2.tpar' 1 &
1.30  '../../../../../ERA5/DCSM_boundary/ERA5_62.70_-12.00.tpar' 1 &
2.50  '../../../../../ERA5/DCSM_boundary/ERA5_61.50_-12.00.tpar' 1 &
3.70  '../../../../../ERA5/DCSM_boundary/ERA5_60.30_-12.00.tpar' 1 &
4.90  '../../../../../ERA5/DCSM_boundary/ERA5_59.10_-12.00.tpar' 1 &
6.10  '../../../../../ERA5/DCSM_boundary/ERA5_57.90_-12.00.tpar' 1 &
7.30  '../../../../../ERA5/DCSM_boundary/ERA5_56.70_-12.00.tpar' 1 &
8.50  '../../../../../ERA5/DCSM_boundary/ERA5_55.50_-12.00.tpar' 1 &
9.70  '../../../../../ERA5/DCSM_boundary/ERA5_54.30_-12.00.tpar' 1 &
10.90  '../../../../../ERA5/DCSM_boundary/ERA5_53.10_-12.00.tpar' 1 &
12.10  '../../../../../ERA5/DCSM_boundary/ERA5_51.90_-12.00.tpar' 1 &
13.30  '../../../../../ERA5/DCSM_boundary/ERA5_50.70_-12.00.tpar' 1 &
14.50  '../../../../../ERA5/DCSM_boundary/ERA5_49.50_-12.00.tpar' 1 &
16.00  '../../../../../ERA5/DCSM_boundary/ERA5_48.00_-12.00.tpar' 1

BOUN SEGM XY -12.00 48.00 -6.00 48.00 VAR FILE &
0.00  '../../../../../ERA5/DCSM_boundary/ERA5_48.00_-12.00_2.tpar' 1 &
1.20  '../../../../../ERA5/DCSM_boundary/ERA5_48.00_-10.80.tpar' 1 &
2.40  '../../../../../ERA5/DCSM_boundary/ERA5_48.00_-9.60.tpar' 1 &
3.60  '../../../../../ERA5/DCSM_boundary/ERA5_48.00_-8.40.tpar' 1 &
4.80  '../../../../../ERA5/DCSM_boundary/ERA5_48.00_-7.20.tpar' 1 &
6.00  '../../../../../ERA5/DCSM_boundary/ERA5_48.00_-6.00.tpar' 1

$************************ PHYSICAL PARAMETERS *****************************

GEN3
```

```
FRIC JONSWAP   0.038
BREA CONST     1.0     0.73

$************************ ISLAND (if modeled) ******************************

OBST TRANS 0 REFL 0.3 RSPEC LINe &
    3.6449368E+00   5.2803519E+01 &
    3.6372299E+00   5.2786061E+01 &
    3.6451503E+00   5.2764934E+01 &
    3.6736261E+00   5.2761373E+01 &
    3.7046235E+00   5.2765127E+01 &
    3.7120959E+00   5.2784927E+01 &
    3.7030310E+00   5.2803739E+01 &
    3.6717297E+00   5.2808660E+01 &
    3.6449368E+00   5.2803519E+01 &

$************************* NUMERICAL PARAMETERS ***************************

LIM      10       1
PROP   BSBT
NUM      DIR      cdd = 0.50 SIGIM    css = 0.50
NUM STOPC 0.010 0.010 0.005 99. STAT 50 0.01 0.1

$**************************** OUTPUT QUANTITIES ***************************

QUANTITY XP        excv=-999.0
QUANTITY YP        excv=-999.0
QUANTITY HSIGN     excv=-999.0
QUANTITY TMM10     excv=-999.0
QUANTITY TM01      excv=-999.0
QUANTITY TPS       excv=-999.0
QUANTITY DIR       excv=-999.0
QUANTITY WIND      excv=-999.0

$**************************** OUTPUT LOCATIONS ****************************

POINTS 'PK' FILE  '../../../../../nesting_points/KUSTROOK_clw_reduced.PNT'

$**************************** OUTPUT REQUEST ******************************

SPECOUT 'PK'  SPEC2D  ABS 'SPEC_PK_SP2.sp2'  OUTPUT 20160101.0000 1 HR

$*************************** COMPUTATION REQUEST **************************

COMPUTE STAT 20160101.0000
```

```
INIT DEF

$ ... the commands in between are not shown here!

COMPUTE STAT 20160102.2200
INIT DEF
COMPUTE STAT 20160102.2300
STOP
```

Example of SWAN-HCWD command file.

```
$** model swan–hcwd (june 2018)
$************************ HEADING ******************************************

PROJ 'OWFs_North_Sea' '001'

$************************ MODEL INPUT ************************************

SET NAUTICAL
SET LEVEL=0
MODE NONSTAT TWOD
COORDINATES SPHERICAL CCM

CGRID CURVI 77 174 EXCE 0.0 0.0 CIRCLE 45 0.03 0.6
READ COORD 1. '../../../../../computation_grid/swan–hcwd.grd' 4 0 1 FREE

INP BOTTOM CURVI 0. 0. 77 174
READ BOTTOM 1. '../../../../../bathymetry/swan–hcwd.BOT' 4 0 FREE

INPGRID WIND REGF '../../../../../ERA5/ERA5_2016_base/Jan.nc' &
NONSTAT 20160101.0000 1 HR 20160102.2300
READINP WIND 1.0 '../../../../../ERA5/ERA5_2016_base/Jan.nc'

$*********************** BOUNDARY CONDITIONS ******************************

BOUND NEST '../01_DCSM/SPEC_PK_SP2.sp2' OPEN

$************************ PHYSICAL PARAMETERS *****************************

GEN3 KOMEN
WCAP KOMEN delta=1
QUAD iquad=2
TRIAD itriad=1 trfac=0.8 cutfr=2.5
FRIC JONSWAP cfjon=0.038
BREA CONST 1.0 0.73

```

```
$************************ ISLAND (if modeled) ****************************

OBST TRANS 0 REFL 0.3 RSPEC LINe &
   3.6449368E+00   5.2803519E+01 &
   3.6372299E+00   5.2786061E+01 &
   3.6451503E+00   5.2764934E+01 &
   3.6736261E+00   5.2761373E+01 &
   3.7046235E+00   5.2765127E+01 &
   3.7120959E+00   5.2784927E+01 &
   3.7030310E+00   5.2803739E+01 &
   3.6717297E+00   5.2808660E+01 &
   3.6449368E+00   5.2803519E+01 &

$************************* NUMERICAL PARAMETERS **************************

NUM STOPC 0.01 0.01 0.005 99. STAT 50 0.01 0.1

$**************************** OUTPUT QUANTITIES **************************

QUANTITY XP        excv=-999.0
QUANTITY YP        excv=-999.0
QUANTITY HSIGN     excv=-999.0
QUANTITY TMM10     excv=-999.0
QUANTITY TM01      excv=-999.0
QUANTITY TPS       excv=-999.0
QUANTITY DIR       excv=-999.0
QUANTITY WIND      excv=-999.0

$**************************** OUTPUT LOCATIONS ***************************

POINTS 'LOC9M' FILE '../../../../../JARKUS/Jarkus_locations_9m.PNT'

$**************************** OUTPUT REQUEST *****************************

TABLE    'LOC9M'   NOHEADER './output_JARKUS_9M.nc' &
   XP YP HSIG TMM10 TM01 TPS DIR WIND OUTPUT 20160101.0000 1 HR

BLOCK    'COMPGRID'   NOHEAD   './output_HCWD.nc'   LAYOUT 3 &
   XP YP HSIG TMM10 TM01 TPS DIR WIND OUTPUT 20160101.0000 1 HR

$*************************** COMPUTATION REQUEST *************************

COMPUTE STAT 20160101.0000
INIT DEF
```

```
$ ... the commands in between are not shown here!

COMPUTE STAT 20160102.2200
INIT DEF
COMPUTE STAT 20160102.2300
STOP
```

SWAN batch submission script.

```
#!/bin/sh

### INPUT VARIABLES
model="HCWD"; ### model: "DCSM" "HCWD"
island="0";   ### island: "0" "1" "2" "3" "4"
for year in "base" ### year: "base" "2018" "2023" "2030" "2050" "2050A"
do
        for change in "0" ### wind change (%): "0" (for baseline) "-20"
        do
                echo "model = ${model}";
                echo "year = ${year}";
                echo "island = ${island}"
                echo "change = ${change}"
                if test "$year" = "base"
                then
                        echo "base case"
                        cd "../../test_runs/quasi_stationary/${year}/"
                else
                        echo "owf case"
                        cd "../../test_runs/quasi_stationary/" \
                        "${year}_${island}/${change}/"
                fi
                for month in "Jan" "Feb" "Mar" "Apr" "May" \
                "Jun" "Jul" "Aug" "Sep" "Oct" "Nov" "Dec"
                do
                        echo "month = ${month}";
                        if test "$month" = "Jan"
                        then
                                cd "./${month}/"
                        else
                                cd "../../${month}/"
                        fi
                        echo "dir: $PWD"
                        ### files split into 2-day runs (16 files per month)
                        cd "./01_${model}/";
                        qsub -N ${month}_${change}_1  run_swan_l64_omp.sh
                        cd "../02_${model}/"
```

```
            qsub -N ${month}_${change}_2  run_swan_l64_omp.sh
            cd "../03_${model}/"
            qsub -N ${month}_${change}_3  run_swan_l64_omp.sh
            cd "../04_${model}/"
            qsub -N ${month}_${change}_4  run_swan_l64_omp.sh
            cd "../05_${model}/"
            qsub -N ${month}_${change}_5  run_swan_l64_omp.sh
            cd "../06_${model}/"
            qsub -N ${month}_${change}_6  run_swan_l64_omp.sh
            cd "../07_${model}/"
            qsub -N ${month}_${change}_7  run_swan_l64_omp.sh
            cd "../08_${model}/"
            qsub -N ${month}_${change}_8  run_swan_l64_omp.sh
            cd "../09_${model}/"
            qsub -N ${month}_${change}_9  run_swan_l64_omp.sh
            cd "../10_${model}/"
            qsub -N ${month}_${change}_10  run_swan_l64_omp.sh
            cd "../11_${model}/"
            qsub -N ${month}_${change}_11  run_swan_l64_omp.sh
            cd "../12_${model}/"
            qsub -N ${month}_${change}_12  run_swan_l64_omp.sh
            cd "../13_${model}/"
            qsub -N ${month}_${change}_13  run_swan_l64_omp.sh
            cd "../14_${model}/"
            qsub -N ${month}_${change}_14  run_swan_l64_omp.sh
            cd "../15_${model}/"
            qsub -N ${month}_${change}_15  run_swan_l64_omp.sh
            cd "../16_${model}/"
            qsub -N ${month}_${change}_16  run_swan_l64_omp.sh
        done
    done
done
```

E.2. Unibest-CL+ simulations

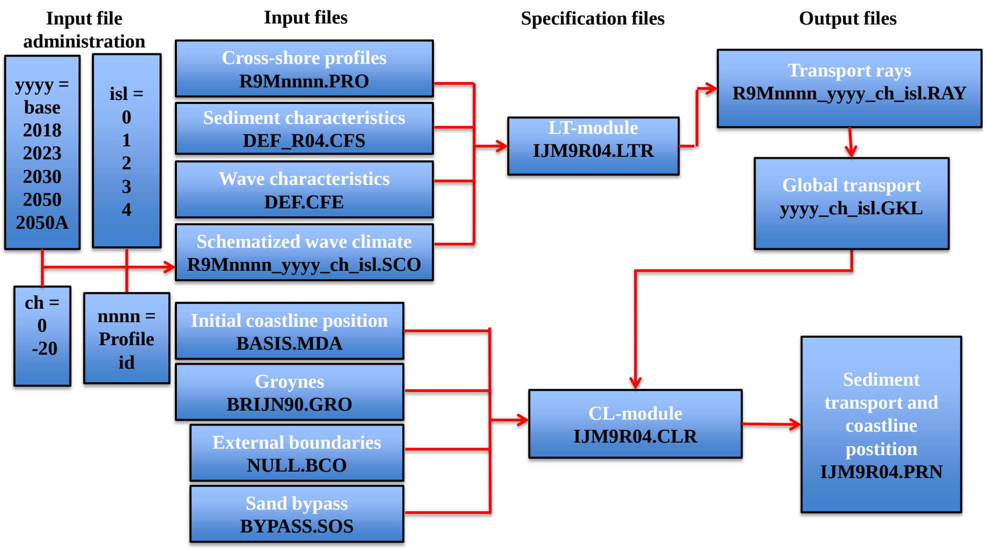

Figure E.2: Flow chart of Unibest-CL+ simulations.

Example of LT-module command file.

```
Number of Climates
 112
ORKST    PROFH  .PRO        .CFS       .CFE       .SCO                      .RAY
300.47 10. 'R9M0000' 'DEF_R04' 'DEF' 'R9M0000_2018_-20_0' 'R9M0000_2018_-20_0'
301.21 10. 'R9M0010' 'DEF_R04' 'DEF' 'R9M0010_2018_-20_0' 'R9M0010_2018_-20_0'
302.14 10. 'R9M0021' 'DEF_R04' 'DEF' 'R9M0021_2018_-20_0' 'R9M0021_2018_-20_0'
302.91 10. 'R9M0032' 'DEF_R04' 'DEF' 'R9M0032_2018_-20_0' 'R9M0032_2018_-20_0'
303.67 10. 'R9M0042' 'DEF_R04' 'DEF' 'R9M0042_2018_-20_0' 'R9M0042_2018_-20_0'
304.44 10. 'R9M0052' 'DEF_R04' 'DEF' 'R9M0052_2018_-20_0' 'R9M0052_2018_-20_0'
305.31 10. 'R9M0063' 'DEF_R04' 'DEF' 'R9M0063_2018_-20_0' 'R9M0063_2018_-20_0'
306.23 10. 'R9M0074' 'DEF_R04' 'DEF' 'R9M0074_2018_-20_0' 'R9M0074_2018_-20_0'
307.29 10. 'R9M0087' 'DEF_R04' 'DEF' 'R9M0087_2018_-20_0' 'R9M0087_2018_-20_0'
308.20 10. 'R9M0099' 'DEF_R04' 'DEF' 'R9M0099_2018_-20_0' 'R9M0099_2018_-20_0'
309.16 10. 'R9M0110' 'DEF_R04' 'DEF' 'R9M0110_2018_-20_0' 'R9M0110_2018_-20_0'
309.59 10. 'R9M0120' 'DEF_R04' 'DEF' 'R9M0120_2018_-20_0' 'R9M0120_2018_-20_0'
310.06 10. 'R9M0131' 'DEF_R04' 'DEF' 'R9M0131_2018_-20_0' 'R9M0131_2018_-20_0'
310.50 10. 'R9M0142' 'DEF_R04' 'DEF' 'R9M0142_2018_-20_0' 'R9M0142_2018_-20_0'
310.95 10. 'R9M0153' 'DEF_R04' 'DEF' 'R9M0153_2018_-20_0' 'R9M0153_2018_-20_0'
311.38 10. 'R9M0164' 'DEF_R04' 'DEF' 'R9M0164_2018_-20_0' 'R9M0164_2018_-20_0'
311.80 10. 'R9M0174' 'DEF_R04' 'DEF' 'R9M0174_2018_-20_0' 'R9M0174_2018_-20_0'
312.19 10. 'R9M0184' 'DEF_R04' 'DEF' 'R9M0184_2018_-20_0' 'R9M0184_2018_-20_0'
312.59 10. 'R9M0193' 'DEF_R04' 'DEF' 'R9M0193_2018_-20_0' 'R9M0193_2018_-20_0'
313.03 10. 'R9M0204' 'DEF_R04' 'DEF' 'R9M0204_2018_-20_0' 'R9M0204_2018_-20_0'
313.51 10. 'R9M0215' 'DEF_R04' 'DEF' 'R9M0215_2018_-20_0' 'R9M0215_2018_-20_0'
311.90 10. 'R9M0228' 'DEF_R04' 'DEF' 'R9M0228_2018_-20_0' 'R9M0228_2018_-20_0'
```

```
310.67 10. 'R9M0238' 'DEF_R04' 'DEF' 'R9M0238_2018_-20_0' 'R9M0238_2018_-20_0'
309.26 10. 'R9M0250' 'DEF_R04' 'DEF' 'R9M0250_2018_-20_0' 'R9M0250_2018_-20_0'
307.78 10. 'R9M0261' 'DEF_R04' 'DEF' 'R9M0261_2018_-20_0' 'R9M0261_2018_-20_0'
306.15 10. 'R9M0274' 'DEF_R04' 'DEF' 'R9M0274_2018_-20_0' 'R9M0274_2018_-20_0'
304.70 10. 'R9M0287' 'DEF_R04' 'DEF' 'R9M0287_2018_-20_0' 'R9M0287_2018_-20_0'
303.20 10. 'R9M0299' 'DEF_R04' 'DEF' 'R9M0299_2018_-20_0' 'R9M0299_2018_-20_0'
301.99 10. 'R9M0309' 'DEF_R04' 'DEF' 'R9M0309_2018_-20_0' 'R9M0309_2018_-20_0'
300.66 10. 'R9M0320' 'DEF_R04' 'DEF' 'R9M0320_2018_-20_0' 'R9M0320_2018_-20_0'
299.38 10. 'R9M0330' 'DEF_R04' 'DEF' 'R9M0330_2018_-20_0' 'R9M0330_2018_-20_0'
298.81 10. 'R9M0341' 'DEF_R04' 'DEF' 'R9M0341_2018_-20_0' 'R9M0341_2018_-20_0'
298.15 10. 'R9M0353' 'DEF_R04' 'DEF' 'R9M0353_2018_-20_0' 'R9M0353_2018_-20_0'
297.50 10. 'R9M0364' 'DEF_R04' 'DEF' 'R9M0364_2018_-20_0' 'R9M0364_2018_-20_0'
296.72 10. 'R9M0379' 'DEF_R04' 'DEF' 'R9M0379_2018_-20_0' 'R9M0379_2018_-20_0'
296.08 10. 'R9M0390' 'DEF_R04' 'DEF' 'R9M0390_2018_-20_0' 'R9M0390_2018_-20_0'
295.35 10. 'R9M0404' 'DEF_R04' 'DEF' 'R9M0404_2018_-20_0' 'R9M0404_2018_-20_0'
294.55 10. 'R9M0418' 'DEF_R04' 'DEF' 'R9M0418_2018_-20_0' 'R9M0418_2018_-20_0'
293.82 10. 'R9M0432' 'DEF_R04' 'DEF' 'R9M0432_2018_-20_0' 'R9M0432_2018_-20_0'
293.12 10. 'R9M0444' 'DEF_R04' 'DEF' 'R9M0444_2018_-20_0' 'R9M0444_2018_-20_0'
292.38 10. 'R9M0458' 'DEF_R04' 'DEF' 'R9M0458_2018_-20_0' 'R9M0458_2018_-20_0'
292.13 10. 'R9M0470' 'DEF_R04' 'DEF' 'R9M0470_2018_-20_0' 'R9M0470_2018_-20_0'
291.83 10. 'R9M0485' 'DEF_R04' 'DEF' 'R9M0485_2018_-20_0' 'R9M0485_2018_-20_0'
291.54 10. 'R9M0499' 'DEF_R04' 'DEF' 'R9M0499_2018_-20_0' 'R9M0499_2018_-20_0'
291.23 10. 'R9M0515' 'DEF_R04' 'DEF' 'R9M0515_2018_-20_0' 'R9M0515_2018_-20_0'
290.99 10. 'R9M0526' 'DEF_R04' 'DEF' 'R9M0526_2018_-20_0' 'R9M0526_2018_-20_0'
290.74 10. 'R9M0539' 'DEF_R04' 'DEF' 'R9M0539_2018_-20_0' 'R9M0539_2018_-20_0'
290.49 10. 'R9M0551' 'DEF_R04' 'DEF' 'R9M0551_2018_-20_0' 'R9M0551_2018_-20_0'
290.22 10. 'R9M0563' 'DEF_R04' 'DEF' 'R9M0563_2018_-20_0' 'R9M0563_2018_-20_0'
290.02 10. 'R9M0572' 'DEF_R04' 'DEF' 'R9M0572_2018_-20_0' 'R9M0572_2018_-20_0'
289.92 10. 'R9M0577' 'DEF_R04' 'DEF' 'R9M0577_2018_-20_0' 'R9M0577_2018_-20_0'
289.42 10. 'R9M0582' 'DEF_R04' 'DEF' 'R9M0582_2018_-20_0' 'R9M0582_2018_-20_0'
288.92 10. 'R9M0587' 'DEF_R04' 'DEF' 'R9M0587_2018_-20_0' 'R9M0587_2018_-20_0'
288.51 10. 'R9M0591' 'DEF_R04' 'DEF' 'R9M0591_2018_-20_0' 'R9M0591_2018_-20_0'
286.60 10. 'R9M0611' 'DEF_R04' 'DEF' 'R9M0611_2018_-20_0' 'R9M0611_2018_-20_0'
286.02 10. 'R9M0616' 'DEF_R04' 'DEF' 'R9M0616_2018_-20_0' 'R9M0616_2018_-20_0'
285.38 10. 'R9M0622' 'DEF_R04' 'DEF' 'R9M0622_2018_-20_0' 'R9M0622_2018_-20_0'
284.84 10. 'R9M0627' 'DEF_R04' 'DEF' 'R9M0627_2018_-20_0' 'R9M0627_2018_-20_0'
284.32 10. 'R9M0633' 'DEF_R04' 'DEF' 'R9M0633_2018_-20_0' 'R9M0633_2018_-20_0'
283.33 10. 'R9M0639' 'DEF_R04' 'DEF' 'R9M0639_2018_-20_0' 'R9M0639_2018_-20_0'
282.73 10. 'R9M0645' 'DEF_R04' 'DEF' 'R9M0645_2018_-20_0' 'R9M0645_2018_-20_0'
282.40 10. 'R9M0652' 'DEF_R04' 'DEF' 'R9M0652_2018_-20_0' 'R9M0652_2018_-20_0'
281.96 10. 'R9M0660' 'DEF_R04' 'DEF' 'R9M0660_2018_-20_0' 'R9M0660_2018_-20_0'
281.39 10. 'R9M0670' 'DEF_R04' 'DEF' 'R9M0670_2018_-20_0' 'R9M0670_2018_-20_0'
280.88 10. 'R9M0680' 'DEF_R04' 'DEF' 'R9M0680_2018_-20_0' 'R9M0680_2018_-20_0'
280.39 10. 'R9M0689' 'DEF_R04' 'DEF' 'R9M0689_2018_-20_0' 'R9M0689_2018_-20_0'
279.88 10. 'R9M0698' 'DEF_R04' 'DEF' 'R9M0698_2018_-20_0' 'R9M0698_2018_-20_0'
```

```
279.32 10. 'R9M0708' 'DEF_R04' 'DEF' 'R9M0708_2018_-20_0' 'R9M0708_2018_-20_0'
278.82 10. 'R9M0717' 'DEF_R04' 'DEF' 'R9M0717_2018_-20_0' 'R9M0717_2018_-20_0'
278.30 10. 'R9M0726' 'DEF_R04' 'DEF' 'R9M0726_2018_-20_0' 'R9M0726_2018_-20_0'
277.74 10. 'R9M0736' 'DEF_R04' 'DEF' 'R9M0736_2018_-20_0' 'R9M0736_2018_-20_0'
277.60 10. 'R9M0746' 'DEF_R04' 'DEF' 'R9M0746_2018_-20_0' 'R9M0746_2018_-20_0'
277.45 10. 'R9M0755' 'DEF_R04' 'DEF' 'R9M0755_2018_-20_0' 'R9M0755_2018_-20_0'
277.32 10. 'R9M0764' 'DEF_R04' 'DEF' 'R9M0764_2018_-20_0' 'R9M0764_2018_-20_0'
277.16 10. 'R9M0775' 'DEF_R04' 'DEF' 'R9M0775_2018_-20_0' 'R9M0775_2018_-20_0'
277.01 10. 'R9M0785' 'DEF_R04' 'DEF' 'R9M0785_2018_-20_0' 'R9M0785_2018_-20_0'
276.88 10. 'R9M0793' 'DEF_R04' 'DEF' 'R9M0793_2018_-20_0' 'R9M0793_2018_-20_0'
276.74 10. 'R9M0803' 'DEF_R04' 'DEF' 'R9M0803_2018_-20_0' 'R9M0803_2018_-20_0'
276.60 10. 'R9M0812' 'DEF_R04' 'DEF' 'R9M0812_2018_-20_0' 'R9M0812_2018_-20_0'
276.45 10. 'R9M0822' 'DEF_R04' 'DEF' 'R9M0822_2018_-20_0' 'R9M0822_2018_-20_0'
276.29 10. 'R9M0833' 'DEF_R04' 'DEF' 'R9M0833_2018_-20_0' 'R9M0833_2018_-20_0'
277.55 10. 'R9M0842' 'DEF_R04' 'DEF' 'R9M0842_2018_-20_0' 'R9M0842_2018_-20_0'
278.67 10. 'R9M0851' 'DEF_R04' 'DEF' 'R9M0851_2018_-20_0' 'R9M0851_2018_-20_0'
279.97 10. 'R9M0861' 'DEF_R04' 'DEF' 'R9M0861_2018_-20_0' 'R9M0861_2018_-20_0'
281.13 10. 'R9M0870' 'DEF_R04' 'DEF' 'R9M0870_2018_-20_0' 'R9M0870_2018_-20_0'
282.34 10. 'R9M0879' 'DEF_R04' 'DEF' 'R9M0879_2018_-20_0' 'R9M0879_2018_-20_0'
283.41 10. 'R9M0888' 'DEF_R04' 'DEF' 'R9M0888_2018_-20_0' 'R9M0888_2018_-20_0'
284.54 10. 'R9M0897' 'DEF_R04' 'DEF' 'R9M0897_2018_-20_0' 'R9M0897_2018_-20_0'
285.77 10. 'R9M0907' 'DEF_R04' 'DEF' 'R9M0907_2018_-20_0' 'R9M0907_2018_-20_0'
287.16 10. 'R9M0918' 'DEF_R04' 'DEF' 'R9M0918_2018_-20_0' 'R9M0918_2018_-20_0'
288.37 10. 'R9M0927' 'DEF_R04' 'DEF' 'R9M0927_2018_-20_0' 'R9M0927_2018_-20_0'
287.84 10. 'R9M0937' 'DEF_R04' 'DEF' 'R9M0937_2018_-20_0' 'R9M0937_2018_-20_0'
287.24 10. 'R9M0948' 'DEF_R04' 'DEF' 'R9M0948_2018_-20_0' 'R9M0948_2018_-20_0'
286.71 10. 'R9M0958' 'DEF_R04' 'DEF' 'R9M0958_2018_-20_0' 'R9M0958_2018_-20_0'
286.17 10. 'R9M0967' 'DEF_R04' 'DEF' 'R9M0967_2018_-20_0' 'R9M0967_2018_-20_0'
285.68 10. 'R9M0976' 'DEF_R04' 'DEF' 'R9M0976_2018_-20_0' 'R9M0976_2018_-20_0'
285.09 10. 'R9M0987' 'DEF_R04' 'DEF' 'R9M0987_2018_-20_0' 'R9M0987_2018_-20_0'
284.56 10. 'R9M0998' 'DEF_R04' 'DEF' 'R9M0998_2018_-20_0' 'R9M0998_2018_-20_0'
283.90 10. 'R9M1009' 'DEF_R04' 'DEF' 'R9M1009_2018_-20_0' 'R9M1009_2018_-20_0'
283.33 10. 'R9M1019' 'DEF_R04' 'DEF' 'R9M1019_2018_-20_0' 'R9M1019_2018_-20_0'
282.76 10. 'R9M1030' 'DEF_R04' 'DEF' 'R9M1030_2018_-20_0' 'R9M1030_2018_-20_0'
283.36 10. 'R9M1040' 'DEF_R04' 'DEF' 'R9M1040_2018_-20_0' 'R9M1040_2018_-20_0'
283.92 10. 'R9M1049' 'DEF_R04' 'DEF' 'R9M1049_2018_-20_0' 'R9M1049_2018_-20_0'
284.40 10. 'R9M1058' 'DEF_R04' 'DEF' 'R9M1058_2018_-20_0' 'R9M1058_2018_-20_0'
284.82 10. 'R9M1067' 'DEF_R04' 'DEF' 'R9M1067_2018_-20_0' 'R9M1067_2018_-20_0'
285.27 10. 'R9M1077' 'DEF_R04' 'DEF' 'R9M1077_2018_-20_0' 'R9M1077_2018_-20_0'
285.74 10. 'R9M1087' 'DEF_R04' 'DEF' 'R9M1087_2018_-20_0' 'R9M1087_2018_-20_0'
286.38 10. 'R9M1099' 'DEF_R04' 'DEF' 'R9M1099_2018_-20_0' 'R9M1099_2018_-20_0'
286.85 10. 'R9M1108' 'DEF_R04' 'DEF' 'R9M1108_2018_-20_0' 'R9M1108_2018_-20_0'
287.45 10. 'R9M1121' 'DEF_R04' 'DEF' 'R9M1121_2018_-20_0' 'R9M1121_2018_-20_0'
287.88 10. 'R9M1130' 'DEF_R04' 'DEF' 'R9M1130_2018_-20_0' 'R9M1130_2018_-20_0'
288.34 10. 'R9M1139' 'DEF_R04' 'DEF' 'R9M1139_2018_-20_0' 'R9M1139_2018_-20_0'
```

LT-module batch submission script.

```
:: inside loops we have to use an extra %
:: remove echoing of commands
@echo off
ECHO starting compuations

cd p:/energy-island/MSc_work/Greg_Ballas/Unibest/LT_R04/base/
p:/energy-island/MSc_work/Greg_Ballas/Unibest/LT_exe/ltrun.exe IJM9R04.LTR
ECHO LT run base case is complete

for %%y in (2018,2023,2030,2050,2050A) do (
for %%c in (-20)  do (
for %%i in (0)  do (
echo year=%%y
echo island=%%i
echo change=%%c percent

cd p:/energy-island/MSc_work/Greg_Ballas/Unibest/LT_R04/%%y_%%i/%%c%/
echo p:/energy-island/MSc_work/Greg_Ballas/Unibest/LT_R04/%%y_%%i/%%c%/
p:/energy-island/MSc_work/Greg_Ballas/Unibest/LT_exe/ltrun.exe IJM9R04.LTR
ECHO LT run year=%%y, island=%%i, change=%%c percent is complete

)
)
)

ECHO Series batch script has completed succesfully
ECHO Returning to batch run directory:
cd p:/energy-island/MSc_work/Greg_Ballas/Unibest/UB_batch_runs/
```

Example of CL-module command file.

```
Fase Unit
 1
Delta t
2.0E+02
Number of Phases
 5
Number of Cycli
 1
Begin time (t0)
0.0E+00
'BASIS'   (MDA-file)
'IJM9R04'(LAT-file)
Fase   From To   .GKL          .BCO    .GRO        .SOS       .REV    .OBW    .BCI
 1     2013 2018 'BASE'        'NULL'  'BRIJN90'   'BYPASS'   'NULL'  'NULL'  'NULL'
```

```
 2      2018  2023  '2018_-20_0'  'NULL'  'BRIJN90'  'BYPASS'  'NULL'  'NULL'  'NULL'
 3      2023  2030  '2023_-20_0'  'NULL'  'BRIJN90'  'BYPASS'  'NULL'  'NULL'  'NULL'
 4      2030  2050  '2030_-20_0'  'NULL'  'BRIJN90'  'BYPASS'  'NULL'  'NULL'  'NULL'
 5      2050  2070  '2050_-20_0'  'NULL'  'BRIJN90'  'BYPASS'  'NULL'  'NULL'  'NULL'
iaant  ifirst  ival
 100    0         200
```

CL-module batch submission script.

```
:: inside loops we have to use an extra %
:: remove echoing of commands
@echo off
ECHO starting compuations

cd p:/energy-island/MSc_work/Greg_Ballas/Unibest/CL_R04/base/
p:/energy-island/MSc_work/Greg_Ballas/Unibest/CL_exe/clrun.exe IJM9R04.CLR
ECHO CL run base case is complete

for %%c in (-20) do (
for %%i in (0,1,2,3,4)  do (
echo island=%%i
echo change=%%c percent

cd p:/energy-island/MSc_work/Greg_Ballas/Unibest/CL_R04/%%c_%%i%/
p:/energy-island/MSc_work/Greg_Ballas/Unibest/CL_exe/clrun.exe IJM9R04.CLR
ECHO CL run: island=%%i, change=%%c percent is complete

)
)

ECHO CL Series batch script has completed succesfully
ECHO Returning to batch run directory:
cd p:/energy-island/MSc_work/Greg_Ballas/Unibest/UB_batch_runs/
```